

EFFECTS OF CLIMATE CHANGE ON WATER RESOURCES IN OMERLI
BASIN

A THESIS SUBMITTED TO
THE GRADUATE SCHOOL OF NATURAL AND APPLIED SCIENCES
OF
MIDDLE EAST TECHNICAL UNIVERSITY

BY

FATİH KARA

IN PARTIAL FULFILLMENT OF THE REQUIREMENTS
FOR
THE DEGREE OF DOCTOR OF PHILOSOPHY
IN
GEODETIC AND GEOGRAPHIC INFORMATION TECHNOLOGIES

SEPTEMBER 2014

Approval of the thesis:

**EFFECTS OF CLIMATE CHANGE ON WATER RESOURCES IN OMERLI
BASIN**

submitted by **FATİH KARA** in partial fulfillment of the requirements for the degree
of **Doctor of Philosophy in Geodetic and Geographic Information Technologies**
Department, Middle East Technical University by,

Prof. Dr. Canan Özgen _____
Dean, Graduate School of **Natural and Applied Sciences**

Prof. Dr. Ahmet Coşar _____
Head of Dept., **Geodetic and Geographic Info. Tech.**

Assoc. Prof. Dr. İsmail Yücel _____
Supervisor, **Civil Engineering Dept., METU**

Prof. Dr. S. Zuhale Akyürek _____
Co-supervisor, **Civil Engineering Dept., METU**

Examining Committee Members:

Prof. Dr. G. M. Vedat Toprak _____
Geological Engineering Dept., METU

Assoc. Prof. Dr. İsmail Yücel _____
Civil Engineering Dept., METU

Assoc. Prof. Dr. Nuri Merzi _____
Civil Engineering Dept., METU

Assist. Prof. Dr. Koray K. Yılmaz _____
Geological Engineering Dept., METU

Assist. Prof. Dr. Reşat Geçen _____
Geography Department, Mustafa Kemal University

Date: 03.09.2014

I hereby declare that all information in this document has been obtained and presented in accordance with academic rules and ethical conduct. I also declare that, as required by these rules and conduct, I have fully cited and referenced all material and results that are not original to this work.

Name, Last Name: Fatih, Kara

Signature :

ABSTRACT

EFFECTS OF CLIMATE CHANGE ON WATER RESOURCES IN OMERLI BASIN

Kara, Fatih

Ph.D., Department of Geodetic and Geographic Information Technologies

Supervisor: Assoc. Prof. Dr. İsmail Yücel

Co-supervisor: Prof. Dr. S. Zuhul Akyürek

September 2014, 133 pages

This study investigates the impacts of climate change on water resources through precipitation and discharge analyses in Omerli catchment Istanbul, Turkey. Precipitation and temperature data are obtained from GCM (Global Circulation Model)/RCM (Regional Climate Model) combinations based on A1B carbon scenario via European Union (EU)-ENSEMBLES project. The data is obtained at 25 km resolution on daily time scale for reference period between 1960 and 1990 and future period between 2071 and 2100. The HBV (Hydrologiska Byråns Vattenbalansavdel-ning) model is used to investigate discharge properties of study area. First the HBV is calibrated by some of catchment properties along with PEST (parameter estimation) method. Because RCM scale is comparatively coarse (25 km) for catchment scale its results are downscaled to 1 km using the Geographically Weighted Regression (GWR) method. RCM precipitation with and without GWR method are evaluated for characteristics of extreme precipitation events and they are used in the HBV model for estimating the extreme discharges along with reference and future periods. All RCMs strongly underestimate precipitation. GWR improves underestimation tendency of RCMs precipitation especially for extreme events. Depending on precipitation input from RCMs with and without GWR the HBV also shows significant underestimation in daily and extreme runoff but it provides better estimates with GWR input. The magnitude of extreme events increases in winter, spring, and summer but decreases in fall from reference to future period. Return periods of the extreme events increase in the future period and therefore, Omerli Basin is under water stress with changing climate.

Keywords: Climate change, precipitation, streamflow, GCM/RCM, downscaling, extreme events.

ÖZ

İKLİM DEĞİŞİKLİKLERİNİN ÖMERLİ HAVZASI'NIN SU KAYNAKLARI ÜZERİNDEKİ ETKİLERİ

Kara, Fatih

Doktora, Jeodezi ve Coğrafi Bilgi Teknolojileri Bölümü

Tez Yöneticisi: Doç. Dr. İsmail Yücel

Ortak Tez Yöneticisi: Prof. Dr. S. Zuhul Akyürek

Eylül 2014, 133 sayfa

Bu çalışmada iklim değişikliklerinin su kaynakları üzerindeki etkileri yağış ve akım analizleri vasıtasıyla Ömerli Havzası-İstanbul, Türkiye’de araştırılmıştır. Çalışmada kullanılan sıcaklık ve yağış verileri Avrupa Birliği’nin ENSEMBLES projesi kapsamında A1B senaryosu ile üretilmiş küresel iklim modelleri (GCM) ile bölgesel iklim modellerinin (RCM) kombinasyonundan elde edilmiş verilerdir. 25 km mekansal çözünürlüğe sahip günlük veriler referans (1961-1990) ve gelecek (2071-2100) dönemler için elde edilmiştir. HBV model çalışma alanının akım özelliklerinin incelenmesi amacıyla kullanılmıştır. Öncelikle HBV hidrolojik modeli havzaya ait bazı özellikler ve PEST parametre tahmini yöntemi ile kalibre edilmiştir. Bölgesel iklim modellerinin çözünürlüğü düşük (25 km) olduğundan ve küçük havzalarda yeterince hassas olmadıklarından dolayı coğrafi ağırlıklı regresyon yöntemi (GWR) ile veriler 1 km çözünürlüğe indirgenmiştir. GWR uygulanmış ve uygulanmamış veriler yardımıyla ekstrem yağışlar incelenmiş ve bu veriler hidrolojik model içinde referans ve gelecek dönem akım tahmininde kullanılmıştır. Bütün bölgesel iklim modelleri yağışı gözlem değerlerine göre daha düşük tahmin etmektedir. GWR bu düşük tahmin eğilimini özellikle ekstrem olaylar için azaltmaktadır. GWR uygulanmış ve uygulanmamış verilerdeki bu düşük tahminden dolayı HBV model de günlük ve ekstrem yağışların simulasyonunda azımsama yapmış, bununla birlikte coğrafi ağırlıklı regresyon verileri daha iyi sonuçlar üretmiştir. Ekstrem olayların şiddeti hem referans hem de gelecek periyotları için kış, ilkbahar ve yaz mevsimlerinde artmış, sonbaharda azalmıştır. Gelecek periyodunda ekstrem olayların tekrar süresi arttığından dolayı Ömerli Havzası’nda iklim değişikliklerinden dolayı su sıkıntısı yaşanabilecektir.

Anahtar Kelimeler: İklim değişiklikleri, yağış, akım, küresel iklim modeli/bölgesel iklim modeli, ölçek küçültme, ekstrem olaylar.

To My Daughter

Nesibe

ACKNOWLEDGEMENTS

I would like to dedicate my special thanks to my supervisor, Assoc. Prof. Dr. İsmail Yücel for his patient and outstanding guidance thorough this research. I also thank to my co-supervisor Prof. Dr. S. Zuhale Akyürek for her valuable contributions. I specially thank to Dr. Deborah Lawrence for her contributions in model calibration stage. Thanks are also due to all the academic staff of Geodetic and Geographic Information Technologies (GGIT) department. I cordially thank my friends, colleagues, and Research Assistants at GGIT; Abdurrahman Belek İsmail and Ertuğrul Boza. This study was supported by TÜBİTAK with project number 110Y036 and COST Action ES0901“European Procedures for Flood Frequency Estimation (FloodFreq)” (<http://www.cost-floodfreq.eu/>).

TABLE OF CONTENTS

ABSTRACT	v
ÖZ	vi
ACKNOWLEDGEMENTS	viii
TABLE OF CONTENTS	ix
LIST OF TABLES	xi
LIST OF FIGURES	xii
ABBREVIATIONS	xv
CHAPTERS	1
1. INTRODUCTION	1
1.1 Background and Motivation	1
1.1.1 Changes in climate system	3
1.1.2 Impacts of climate change on the water cycle	4
1.1.3 Projected changes on the water cycle	7
1.1.4 Water availability and water demand in the future	9
1.2 Problem Definition	11
1.3 Historical Overview	12
1.4 Goals and Objectives	21
1.5 Thesis Summary	22
2. STUDY AREA AND METHODOLOGY	23
2.1 Introduction	23
2.2 Study Area and Data	25
2.2.1 Morphology of Omerli Basin	26
2.2.2 Observational data preparation	31
2.3 GCM/RCM Combination	34
2.4 Spatial Interpolation	37
2.5 Hydrological Model	40
3. DOWNSCALING RCM DATA WITH GWR	45
3.1 GWR Setting with Station Data	45
3.2 Determining Explanatory Variables for Grids	47
3.3 Downscaling of Monthly Precipitation and Temperature Data	55

4. THE HBV SETUP AND CALIBRATION	57
4.1 Introduction	57
4.2 Sub-catchment Properties	59
4.3 Calibration procedure	62
5. PRECIPITATION ANALYSIS	71
5.1 General Precipitation Evaluation for RCMs and GWR	71
5.2 Extreme Precipitation Index Calculation	75
5.2.1 Extreme precipitation evaluation for RCMs and GWR	76
5.2.2 Changes in extreme precipitation	78
5.3 Frequency Analysis	81
6. DISCHARGE ANALYSIS	85
6.1 Model Performance Evaluation	85
6.2 Extreme Flow Index Calculation	89
6.2.1 Extreme flow evaluation	90
6.2.2 Changes in extreme flow	92
6.2.3 Changes in extreme flow volume	93
6.3 Frequency Analysis	95
7. SUMMARY, CONCLUSIONS, AND RECOMMENDATIONS.....	99
4.1 Summary	99
4.2 Conclusions	101
4.3 Recommendations	103
REFERENCES.....	105
APPENDICES.....	123
APPENDIX A: PARAMETER FILE OF SUB-CATCHMENT 02-67	123
APPENDIX B: A SAMPLE INPUT FILE FOR THE HBV MODEL	127
APPENDIX C: A SAMPLE RESULT FILE OF THE HBV MODEL	129
CURRICULUM VITAE	131

LIST OF TABLES

TABLES

Table 2.1 Meteorology Stations around Omerli Basin	32
Table 2.2 GCM/RCM Matrix of ENSEMBLES with 25 km Resolution	36
Table 3.1 Explanatory Variables Used in GWR Calibration.	46
Table 3.2 Surface Roughness Values of Land Cover Types.....	54
Table 3.3 Explanatory Variable Values of 16 Grids around Omerli Basin	55
Table 4.1 Elevation Zones, Primary, and Secondary Land Cover Types of Sub-catchments.....	62
Table 4.2 The HBV Parameter Ranges for Optimization	63

LIST OF FIGURES

FIGURES

Figure 2.1 Flow Chart of the Study.....	24
Figure 2.2 Study Area-Omerli Basin.....	25
Figure 2.3 Digital Elevation Model of Omerli Basin.....	27
Figure 2.4 Hypsometric Curves of Sub-catchment Areas.....	28
Figure 2.5 Slope Map of Omerli Basin	29
Figure 2.6 Aspect Map of Omerli Basin	30
Figure 2.7 Land Use/Land Cover (LU/LC) Map of Omerli Basin.	31
Figure 2.8 Thiessen Polygons in Omerli Basin.....	33
Figure 2.9 Streamflow Components in the Sub-catchments of Omerli Basin	34
Figure 2.10 CO ₂ Emissions of Families (Storylines).....	36
Figure 2.11 The Coverage Area of ENSEMBLES Project	37
Figure 2.12 The HBV Model Structure	42
Figure 3.1 RMSE and Bias Ratio Values between Observations and Simulations ...	47
Figure 3.2 Study area and RCM grids around it	48
Figure 3.3 Automatic Calculation of Mean and Median for Altitude, Slope, and Aspect Values of Grids	49
Figure 3.4 DEM Map of RCM Grids	50
Figure 3.5 Slope Map of RCM Grids.....	51
Figure 3.6 Aspect Map of RCM Grids	52
Figure 3.7 LU/LC Types of RCM Grids	53
Figure 3.8 Grid Centers and Prediction Points.....	56
Figure 4.1 The HBV Model Structure: Storage Zones and Main Fluxes	58
Figure 4.2 LU/LC Types of Sub-catchments of Omerli Basin.	60
Figure 4.3 Equal Area Elevation Zones of Sub-catchment 02-55 (A-Upper Image) and Sub-catchment 02-67 (B-Lower Image).....	61
Figure 4.4 Daily Precipitation and Discharge Values of Sub-catchment 02-55 (A-Upper Image) and sub-catchment 02-67 (B-Lower Image).....	65
Figure 4.5 Scatterplots Created by Param1.dat (a, b) and Param2.dat (c,d) Files.	66
Figure 4.6 The HBV Calibration Results by Param1.dat file for Sub-catchment 02-67	67

Figure 4.7 The HBV Calibration Results by Param2.dat file for Sub-Catchment 02-67	68
Figure 4.8 Simulated Versus Observed Cumulative Volumes	69
Figure 4.9 Simulated Versus Observed Empirical Peak Flow Distribution	69
Figure 5.1 Comparison Of Observed (Bold-Blue Line) and Modelled Precipitation Values for Sub-Catchment 02-67 between 1961 and 1990.....	72
Figure 5.2 Comparison Of Observed (Bold-Blue Line) and Modelled Precipitation Values for Sub-Catchment 02-67 between 2071 and 2100. Observed values belong to years between 1961 and 1990	72
Figure 5.3 Comparison of Observed Precipitations and RCM Mean Precipitations.	73
Figure 5.4 Comparison of RCMs Averages and Observation Values for Reference Period. Standard Deviation Values are Also Imposed to the Figures	74
Figure 5.5 Comparison of Observed and Modeled Precipitation Values in Scatterplots for Reference Period.....	75
Figure 5.6 Performance test of 5 RCMs in Index Value Calculation for 1 Year and 5 Year Analysis Time. Each Boxes are Representing Different Search Window Such as Red Box (1.) 1 Day, Yellow Box (2.) 2 Days, Green Box (3.) 5 Days, Blue Box (4.) 10 Days, And Purple Box (5.) 30 Days	77
Figure 5.7 Performance Test of 5 GWRs in Index Value Calculation for 1 Year and 5 Year Analysis Time	78
Figure 5.8 Index Values of Extreme Precipitations of Daily RCMs for 1 Year and 5 Year Time Periods. Each Boxes are Representing Different Search Window Such as Red Box (1.) 1 Day, Yellow Box (2.) 2 Days, Green Box (3.) 5 Days, Blue Box (4.) 10 Days, And Purple Box (5.) 30 Days.....	79
Figure 5.9 Index Values of Extreme Precipitations of Daily GWRs for 1 and 5 Year Time Analysis Time. Each Boxes are Representing Different Search Window Such as Red Box (1.) 1 Day, Yellow Box (2.) 2 Days, Green Box (3.) 5 Days, Blue Box (4.) 10 Days, And Purple Box (5.) 30 Days.....	80
Figure 5.10 Probability of Extreme Precipitations of Observation and Modeled Daily RCMs for Reference and Future Period	82
Figure 5.11 Probability of Extreme Precipitations of Observation and Modeled Monthly RCMs for Reference and Future Period	83
Figure 5.12 Probability of Extreme Precipitations of Observation and Modeled Monthly GWRs for Reference and Future Period	83
Figure 6.1 Comparison of RCMs and GWRs with Observed Discharge Values for Reference (1961-1990) Period	86

Figure 6.2 Comparison of RCMs and GWRs with Observed Discharge Values for Future (2071-2100) Period. As a Reference Observed Daily Discharges from Reference Period are also Shown	87
Figure 6.3 Comparison of Precipitation and Discharge Values of Observation, Mean RCMs, and Mean GWR Simulations	88
Figure 6.4 Scatterplots of RCM via Observed Discharges and GWR via Observed Discharges	89
Figure 6.5 Performance Test of 5 RCMs and 5 GWRs in Index Value Calculation .	91
Figure 6.6 Index Values of 5 RCMs and 5 GWRs	93
Figure 6.7 Index Values of flow volume for 5 RCMs and 5 GWRs	95
Figure 6.8 Frequency Analysis of Extreme Discharge Events of 5 RCMs That are Used in GWR Method.....	96
Figure 6.9 Frequency Analysis of Extreme Discharge Events of 5 GWRs	97

ABREVIATIONS

AIC	Akaike Information Criteria
ASTER	Advanced Spaceborne Thermal Emission and Reflection
CACC	Canada's Action on Climate Change
DEM	Digital Elevation Model
DSI	State Hydraulic Works of Turkey
EC	European Commission
ESRI	Environmental Systems Research Institute
EU	European Union
EU-CC	European Union Climate Action
GAWR	Geographically and Altitudinal Weighted Regression
GCM	Global Circulation Model
GDEM	Global Digital Elevation Model
GIDS	Gradient Plus Inverse-Distance-Squared
GIS	Geographic Information Systems
GML	Gauss-Marquardt-Levenberg
GWR	Geographically Weighted Regression
HBV	Hydrologiska Byråns Vattenbalansavdelning
IDW	Inverse Distance Weighting
IMM	Istanbul Metropolitan Municipality
IPCC	International Government on Climate Change
IWSA	Istanbul Water and Sewerage Administration
LTS	Local Trend Surfaces
LU/LC	Land Use Land Cover
NAO	North Atlantic Oscillation
OLS	Ordinary Least Squares
PEST	Parameter Estimation
RBF	Radial Basis Functions
RCM	Regional Climate Model
RMSE	Root Mean Squared Error
SD	Standard Deviation
SMHI	Swedish Meteorological and Hydrological Institute
SRES	Special Report on Emissions Scenarios
TSA	Trend Surface Analysis
USGS	United States Geological Survey
VI	Vegetation Index

CHAPTER 1

INTRODUCTION

1.1 Background and Motivation

Weather is defined as the conditions of temperature, pressure, humidity, wind, and other meteorological elements (cloudiness, precipitation, storms, etc.) in a certain time and at a particular place. Climate is defined as the average of weather conditions; more specifically, climate is the statistical average of weather conditions and changes in weather conditions during a certain time period. Climate not only defines the average values but, through analyzing frequency and trends, other climatological events, such as drought and floods.

Solar radiation is the main determinative effect of the world's climates. It can be claimed that the average temperature of the earth has remained the same for centuries because of the balance between incoming and outgoing solar radiation. While incoming solar radiation has remained the same, the amount of outgoing radiation (long wave radiation) has become less owing to increased concentrations of aerosols, clouds, and greenhouse gases in the atmosphere (IPCC, 2013; NASA, 2014; EPA, 2014) this issue is the main driver of climate change. Climate change is defined as the long-term changes in weather conditions including temperature, precipitation, and other indicators; it may be observed in both average conditions and during variable periods, such as during extreme events (CACCC, 2013).

Human activity is altering the energy and water budgets of the world by modifying land use/land cover (LU/LC) classes, which cause an imbalance between latent heat flux and sensible heat flux (Salvati et al. 2013). For example, intentional forest fires

and cutting trees for expanding agricultural areas are changing the amount of carbon in plants, carbon dioxide (CO₂) emissions, outgoing radiation (surface albedo), evaporation, and the amount of long wave radiation released from the earth's surface (IPCC, 2013).

Human activity has changed the land cover of the earth and because of this, the emission of some important gases, aerosols, and the concentration of gasses in the atmosphere is changing (EPA, 2014). These events in the atmosphere change the energy budget of the earth. Several studies have demonstrated multiple impacts of climate change that are the result of human activity. The most important effects of climate change occur in the atmosphere, on land surfaces, in oceans, and on land glaciers. According to *in situ* observations and glacier explorations, there has been an increase in the quantities of greenhouse gases, such as CO₂, methane (CH₄), and nitrous oxide (N₂O), in the atmosphere during recent centuries (IPCC, 2013; Lu and Cheng, 2009; Williams et al. 2012). Furthermore, instrumental observations have revealed an increase in temperatures on land and ocean surfaces that started more than one hundred years ago. Instrumental observations have demonstrated temperature increases on ocean surfaces, and satellite images and *in situ* observations have indicated that there has been a mass shrinkage in polar glaciers (UK Met Office, 2014), land glaciers (Stoffel et al. 2014), and icebergs that has occurred since the 1950s.

It is expected that climate change will have both global and local effects on the earth's surface. One of these effects will be decreasing quantities of fresh water and, consequently, increasing water need (Kusangaya et al. 2014; Lespinas et al. 2014). Management of water resources has already become a very important issue. The Intergovernmental Panel on Climate Change (IPCC) was established in 1988 under the World Meteorological Organization and the United Nations Environment Program for the purpose of understanding nature and the effects of climate change, and to determine mitigation and adaptation strategies to climate change. Thereafter, assessments were performed in order to further understand the relationships between greenhouse gases

and global warming, and research began to focus on the impact of emissions on climate (Beare and Heaney, 2002).

1.1.1 Changes in climate system

Observations on climate systems can be made using both in situ physical and biochemical observations, and through remote sensing satellites or ground stations. Climate change is known to have many effects and the known effects of climate change include, increases in surface temperatures, changes in the humidity of the atmosphere, changes in the amount of precipitation, changes in the frequency and intensity of extreme events, shrinkages of land and ocean glaciers, and sea level changes. The IPCC performs extensive research into the impacts of climate change and according to their report, released in 2013, the impact of climate change can be summarized as:

- Instrumental observations identified that global surface temperature increased since the 19th century. Each 30-year time scale is warmer than the previous one and the decade after 2000 is the warmest decade of the last two centuries. If land and ocean temperatures are considered together, there is a linear increasing trend in temperatures and the level of the increase is 0.85°C between 1880 and 2012 (UK Met Office, 2014). Land surface temperatures increased alongside ocean surface temperatures. Temperature increases were determined in the upper 700 m parts of oceans after 1870.
- The frequency of westerly winds and the North Atlantic Oscillation (NAO) are increased at the mid-latitudes of the northern hemisphere after the 1950s (Visbeck et al. 2001; Prasad et al. 2009).
- Changes in patterns of precipitation have been observed since 1951. There has been an increase in the amount of precipitation in the mid-latitudes of the northern hemisphere but no increase or decrease in precipitation has been observed in the other parts of the world. Humidity has been found to be

increasing since the 1970s (Givati and Rosenfeld, 2013; Willems and Vrac 2013; Trambly et al. 2012).

- Ocean salinity increased in at mid-latitudes, where evaporation is a dominant factor and salinity decreased in the tropics because of high amounts of precipitation (Omstedt and Hansson, 2006). Furthermore, ocean salinity decreased in the Polar Regions owing to increased amounts of water flow to the oceans (Bijma et al. 2013).
- It has been observed that permanent and annual glaciers have decreased in arctic regions since 1979. Moreover, the thickness of glaciers decreased between 1980 and 2008. There has been a decrease in the length, width, thickness, and mass of glaciers on a global scale. The regions where glaciers lost the most mass are Greenland, Alaska, and arctic Canada (Dowdeswell et al. 1997; Aniya, 1999). Snowfall decreased and snow cover narrowed where winter temperatures increased (Karl et al. 1993).
- Global sea level has risen 0.19 m between 1901 and 2010 (Toan, 2014; Anderson et al. 2014; Mori et al. 2013).
- An increase has been observed in the frequency and intensity of extreme weather events in the atmosphere (Mirza, 2003). There has been a global increase in the number of hot days and cold days between 1951 and 2010. Increases have been observed in the number of heat waves, instances of intense precipitation, droughts, storms, and flood frequency and intensity since the beginning of the 20th century (Linnenluecke et al. 2011).

1.1.2 Impacts of climate change on the water cycle

Temperature increases, rising sea levels, and changes in the amount and frequency of local precipitation are the main reasons climate change impacts fresh water resources.

The cryosphere is one of the largest water bodies on earth. The main objects of the cryosphere are ice caps, mobile land glaciers, continental glaciers, seasonal snow covers, permafrost, and glaciers on water bodies (lake and sea ices). The impact of climate change on the cryosphere has been studied in many works. In particular, the impact of warming on surface runoff has been examined in many studies (Haeberli and Burn, 2002), because surface runoff increases because of glacial melting discharges (Boon et al. 2003; Juen et al. 2007).

The main impacts of climate change on water bodies are changes in the surface runoff (Hao et al. 2008; Li et al. 2013; Shi et al. 2013), increases in stream flows from melted ice caps (Hoelze et al. 2007), glacier melting (Brunnabend et al. 2012), increased extreme precipitation (Kay et al. 2011), decreased surface runoff in summer (Bavay et al. 2013), decreased ground water reservoir (Okkonen and Klove, 2010), and increased carbon and nutrients in water (Statham, 2012; Tibby and Tiller, 2007).

According to instrumental observations, the last two decades have been the worst years in terms of instances of drought and extreme precipitation-flood events along with 1950s (Arndt et al. 2010) and there are absolute trends in extreme precipitation events. The frequency and intensity of local precipitation have changed owing to global warming or changes in atmospheric circulation in the 20th century (Zhang et al. 2007). There are serious changes in snowfall events and the number of snowy days, and snow melts start earlier than before in the northern hemisphere (Takala et al. 2009). Since the 1960s, evaporation has increased and alterations have been observed in soil humidity (Wang et al. 2011). Another important impact of climate change on water resources is extended drought periods (Fischer et al. 2013). Permafrosts are narrowed and their thickness is decreased owing to temperature increases in arctic regions (Rabassa, 2009). Glaciers and ice caps are decreasing all around the world (Gardner et al. 2013).

Surface runoff is altering owing to variations in temperature and precipitation since 1950 (IPCC, 2014). Stream flows decreased in southern and eastern parts of Europe

but increased in all other areas (Stahl et al., 2010), especially in northern Europe (Wilson et al., 2010). Dai et al. (2009) studied simulations of stream flows for 200 rivers from around the world between 1984 and 2004 and determined a decreasing trend in 45 rivers and an increasing trend in 19 rivers. Decreasing trends in stream flows are observed, especially in low and mid latitudes and these trends are common in western Africa, southern Europe, southern and eastern Asia, eastern Australia, and northern parts of South America (Dai, 2013). Since the 1970s, spring peaks in stream flows arrive earlier where snowfall is altered to precipitation and snow melts before the expected time because of increased winter temperatures (Clow, 2010; Korhonen and Kuusisto, 2010; Tan et al. 2011; Akyürek et al. 2011).

There are fewer studies examining the impacts of climate change on ground water in comparison with surface water runoff. Jeelani (2008) determined a decreasing trend in runoffs from rivers that are fed by ground water in Kashmir-India since 1980. Model-based studies have indicated that, in Spain, the reason for decreasing trends in ground water are not only related to decreased precipitation but also increased evaporation (Aguilera and Murillo, 2009). Increased water temperatures have altered the amount of organic compounds, salt, and heavy metals in water resources (Paerl and Huisman, 2008; Pednekar et al. 2005), thus water quality is decreasing.

Extreme rainfall events have increased since the 1950s (Seneviratne et al. 2012), consequently, erosion effects of precipitation, the extent of soil erosion, and the amount of sediment accumulation by rivers has increased. Soil moisture has decreased and forest fires have increased because of decreasing precipitation in different places of the world (Bussi et al. 2013). Soil erosion has decreased in the Yellow River Basin (Miao et al. 2011) and the Yangtze River Basin (Dai et al. 2008) because of decreased precipitation.

Flood frequency and magnitude has increased on a global scale because of the anthropogenic factors of climate change (Kundzewicz et al. 2013). Trends in extreme precipitations and stream flows indicate that flood risk has increased all around the

world (IPCC, 2014). Property damage by floods has increased since 1970 (Handmer et al. 2012). Maximum surface runoff has increased on a local scale in northwestern Europe (Hatterman et al. 2012; Petrow and Merz, 2009). However, flood frequency and magnitude has decreased in southern France (Giuntoli et al. 2012), southern Australia (Ishak et al. 2010), and Canada.

1.1.3 Projected changes on the water cycle

Climate projections for the future are accomplished using physical-based climate models. According to these global and regional climate models, evaporation will increase because of warmer climate conditions in the future (IPCC, 2014). Long-term projections of evaporation do not show certain results because evaporation is affected not only by air temperatures, but also by soil moisture, CO₂ concentrations, and plant cover changes (Katul and Novick, 2009). It is expected that evaporation will increase in southern Europe, Central America, southern Africa, and Siberia (Seneviratne et al. 2010). The number of hot days (Hirschi et al. 2011) and heat waves will increase along with evaporation.

It is anticipated that fresh water shortages will increase all around the world due to higher demands by growing populations (Vineis et al. 2011) and increased evaporation (Chattopadhyay and Hulme 1997). Therefore, direct and indirect water needs of populations will increase. Agricultural areas are one of the biggest consumers of both surface water and ground water. If precipitation decreases, soil moisture will decrease and the water needs of soils will increase.

Fresh water resources and permafrosts are decreasing in arctic regions and these events will remain the same until the mid-21st century (IPCC, 2014). All glacier simulations indicate a melting trend in glaciers and ice caps during the 21st century. In the future, it is expected that rivers will reach their peak in spring instead of summer owing to vanishing glaciers and ice caps (Huss, 2011). It is estimated that if glacier melt continues, glacier-covered areas will narrow and this will increase surface runoff and

stream flows. Rivers will peak in China between 2010 and 2050 (Xie et al. 2006) and Scandinavia after 2050s (Johannesson et al. 2012) because of this glacier melting events.

Climate simulations indicate that average annual precipitation will increase in high latitudes and the humid tropics, but it will decrease in the dry tropics. There are constant uncertainties the amount of precipitation in China, south Asia, and large parts of South America (IPCC, 2014). There are several examples of the effects of snowfalls and snow melts on stream flows. On a global scale, it is anticipated that rivers will peak earlier than before owing to earlier snow melt (Adam et al. 2009).

Despite increased snow melt, it is expected that the amount and level of ground water will decrease in the future (Taylor R. et al. 2013). Generally, ground water levels and the number of fountains, which are fed by ground water, will increase where surface runoff is increased (IPCC, 2014). Ground water level is expected to decrease despite the amount of rainfall remaining the same where the amount of snowfall decrease in North America (Earman et al. 2006). Increases in sea level rise result in ground water being invaded by salty water, and this will make ground waters salty and decrease fresh water resources (Werner et al. 2012). Deltas will be affected from rising sea levels and fresh water resources in deltas will become salty (Masterson and Garabedian, 2007).

The frequency and intensity of heavy precipitations and soil erosion will increase (Seneviratne et al. 2012) while total precipitation decreases. Soil erosion is expected to increase in dry and semi-dry areas where only one rainfall accounts for more than 80% of total annual rainfall (Bussi et al. 2013). Climate change will affect the amount of sediment carried in rivers by affecting discharge and land cover. Thodsen et al. (2008) suggested that and 11–14% increased discharge will increase sediment load 9–16%. Soil erosion and suspended sediments in rivers will increase in cold regions owing to increased precipitation, glacier melting, permafrost melting, and transformation of snowfalls to rainfalls (Lu et al. 2010). Soil erosions and landslides

are expected to increase in the tropics too, owing to increased heavy rainfalls (Knutson et al. 2010).

Flood events will increase across almost half of the world's surface according to united global hydrology and land cover models, but this increase will occur on a regional scale rather than a global scale (Dankers et al. 2013; Hirabayashi et al. 2013). The impact of floods will increase in south East Asia, north east Europe, tropical Africa, and South America, but will decrease in central Asia, Eastern Europe, central North America, and Anatolia (Seneviratne et al. 2012). Many studies have suggested decreased discharge in rivers in the future. Taylor I. et al. (2013) compared meteorological and agricultural drought with hydrological drought in an ensemble-based study and suggested that drought events will increase 18–30% in the future. The study also suggested that the impact of floods and droughts would increase because of an increase in flood frequency, despite the fact that the hazard remains the same (Kundzewicz et al. 2013).

1.1.4 Water availability and water demand in the future

80% of the world's population is already affected by water security due to increased water demands, decreased availability, and pollution factors (Vörösmarty et al. 2010). Climate change may affect water security by affecting the availability of water. Studies have demonstrated that fresh water resources will decrease, especially in Mediterranean environments (Ludwig et al. 2011) and southern Africa, and that variations in water availability will increase in southern and eastern Asia (IPCC, 2014). However, increased surface runoff will prevent increases in agricultural water demand in some parts of the world. Schewe et al. (2013) suggested that if temperatures increase 1°C, 8% of the global population would experience severe water scarcity. If the amount increases 2°C, 14% of the global population will be affected. Due to climate change, rainfall variations will increase and these variations will alter some climate-related events such increased stream flows and decreased surface runoff through decreased snow and ice deposits. Similarly, climate simulations predict a decreasing

trend in ground water resources as well. Some simulations suggest a linear decreasing trend in ground water owing to global temperature increases (Portman et al. 2013).

Climate change will alter temperature, precipitation, and radiation time, and these alterations will affect the water needs of vegetation, which are fed by precipitation or irrigation. It is likely to increase the amount of irrigation in 40% of Europe, USA, and some parts of Asia. Wada et al. (2013) used seven different global hydrological models in their study and suggested that water demands will increase in agricultural areas, making up 7–21% of the World by the 2080s. However, some researchers suggest water demands in agricultural areas will change by only very small amounts in the future (Zhang and Cai, 2013). Rivers that are fed by rainfall are more sensitive to the impacts of climate change. Types of agricultural products will be altered with changing quantities of precipitation in the future. The negative impacts of climate change on agricultural areas may be decreased by widening irrigated agricultural areas and increasing irrigation (McDonald and Girvets, 2013).

Some important aspects of climate change are temperature increase, decreased snow and ice cover, and temperature and evaporation increases in lakes and rivers, and these changes will decrease the amount of fresh water available where they occur (EPA, 2014; CACC, 2014; EU-CC, 2014). Consequently, water demands will increase and central and local governments will need to secure fresh water resources (Beck and Bernauer, 2011). The need for human-developed water depots will increase owing to decreased stream flows, and severe and intense droughts. Increased water temperatures will increase organic material compounds in water and different purification and cleaning processes will be required. Drier climate conditions will increase pollutant intensity in water. This issue is a more important problem where ground water resources are already polluted. Flood-affected surface runoff will increase and, owing to this, the amount of pathogens, nutrients, and suspending sediments in waters will increase. Increases in sea level will affect both surface and ground water negatively and, in particular, areas where the ground water level is low will be negatively affected more significantly (IPCC, 2014).

1.2 Problem Definition

Water is one of the main requirements for human life and the distribution of fresh water resources is being affected by the climatic conditions of the earth. Scientific studies have demonstrated that the climate of the earth has changed since the beginning of 20th century owing to anthropogenic factors. Consequently, the frequency and magnitude of extreme weather events such as floods and droughts, have increased across almost the whole world. As a result, it is important to determine possible changes in climates and their effects on the environment in order to take necessary precautions. It is expected that climate change will affect water resources in a positive way in some parts of the world like the Arabian Peninsula and the Polar Regions, but most of the world's water resources, including Turkey's, are going to be negatively affected. Particularly, in Turkey, Istanbul shows a sharp increase in population (14,160,467 (IMM, 2014) and therefore, together with consequences coming from climate change and global warming water scarcity is already becoming a serious problem for residents. The city has experienced droughts in 2006 and 2008, when the lowest precipitation in the last 50 years were recorded (Baban et al. 2011). Although this study focusses on Istanbul, it may be an example for all of Turkey in determining the impact of climate change.

Climate change is expected to increase the frequency and intensity of extreme precipitation events all around the world (IPCC, 2014). Several climate change studies have been conducted to assess the impact of these changing conditions (Fowler and Ekström, 2009). These studies are usually conducted using GCM (Global Circulation Model)/RCM (Regional Climate Model) combinations and downscaling methods. Following this, high-resolution data are used in hydrological models to estimate changes in hydrological variables. GCM data are widely used in climate change studies but the spatial resolution of these data is approximately 2°-200 km. It is not possible to use these coarse resolution data in hydrologic models. RCMs provide data in 25-km spatial resolution but these data may still be too coarse for some small areas.

Consequently, further downscaling operations might be needed for local-scale studies (Fowler et al. 2007).

There are not many studies that have investigated the water resources of Istanbul in the context of climate change. In this study, precipitation and discharge properties of the biggest fresh water resource of Istanbul, Omerli Basin, are investigated by GCM/RCM combinations for the past (1961–1990) and the future (2071–2100). Geographically weighted regression (GWR) is selected as the downscaling method as it considers local geo-physical parameters that may influence precipitation distribution. From this point of view, it differs from other conventional methods such as dynamical and statistical downscaling methods used in many applications.

1.3 Historical Overview

Several studies have examined the impact of climate change on precipitation and water resources. Gobiet et al. (2014) simulated the impact of climate change according to the A1B emission scenario in the European Alps in the 21st century and investigated how temperature, precipitation, global radiation, and humidity will be affected. The authors claimed that temperatures will increase more rapidly after the 2050s, and that today's extreme weather events will be accepted as normal. The study also suggested droughts, floods, the number of hot days, and relative humidity will show severe alterations and the number of snow covered days will decrease excessively.

Chaouche et al. (2010) investigated precipitation, temperature, and evaporation in the context of climate change in the Mediterranean shorelines of France, suggesting that water resources of the region are sensitive to climate change. The investigators discovered high local trends both in observation and model simulation values, and suggested that this is related to the characteristics of Mediterranean climate properties. The study discovered increases in monthly temperatures in spring and June, decreases in precipitation in June but increases in November from 1970 to 2006.

Vrochidou et al. (2013) investigated the impact of climate change on hydro-meteorological drought on the basin scale on the island of Crete, using three different GCM temperature and precipitation data sets, along with A2 and B1 emission scenarios. In the study, discharge, soil moisture, and lower groundwater reservoir volumes were simulated using bias-corrected precipitation and temperature data along with the HBV hydrological model. The study evaluated the hydro-meteorological situation of the study area and investigated drought events.

Koutroulis et al. (2013) examined the effects of climate change on water resources by using 24 different climate scenarios, produced by 24 hydro-climatological regimes. Runoff simulations were applied by using both GCM and RCM, which were produced by varied emission scenarios such as B1, A2 and A1B, and bias correction was performed by comparing these data with observation values. The study suggested that RCMs used in A1B emission scenario have better simulation results than RCMs used in other scenarios. Furthermore, the study's authors claimed that the ECHAM model produced more accurate precipitation data than IPSL and CNRM models. Runoff was simulated until 2100 and suggested that climate change will effect fresh water resources severely.

Teutschbein and Seibert (2012) studied bias correction in RCM simulations and suggested that using RCM simulations in hydrological modeling is a challenging task because of bias risk. The reliability of several bias correction methods was tested using temperature and precipitation data from 11 different RCMs. In the study, it is claimed that all bias correction methods provide adjustments in mean values but that there are big differences between methods in standard deviation and percentile values.

Kysely et al. (2012) investigated the impact of climate change on extreme precipitation scenarios for western and central Mediterranean basins for the future (2070–2099), using high-resolution RCM data as an input from the EU-ENSEMBLES project. Precipitation was investigated across very different time periods, including hours, days, and seasons, and the results suggested that RCMs have very different

precipitation patterns in West Africa. The authors claimed annual total precipitation demonstrates a decreasing trend but that extreme rainfalls exhibit a different tendency.

The following paragraphs cover the studies of climate change impacts on water resources performed in Turkey:

Dalfes et al. (2007) studied climate change scenarios for Turkey during the last century, made future projections, and investigated changes in temperature, precipitation and stream flow. No persistent changes in precipitation patterns were found and it was hard to identify changing signals of climate change on precipitation. However, some short time trends were detected, which might be an indicator of long-term variability. A Mann-Kendall test was used to determine trends in seasonal precipitation and significant changes in winter and fall seasons were detected. It was determined that winter precipitations significantly decreased in western parts of Turkey. Conversely, fall precipitations increased in northern parts of Anatolia. It was also suggested that there is a significant decrease in stream flows in western and southwestern parts of Turkey. However, there are a few stations on the northern parts of Anatolia that reported significant increases in stream flow.

Tayanç et al. (2009) investigated temperature and precipitation patterns in Turkey during the period 1950–2004, using a Mann–Kendall test for calculating the maximum, minimum, and mean temperature, and precipitation series. A cooling period was detected from the 1960s to 1993 and 2000–2002 temperatures were the highest in the study period. The study found that precipitation variability is higher in urban areas than rural areas and that urban meteorological stations recorded more severe floods and droughts. Furthermore, spatial analyses displayed significant temperature increases in southern and southeastern parts of Turkey. Moreover, some important decreases in precipitation in the Aegean and Thrace regions were detected while some northern stations showed increases in precipitation.

Türkeş et al. (2002) investigated trends in mean, maximum, and minimum temperatures of 70 stations of Turkey between 1929 and 1999. In the study, increasing tendencies were found for annual, winter, and spring mean temperatures whereas summer and, particularly autumn, mean temperatures decreased over the northern and continental inner regions. An increasing trend was also found for maximum temperatures, except for during the fall season at many stations, with the only exceptions to this trend being central Anatolia and the Black Sea region. Minimum temperatures exhibited positive trends at different locations in different seasons of the year. Furthermore, winter and autumn minimum temperatures displayed negative trends in some parts of the Marmara, Black Sea, and Eastern Anatolia regions.

Kadioğlu (1997) investigated trends in surface air temperature over Turkey using Mann–Kendall rank statistics, analyzing mean, unfiltered, seasonal, and annual maximum and minimum temperatures. A warming trend in mean annual temperature was found from 1939 to 1989 but a cooling trend from 1955 to 1989 was found, without significance. Kadioğlu claimed spring and winter warming effects were greater in minimum temperature trends than maximums, and increasing trends in mean minimum temperatures were attributed to the urban heat island effect.

Ezber et al. (2007) studied climatic impacts of urbanization in Istanbul and used statistical and numerical modeling tools. A Mann–Kendall test was applied to minimum temperatures and the significance of trends was determined. Furthermore, a mesoscale atmospheric model was used for sensitivity experiments exploring atmospheric effects of urbanization. The results suggested that there was a significant warming over urban areas and a positive trend in minimum temperatures between urban and rural stations was detected. It was suggested that the urbanization effect is influential mostly in summer, and urban heat islands significantly expanded from 1951 to 2004. It was also claimed that the velocity of northeasterly winds and water vapor mixing ratio were decreased over the city.

Türkeş (1996) studied spatial and temporal characteristics of annual rainfall variability in Turkey and analyzed monthly rainfall data taken from 91 stations between 1930 and 1993. Long-term trends, fluctuations, and changes in runs of dry and wet years were analyzed. It was found that area-averaged annual rainfalls decreased slightly all around Turkey, particularly in the Black Sea and Mediterranean regions. There was no trend in area-averaged rainfall series according to Mann–Kendall test results and many of stations showed low-frequency fluctuations in the annual rainfall.

Kahya and Kalaycı (2004) performed an analysis of monthly stream flows from 26 basins in Turkey using non-parametric tests. The study results suggested a downward trend with 0.05 or lower level occurred in western Turkey, with no trend found in eastern Turkey.

Yıldız and Saraç (2008) investigated trends in discharges in Turkish Rivers, trends in floods, and mean and minimum discharges. There were decreasing trends found in most research stations' mean and minimum discharges rather than maximum discharges in the Marmara, Aegean, and central Anatolia regions. There was a decreasing trend found in mean and minimum discharges of rivers in western, central, and southern parts of Turkey, but increasing trends were found in the other parts of Turkey.

Türkeş et al. (2009) investigated long-term changes and trends in monthly, seasonal, and annual precipitation stations in Turkey along with spatial variation and relationships. This was performed using a Mann–Kendall correlation test and principal component analysis conducted for the period 1930–2002. It was suggested that there is an increasing trend in precipitation totals during the spring, summer, and autumn seasons, and a decreasing trend in the winter season. Mediterranean and the Mediterranean transition regions are the areas where the greatest decreasing trends were observed.

Yılmaz and Yazıcıgil (2011) reviewed the potential impact of climate change on Turkish water resources and divided studies into two major groups. Current knowledge was summarized on the impact of climate change on precipitation, temperature, stream flow, and groundwater levels for both the past and predicted future trends. It was suggested that there were many studies reporting warming trends since the 1990s and the most significant changes were observed in Mediterranean climate regions with increases in temperatures and decreases in precipitation. According to this analysis, the important observed trends were an increase in annual minimum temperatures and summer temperatures and a decrease in winter precipitation. It was reported that stream flows and groundwater levels responded to changes in atmospheric variables and exhibited a decreasing trend in many regions of Turkey. It was also suggested that existing water scarcity and water allocation problems in Turkey would worsen in the future.

Harmancıoğlu et al. (2007) modeled climate change effects in the Gediz and Büyük Menderes river basins and stated that there were tremendous decreases in stream runoffs between 1960 and 2000. Therefore, there might be water scarcity and water allocation problems already in these study areas. According to model simulations, warmer winters and hotter summers are expected to occur along with precipitation decreases in all months.

Bozkurt and Sen (2013) investigated the impact of climate change in the Euphrates–Tigris Basin using different GCMs and emission scenarios, stating that precipitation will decrease in winter in the highlands and northern regions, while it is going the decrease in the southern parts of the study area. It was also suggested that significant declines in surface runoff would occur and that all projections of surface runoff showed that the territories of Turkey and Syria within the basin are most vulnerable to climate change. In the future, stream flows will decrease significantly and dam reservoirs and hydropower plants will be significantly affected.

Fujihara et al. (2008) investigated the potential impact of climate change on water resources in the Seyhan River Basin and produced high-resolution data from GCM's for hydrologic models using dynamic downscaling. The study suggested that average annual temperature will increase by 2.0–2.7°C and that annual precipitation is going to decrease by 157–182 mm until 2070, according to different models. The authors also stated that water scarcity would not occur in the future if water demand remains the same.

Ertürk et al. (2014) evaluated the impact of climate change on groundwater resources in the Köyceğiz-Dalyan watershed and observed decreases in annual and winter precipitation, and increases in temperatures since the 1960s. A combination of hydrological modeling of climate change and land-use scenarios were used to calculate the impact of climate change on water budgets. The authors claimed that almost all water budget components showed a decrease and that this might be a problem for agriculture in the future.

Aksoy et al. (2008) performed a hydro-meteorological analysis for northwestern Turkey from a climate change perspective and analyzed precipitation, temperature, and stream flow data of the European part of Turkey. Structural characteristics were determined including randomness, jump, trend, and a best-fit probability distribution function; no significant trend was found in jump and time series of stream flow data. It was suggested that increased evapotranspiration and severe groundwater extraction are the main causes of low groundwater levels in the area. According to climate models, air temperature will increase and precipitation will decrease during the 21st century with high variability. It was also suggested that an increase in the frequency of extreme events, floods, and droughts would occur in the region.

Kum and Çelik (2014) investigated the effects of climate change in the Adana region by analyzing temperature, precipitation, and water resources. A Mann–Kendall test and Humidex index were applied to perform a trend analysis of temperature, precipitation, and humidity. A strong positive trend in average and minimum

temperature values, and both strong positive and negative trends in humidity variables were observed. It was suggested that small decreases in winter precipitation and an increase in the frequency and magnitude of heat waves would occur.

In most recent study, Yucel et al. (2014) investigated the impact of climate change on the hydrometeorology of the eastern Anatolia and specifically showed if there is any temporal shifts in snowmelt runoff because of the warming in the region. The results of the study suggested significant temperature increases during the study period (1970–2010). The authors also claimed that no significant increase in precipitation and shift in stream flow timings occurred. The study revealed declines in surface runoffs in the Aras, Euphrates, and Tigris Basins, and a slight increase in the Coruh Basin by the end of 20th century. The authors stated that the timing of peak flows would continue to shift to earlier times in response to the warming effects of climate change.

Demir et al. (2008) studied changes and tendencies in maximum, minimum, mean temperatures and precipitation series. The study suggested increasing trends were occurring in mean temperatures in southern and southwestern parts of Turkey, maximum temperatures in Mediterranean shorelines, southeastern and eastern Anatolia, and minimum temperatures in most of Turkey. The authors also claimed that significant precipitation changes might be seen in winter and that Mediterranean, Mediterranean transition, continental central Anatolia and continental Mediterranean areas are the places where winter precipitation exhibited decreasing trends. However, the study found that precipitation is increased in important parts of Turkey during the fall season. Finally, the study also suggested that changes in air circulation systems affected drought conditions and positive periods of North Atlantic Oscillations (NAO) were consistent with drought terms in Turkey.

Baban et al. (2011) studied a conceptual scheme for rainwater harvesting and grey water management for Istanbul, examining water resources in Istanbul as one of the most rapid growing cities of Europe, with a population of 13 million at the time. The study revealed that a majority of water resources for Istanbul are located in the Asian

side of the city and that domestic water use was the major type of water consumption. Consequently, development of a water management plan was a necessity owing to increasing water demands of growing population.

Dikici (2009) analyzed drought periods of Istanbul's rainfall using observed precipitation data and performed simulations for estimating future droughts. This study stated that the length of average dry terms is about 4 years for meteorology stations in Istanbul. The author claimed that there was no important difference between dry seasons of the European and Asian sides of Istanbul. However, return periods of droughts were shorter in the Asian side in comparison with the European side of Istanbul. It was also suggested that it was hard to mention long droughts owing to climate change. The author discovered that there were some wet periods just after dry periods in Istanbul. Moreover, urbanization is more intense in the European side of the city and this increases temperature values in urban areas and makes relative humidity lower.

The most comprehensive study into the impact of climate change on water resources of Istanbul and Turkey is a report prepared by a project group under management of IWSA (2010). The main aim of that project was to perform simulations of precipitation and discharges that might happen anywhere in Istanbul between 2000 and 2050. According to this study, a reduction of stream flows is already occurring and it is expected to impact on water resource management. A reduction in snowfall will decrease streamflows, especially after the 2040s. This study stated global drought risk was increased and that a 1°C increase in global temperature will move the southern dry regions of Turkey 250–300 km to the north. This report also claimed uncertainties in river discharges will increase after the 2040s. The study's authors suggested that it was possible there would be a decline in mountain glaciers, with most of the small ones disappearing.

Most of the climate studies of Turkey have investigated trends in temperature, precipitation, and discharge for past terms so far. Generally statistical changes of

precipitation or temperature in a certain time period were investigated in those studies. The number of temperature and precipitation simulation studies in Turkey for future (IWSA, 2010) is very limited. In this study precipitation and discharge conditions of Istanbul is investigated both in reference (1961-1990) and future (2071-2100) periods through using 15 GCM/RCMs data. Furthermore Geographical Information System (GIS) based interpolation method of GWR is used to investigate the effects on precipitation downscaling.

1.4 Goals and Objectives

The Omerli Basin has been selected as the study area for this work because of its importance to the water resources of Istanbul. The main goal of this study is to determine the impact of climate change on the water resources of the Omerli Basin using a number of GCM/RCM combinations together with a downscaling method based on spatially weighted regression and a hydrological model. The research objectives in reaching this main goal are presented as follows:

- Download/extract daily and monthly GCM/RCM data, prepare the observed temperature and precipitation data for the study basins, and make initial spatial assessments.
- Develop and calibrate downscaling method using geo-physical variables representing station points and RCM grids.
- Evaluate the performance of simulated precipitation and runoff.
- Determine changes in precipitation patterns including extreme events in the current and future climate conditions.
- Determine changes in runoff patterns including extreme events in the present and future climate conditions.

- Assess the impacts of downscaling RCM results on average and extreme precipitation and runoff for current and future climate conditions.
- Determine frequency behavior of extreme precipitation and runoff for current and future climate.
- How these changes will impact Istanbul's water need?

1.5 Thesis Summary

The first chapter provides an introduction, a definition of the problem, a historical overview, and the research objectives and goals. The second chapter describes the general methodology, the study area, and the data. The third chapter introduces the application of downscaling methods through GWR technique, while the fourth chapter describes the hydrological model setup and calibration processes. The fifth and sixth chapters present the analysis of the results obtained regarding precipitation and discharge, respectively. Finally, the last chapter (6) provides an overall summary and the main conclusions derived from this study.

CHAPTER 2

STUDY AREA AND METHODOLOGY

2.1 Introduction

The methodology including all of the steps utilized in the study is described and illustrated in the flow chart provided below (figure 2.1). Daily and monthly climate data were acquired from meteorology stations and the area-averaged time-series of precipitation and temperature data sets were produced for the sub-catchment areas using the Thiessen polygons method of the data collected during the reference period (1961–1990). These observed time-series climate data sets were used directly in the precipitation analysis. Additionally, daily observed climate data sets were used in the HBV model calibration and validation, although the monthly time series data were used in the GWR model calibration and validation as well.

The model values were downloaded from one of the pioneer climate projects of the European Union (EU): the ENSEMBLES program. Daily precipitation data sets were produced for 15 RCMs by using area percentages of RCM grids both from the reference (1961–1990) and future (2071–2100) periods of the study. Monthly RCM values were downloaded and monthly time series precipitation and temperature data sets were produced with and without using the GWR method for both the reference and future time periods. These data were used in the daily and monthly precipitation analyses. Furthermore, GWR-based monthly values were converted to daily values and used in the HBV model for the discharge simulations during reference and future periods. The general assessment includes performance tests for precipitation and discharge and changes in these variables from reference to future periods for different indices.

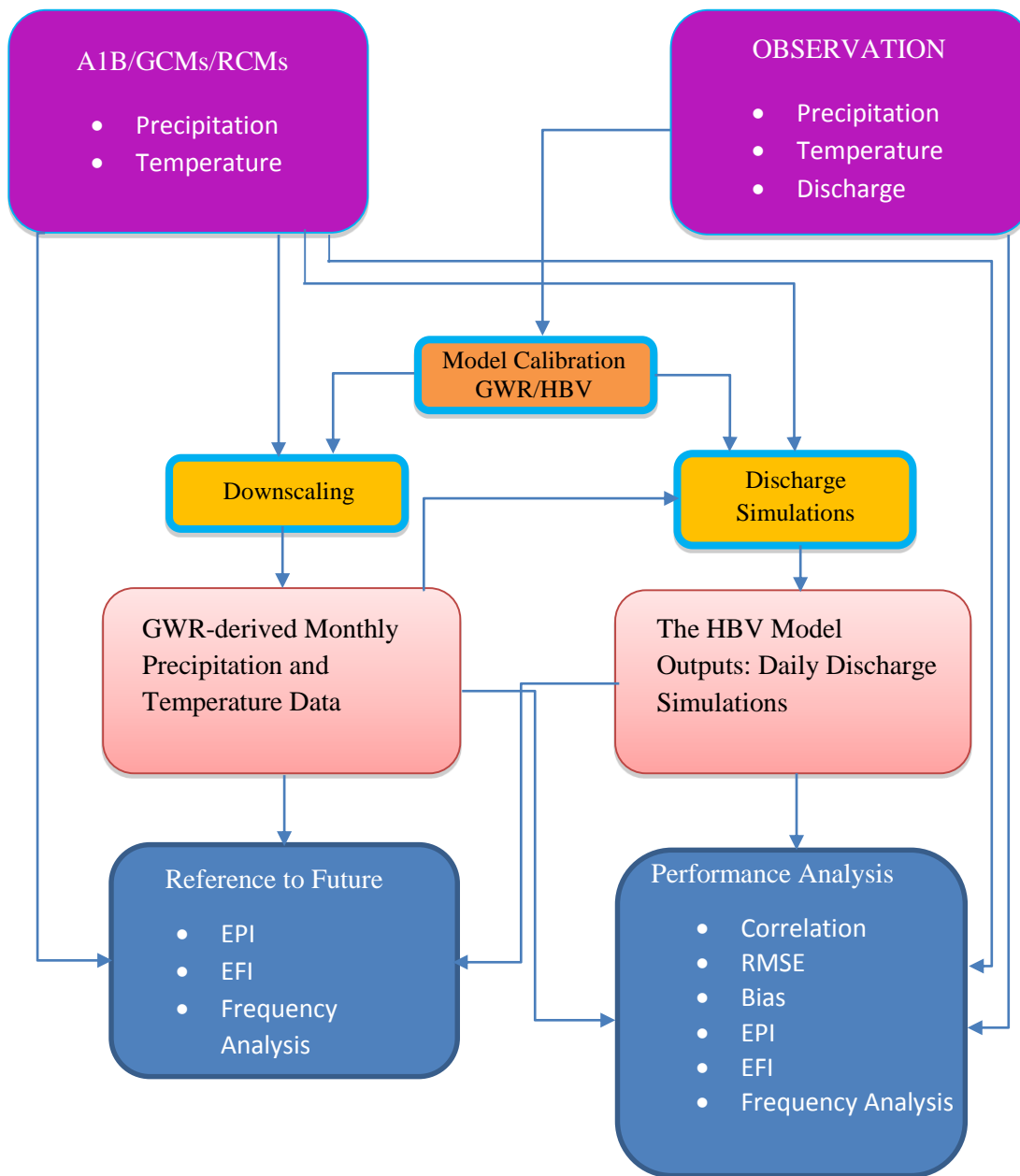


Figure 2.1 Flow chart of the study.

2.2 Study Area and Data

The Omerli Basin was selected as the study area. It is located on two north-western provinces of Turkey, Istanbul and Kocaeli, and lies between 29° 11' – 29° 40' latitudes and 40° 51' – 41° 07' longitudes. It has an area of approximately 621 km² and its length is 28 km in the N–S and 39 km in E–W directions (Figure 2.2). Distribution of meteorological stations used in the study is also shown in Figure 2.2.

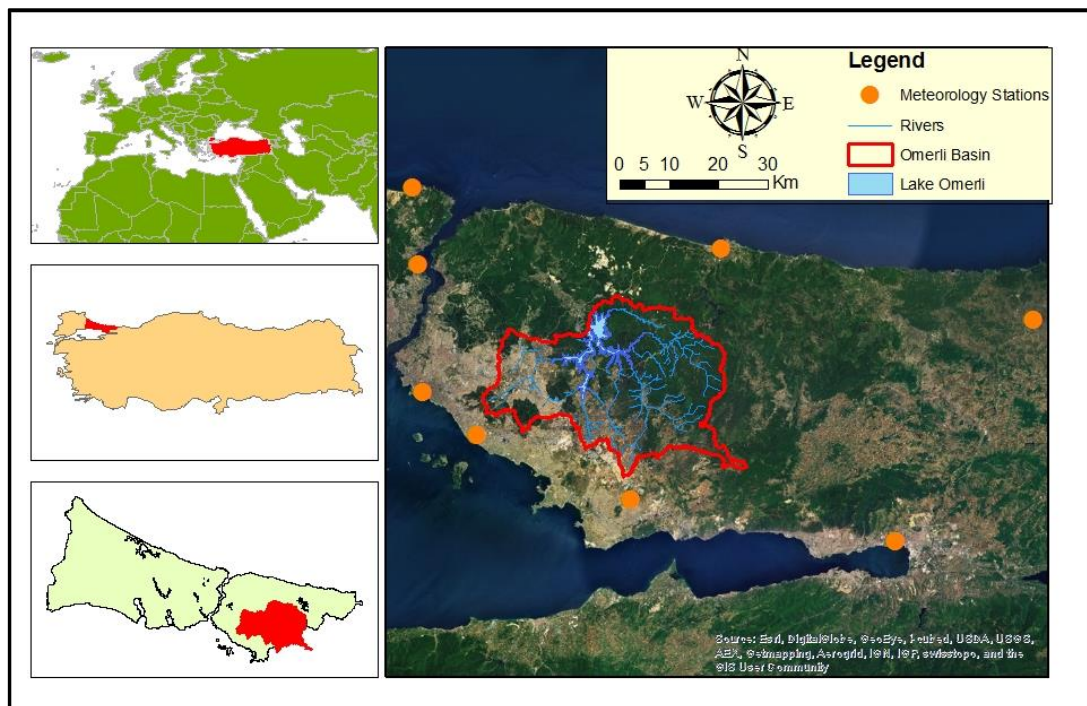


Figure 2.2 Study area-Omerli Basin.

The Omerli Dam, located within this basin, was constructed on Riva Creek in 1972 and it is the biggest dam located in Istanbul with a 220,000,000 m³/year service capacity. With an area of 21.07 km², it is the third largest water depot of Istanbul after the Terkos and Büyükçekmece Lakes, but it is the biggest fresh water resource for Istanbul, according to service capacity. The yearly service capacities of Terkos and Büyükçekmece Lakes are 142,000,000 and 100,000,000 m³/year, respectively (IWSA, 2009) and the Omerli Dam provides a volume of water equal to almost the total of these lakes. The Omerli Dam provides water to the entire Asian part of Istanbul, which

has a population of 4,997,548 (2013), along with the Darlık Dam and the Elmalı Dam (IMM, 2014). Furthermore, if necessary, it can also provide water to residents of the European part of Istanbul. The lowest and the highest usage altitudes of the dam are 46 and 62 m, respectively.

The Omerli Basin has a transitional climate, which is very common in the entire Marmara Region. This climate is impacted by the Black Sea to the north, and the Marmara Sea and Aegean Sea to the south. Consequently, the effects of both maritime and Mediterranean climates can be seen in the region. The average temperature during January is 5.83°C; this is the lowest monthly average value during a 52-year period between 1961 and 2012. February is the second coldest month of the year with an average temperature of 5.97°C. July (23.43°C) and August (23.38°C) are the warmest months in the Omerli Basin. The average annual precipitation in the Omerli Basin is 795.24 mm. December (118.19 mm) and January (97.78 mm) are known to be the wettest months, while July (27.51 mm) and June (31.54 mm) are the driest months for the study area.

2.2.1 Morphology of Omerli Basin

The Digital Elevation Model (DEM) of the Omerli Basin, produced using the Advanced Spaceborne Thermal Emission and Reflection Radiometer Global Digital Elevation Model (ASTER GDEM), with a spatial resolution of 30 m, is shown in Figure 2.3. In this figure, boundaries and outlet points of two sub-catchments are also shown. This DEM is used to acquire elevation information along and to produce the slope and aspect maps of the study area. Altitude, slope, and aspect maps are generated by using the ASTER GDEM data, along with ArcGIS 10.1 and Erdas Imagine 2011 software.

In general, the Omerli Basin has a gentle surface with small hills, mountains, and shallow valleys. The lowest area of the basin is the lake surface, with an altitude of 47 m; the highest peak is the Aydos Mountain, with an altitude of 536 m. Other high

elevations in the basin are Taşlık Hill (256 m) on the east, Ayazma Hill (242 m), Çatal Hill (392 m), and Pınar Hill (172 m) on the west, and Koru Hill (173 m), Kara Hill (254 m), and Sazak Hill (273 m) in the middle of the study area. The altitude of the basin increases from west to east, reaching higher than 300 m on the eastern side of the dam. The altitude changes from approximately 60 to 150 m on the western side of the basin. In general, flat surfaces and low sloped areas are located in the southern areas of the basin, with the hills being located on the eastern side. The direction of the valleys runs from north to south in the southern part of the basin and west to east in the northern region of the basin. Most of the area of the Omerli Basin lies between elevations of 100 and 200 m, and this elevation zone covers 52.5% (326 km²) of the study area (Figure 2.3).

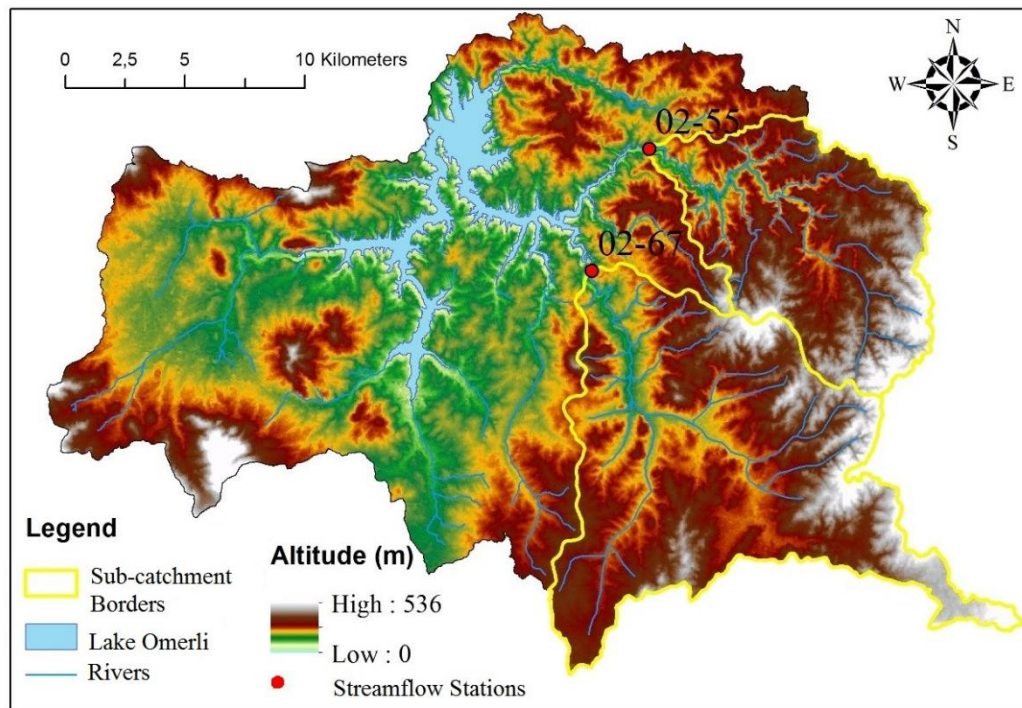


Figure 2.3 Digital elevation model of Omerli Basin.

Hypsometric (area-elevation) curves of the two sub-catchments (02-55 and 02-67) were generated using the DEM data (Figure 2.4). The curves of the neighboring sub-catchment areas are very similar to each other, meaning the elevation properties of sub-catchments are similar. The altitudes of the lowest points in the areas are 64 m for

sub-catchment 02-55 and 65 m for sub-catchment 02-67. The elevation of the highest points within the sub-catchments are 414 and 479 m for sub-catchments 02-55 and 02-67, respectively (Figure 2.4). The median elevation values of the two catchments are 250 m for 02-55 and 325 m for 02-67. The hypsometric curve is also required for the application of the hydrological model (the HBV).

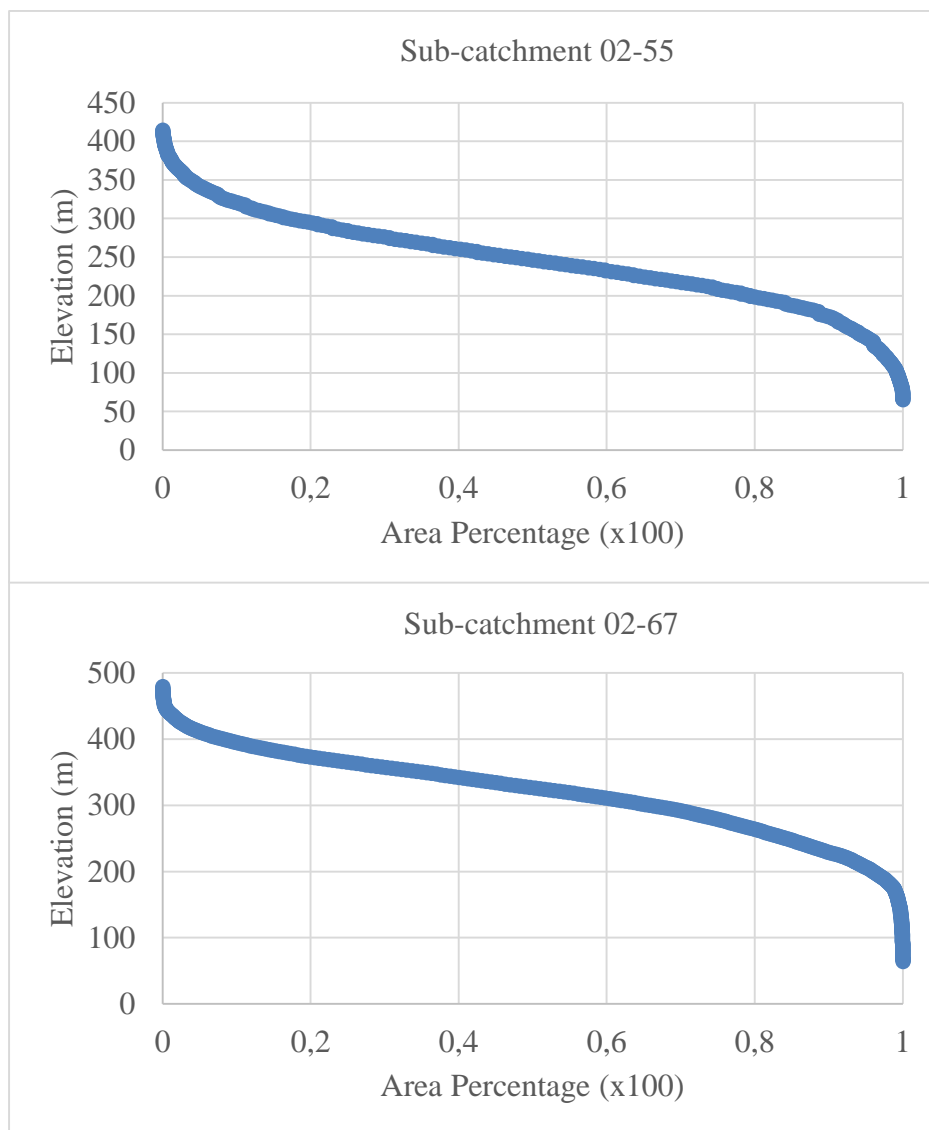


Figure 2.4 Hypsometric curves of sub-catchment areas.

The slope map of the Omerli Basin produced automatically using the spatial terrain tool of ERDAS Imagine 2011 software is shown in Figure 2.5. According to the results

of the slope analysis, slope values between 0 and 10% cover 68.6% of the study area. The size of these low slope areas is 426.3 km² and they represent abrasion surfaces, sediment deposits, and plateaus. Approximately 166.6 km² (26.8%) of the study area contains slopes between 10.1 and 20%, and these areas are mostly plateaus and semi-matured slopes. Only 25 km² of (4%) of the study area contains slopes between 20.1 and 30%, and these are the steeper areas of the basin. The steepest locations within the basin have slopes between 30.1 and 53%; these areas cover only 3.1 km² (0.6%) of the entire study area (Figure 2.5).

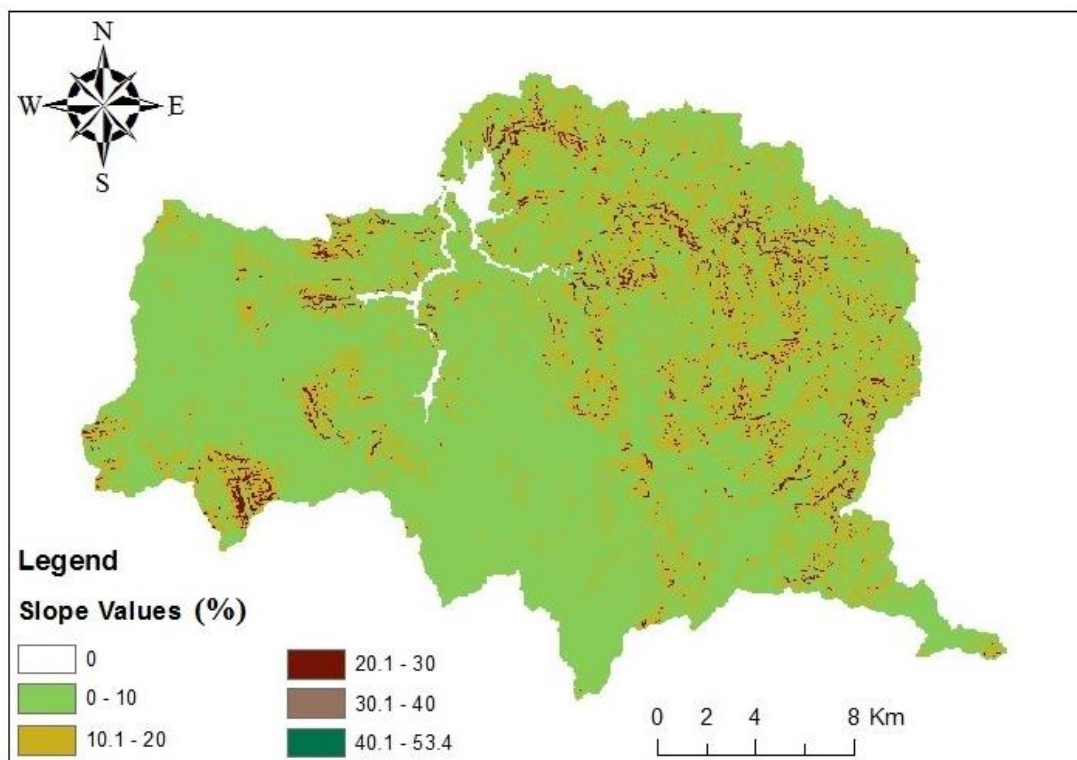


Figure 2.5 Slope map of Omerli Basin.

The aspect map of the study area was produced using the same methods as the slope map. The aspects of the slopes shown in Figure 2.6 are distributed almost uniformly in the Omerli Basin. The western region (SW–W–NW) is the most common aspect, with 28.01% and northern region is the least common, with 23.07% aspect values in the study area. The lake surface is a flat surface without any degree of slope and it is considered to have no aspect (Figure 2.6).

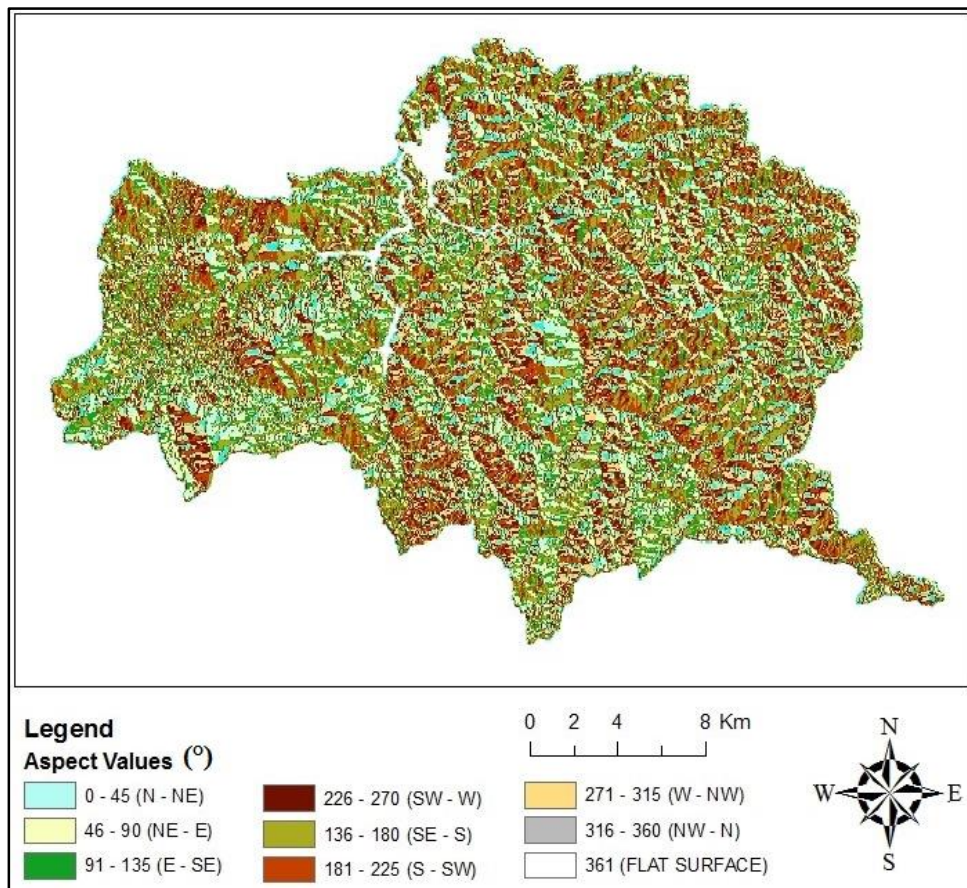


Figure 2.6 Aspect map of Omerli Basin.

Landsat 5 TM satellite images, which have 30-m spatial resolution, were classified using Erdas Imagine 2011 software according to the USGS 2006 land cover class definitions. According to these definitions, six major land cover classes were determined within the study area as shown in Figure 2.7; these classes were open water, high intensity residential, deciduous forest, evergreen forest, herbaceous/grasslands, and small grains. The classification results revealed that the Omerli Basin is covered by forested areas and bushes in the north, and narrow agricultural and large settlement areas in the west. The southern region of the study area is covered by large agricultural and small settlement areas. There are also some small forested areas located in the southern part of the basin. The eastern region of the study area is mostly covered by deciduous forests, along with agricultural and settlements areas. There are only a few small settlements in the northern and eastern regions of the Omerli Basin (Figure 2.7).

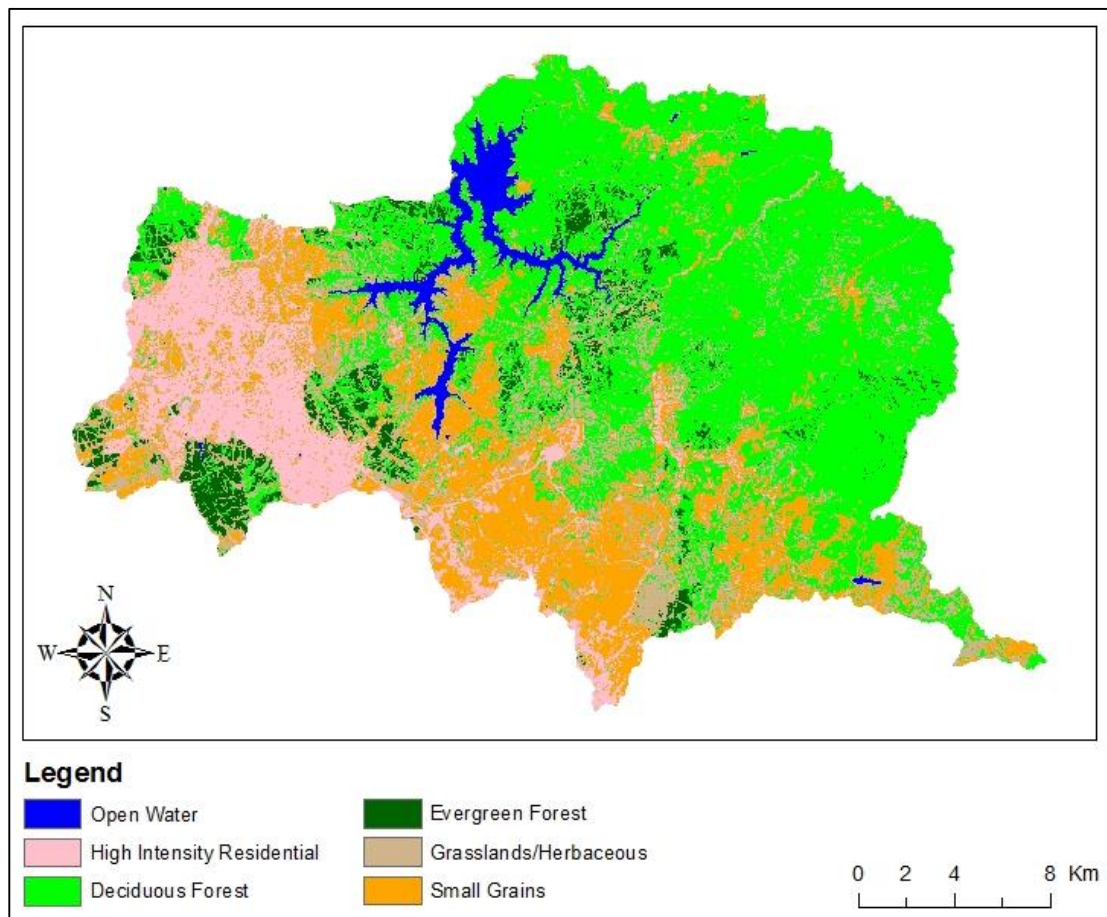


Figure 2.7 Land use/land cover (LU/LC) map of Omerli Basin.

2.2.2 Observational data preparation

The observed precipitation and temperature data were taken from eight meteorology stations (see Figure 2.2) and their relevant logistical information is presented in Table 2.1.

Table 2.1 Meteorology Stations around Omerli Basin

Name	Latitude (°)	Longitude (°)	Altitude (m)
Göztepe	40.9712	29.0576	16
Kireçburnu	41.1464	29.0502	59
Kartal-Istanbul Bölge	40.9120	29.1567	18
Kumkoy-Kilyos	41.2505	29.0384	38
Şile	41.1688	29.6007	83
Gebze	40.8230	29.4342	130
Kandıra	41.0700	30.1700	32
Kocaeli	40.7663	29.9173	74

The observed daily and monthly precipitation and temperature values were used to generate basin averaged time series during the reference period (1961–1990) for two sub-catchments 02-55 and 02-67 using the Thiessen polygons method (Figure 2.8). The Thiessen polygons method is a proximity method used in GIS (Geographic Information Systems) for finding the “region of influence” of points (stations) by creating polygons around them using Euclidean distance information (DeMers, 2003). The Thiessen polygons method is used to make approximations in several disciplines, including meteorology (Bayraktar and Turalioglu, 2005; Derakshan and Talebbeydokhti, 2011; Zhenyao et al. 2012; Wagner et al. 2012), forestry (Butler et al. 2014; Dobbertin et al. 2001), land use/land cover (Ziadat, 2007; Aubrecht et al. 2009), hydrology (Jarvis et al. 2013; Ruelland et al, 2008), remote sensing (Guang and Weili, 2011; Alexander, 2013), health (Gething et al. 2004), vegetation cover (Hühn, 2000; Kristensen et al. 2006; Viana et al. 2012), and solar radiation (Grant et al. 2004).

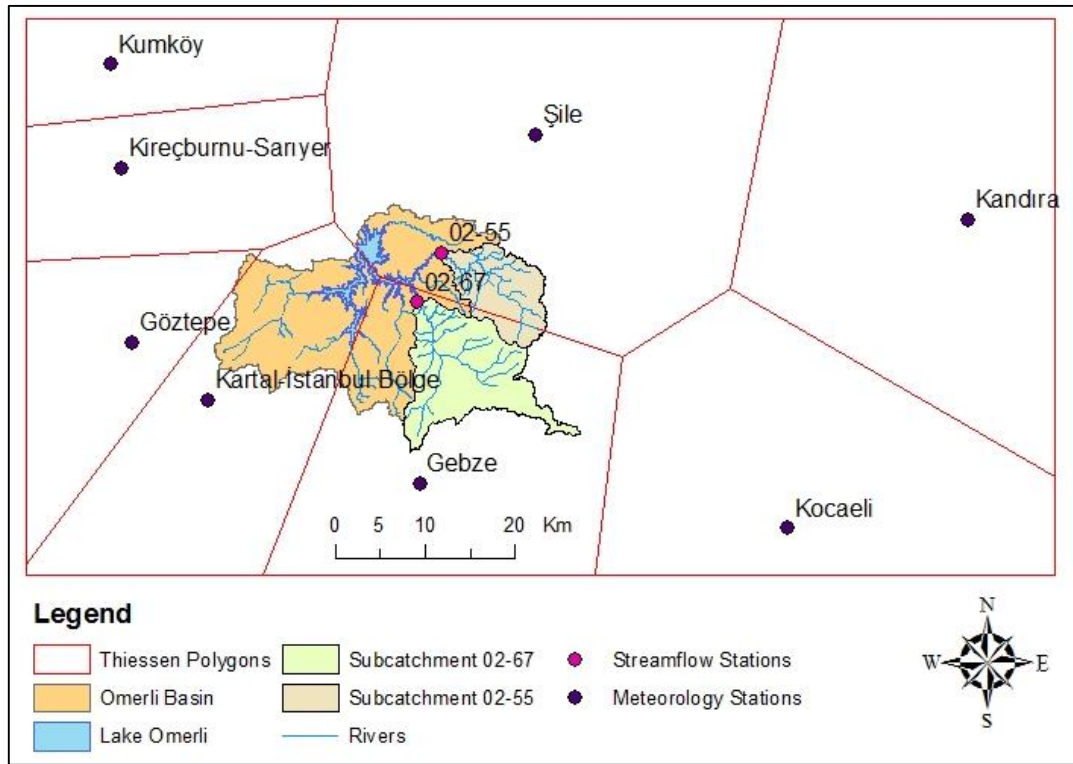


Figure 2.8 Thiessen polygons in Omerli Basin.

A significant problem with the data in this study is the distribution of meteorological stations across in the study area. As can be seen in the available data network (Fig. 2.2 and 2.8), there is only one meteorology station (Şile) on the northern side of the study area, and there is quite a long distance between stations. Consequently, the accuracy of the Thiessen polygons method in calculating the basin-averaged variables for both sub-catchments is influenced.

Daily streamflow data, obtained from locations that are illustrated at the outlet of two sub-catchments in Figure 2.8, were obtained from State Hydraulic Works of Turkey (DSI) for the period from 1978 to 2004; these were used to calibrate and validate the hydrological model. Using the daily streamflow data from 02-67 catchment, streamflow components of the river were investigated using the Wetspro tool (Willems, 2009). The observed flow series were introduced into this program and surface flow (quick flow), interflow, and groundwater (base flow) flows were

identified from the streamflow data; the results are illustrated in Figure 2.9. With this separation recession constants of quick flow, interflow, and base flow were identified as 1 day, 4 days, and 30 days, respectively. The program also assisted in determining the overall water balance in the sub-basin. The results of this analysis revealed that the base flow (slow flow), interflow and quick flows contribute 40, 30, and 30% of the total runoff, respectively.

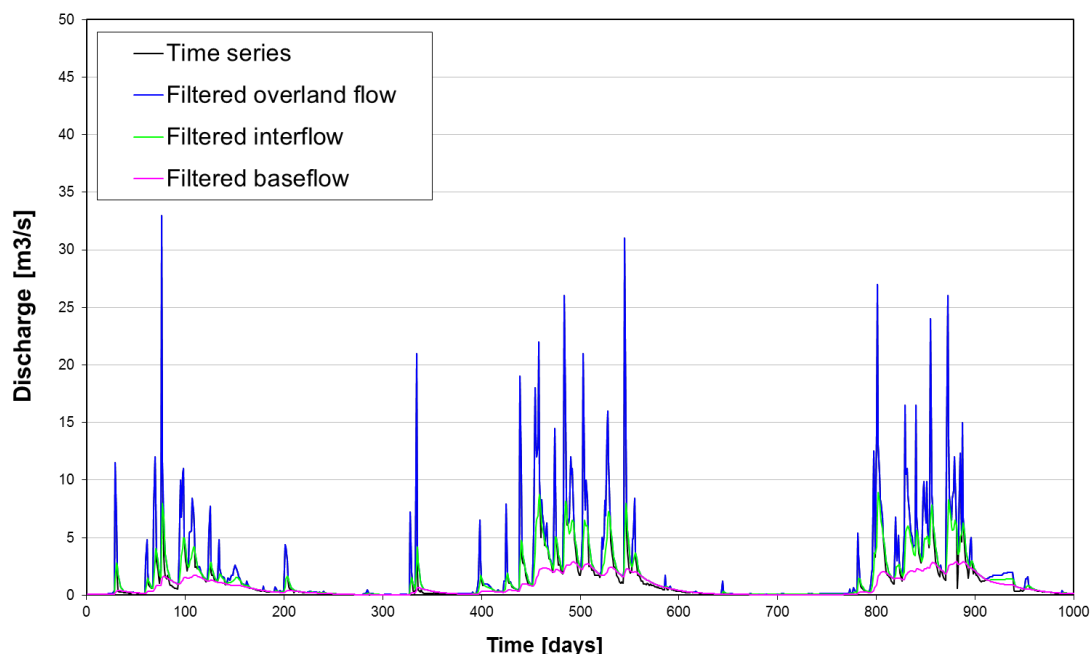


Figure 2.9 Streamflow components in the 02-67 subcatchment of Omerli Basin.

2.3 GCM/RCM Combination

Daily and monthly precipitation and temperature data were downloaded from the ENSEMBLES project database (van der Linden and Mitchell, 2009) and were used as primary data in this study. The ENSEMBLES project was conducted by the European Commission (EC) in order to provide information about latest climate change effects to scientists, the business sector, and decision makers, using the most developed modelling and analytical tools. In order to improve the accuracy of the forecasts of the project, multiple climate models ('ensembles') were used in this project.

Many hydrological modeling studies (Seaby et al. 2013; Burke et al. 2010; Hanel and Buishand 2012) have used data from ENSEMBLES.

In the ENSEMBLES project, an ensembles prediction system based on GCMs was developed to perform simulations of the future climate across seasonal and multi-decadal time spans. The scope of the project was modeling the effects of uncertainties arising from key physical, chemical, and biological processes, and the assembly and testing of new GCMs. Further, imperfections arising from model uncertainties and climate variability quantified well in this project. GCMs ran with four different emission scenarios (B1, A1B, A2, 1%CO₂) at seven climate centers and all centers created multi-simulation ensembles for more than one scenario. Finally, multi-model ensembles were created for Europe.

RCMs with 25-km and 50-km spatial resolutions were used and nested within 5 GCMs to provide the boundary conditions for RCMs.

RCM climate data from the ENSEMBLES project are produced by considering the A1B carbon emission scenario. A1B is a sub-member of the A1 family, which predicts rapid economic growth and population increases until the middle of the 21st century, followed by the development of more efficient technologies and a population decrease. The main features of this family are social interaction between societies, removing borders between countries, and more balanced distribution of per capita income. The A1 family can be divided into three groups based on technological preferences: fossil dominated (A1F1), non-fossil (clean energy) sources (A1T), or a balance of all energy sources (A1B) (Figure 2.10).

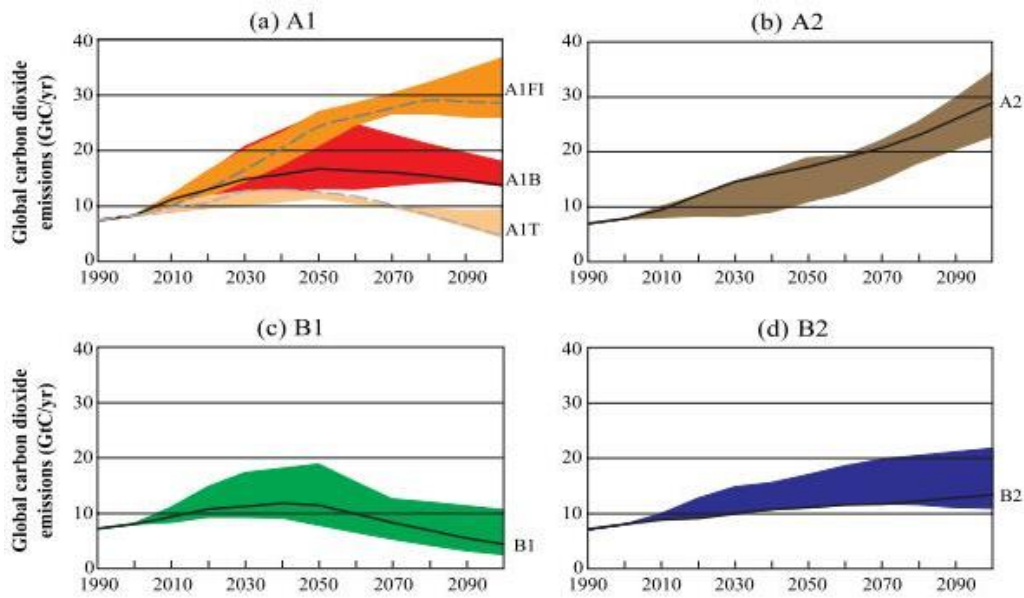


Figure 2.10 CO₂ emissions of families (storylines) (IPCC, 2000).

In this study, the data with 25-km resolution is used as it shows more detailed spatial coverage in the study area, which is relatively small in size. Table 2.2 gives the combination of GCM and RCM model pairs together with their acronym used in this study.

Table 2.2 GCM/RCM matrix of ENSEMBLES with 25 km resolution

Scenario	Driving GCM	Model	Acronym	Resolution
A1B	ARPEGE	HIRHAM	DMI-HIRHAM5	25km
A1B	ARPEGE_RM5.1	Aladin	CNRM-RM5.1	25km
A1B	BCM	DMI-HIRHAM5	DMI-HIRHAM5	25km
A1B	BCM	RCA	SMHIRCA	25km
A1B	ECHAM5-r3	DMI-HIRHAM5	DMI-HIRHAM5	25km
A1B	ECHAM5-r3	RegCM	ICTP-REGCM3	25km
A1B	ECHAM5-r3	RACMO	KNMI-RACMO2	25km
A1B	ECHAM5-r3	RCA	SMHIRCA	25km
A1B	ECHAM5-r3	REMO	MPI-M-REMO	25km
A1B	HadCM3Q0	CLM	ETHZ-CLM	25km
A1B	HadCM3Q0	HadRM3Q0	METO-HC-HadRM3Q0	25km
A1B	HadCM3Q3	HadRM3Q3	METO-HC-HadRM3Q3	25km
A1B	HadCM3Q3	RCA	SMHIRCA	25km
A1B	HadCM3Q16	RCA3	C4IRCA3	25km
A1B	HadCM3Q16	HadRM3Q16	METO-HC-HadRM3Q16	25km

The ENSEMBLES project was developed for almost the entire of Europe, Northern Africa, and Western parts of Turkey and it has climate data (simulations) for all of Europe except for the northern regions of Norway. Additionally, simulations are produced for northern regions of Africa (Figure 2.11).

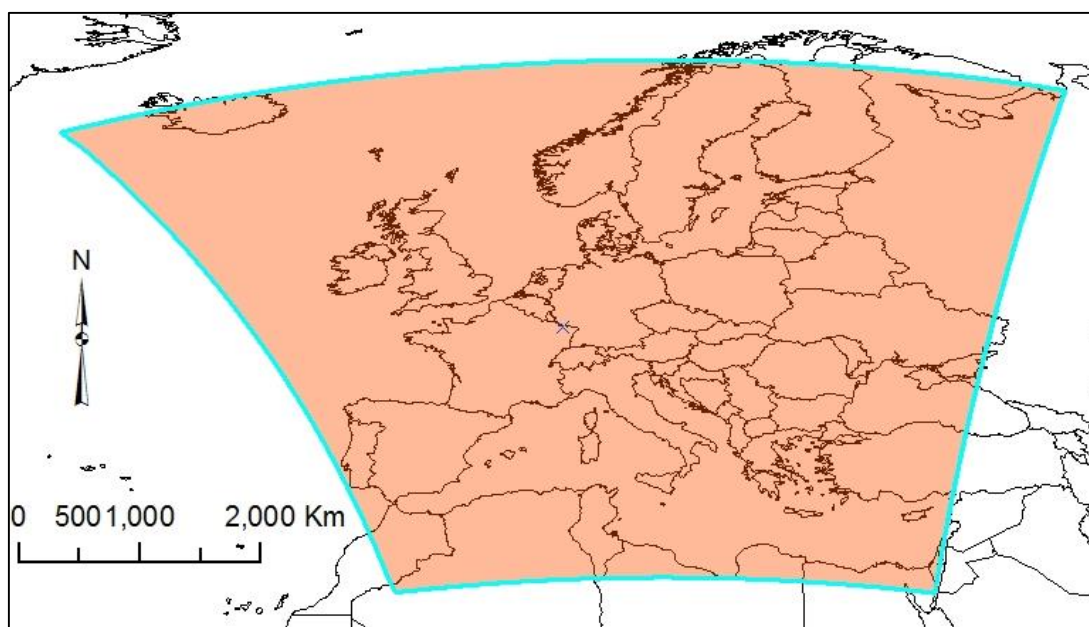


Figure 2.11 The coverage area of ENSEMBLES project.

2.4 Spatial Interpolation

Interpolation is a method for making estimations for points or stations where there are no data by using existing points (stations). Spatial interpolation techniques allow estimations to be made for points (stations) where no observation values exist by using existing observation data. Spatial data are used commonly in planning, decision making, climatological applications, and environmental management. However, it is very hard to find spatial data for all locations and producing spatial data is a time-consuming undertaking. Random and systematic errors and gaps (Vieux, 2001) are the most significant problems in hydrological studies that utilize estimations of precipitation, temperature, and streamflow (Di Piazza et al. 2011). These reasons necessitate the use of interpolation methods in space-related studies. Performing

estimations for outside of observation stations is defined as extrapolation (Burrough and McDonnell, 1998).

There are two kinds of spatial interpolation techniques: deterministic methods and geostatistical methods. Deterministic methods include inverse distance weighting (IDW), trend surface analysis (TSA), local trend surfaces (LTS), and radial basis functions (RBF). Geostatistic methods are defined as statistics of the earth, and they are used very widely within spatial statistics.

Kriging methods are mathematical- and statistics-based models. Having a statistical model with a probability function separates kriging from deterministic methods. Kriging methods are autocorrelation-based methods and autocorrelation is a distance function. In classical statistics, observation values are considered independent while geostatistics allows the calculation of distances between observation points and modeling of an autocorrelation as a function of distance. In general, kriging performs two main roles: the analysis of the structure of spatial data and making estimations (ESRI, 2014). Deterministic methods have been used along with geostatistical methods in several studies. Interpolation techniques are commonly used in making estimations of climatological data, such as precipitation and temperature. Wagner et al. (2012) made estimations of precipitation in monsoon climate regions where climate stations are rare using interpolation techniques. The authors used seven different interpolation techniques including Thiessen polygons, and statistical and geostatistical methods, claiming that geostatistical regression methods provided more accurate results.

Regression techniques are the most widely applied statistical modeling methods that are utilized. When using traditional regression techniques, the relationship between one dependent variable and other variables is summarized by only one equation. GWR is a spatial statistics method used for analyzing “spatial non-stationary”, which is defined as being alterations in relationships between variables from one point (station) to another. GWR develops different equations for every stations (points) in the datasets through the dependent and explanatory variables of stations (ESRI, 2014).

Consequently, GWR provides valuable information about the nature of an investigated relationship, and, in this way, it is separated from the other regression methods (Fotheringham et al. 2002).

In traditional regression methods (2.8);

$$\hat{y}_i = \beta_0 + \sum_k \beta_k x_{ik} + \varepsilon_i \quad (2.8)$$

where \hat{y}_i is the dependent variable for observation i , β_0 is the intercept, β_k is k 's estimated parameter, x_{ik} is the value of the k^{th} variable for i , ε_i is the error term. GWR produces new equations for each observation, instead of calibrating the existing equation. Each equation is calibrated by using different coefficients of observation values in the data set. GWR may be introduced (2.9);

$$\hat{y}_i = \beta_0(u_i, v_i) + \sum_k \beta_k(u_i, v_i) x_{ik} + \varepsilon_i \quad (2.9)$$

where (u_i, v_i) are coordinates of i (Fotheringham et al. 2002). The concept here is that closer observations may effect each other's parameters to a greater extent in comparison with farther ones. Weighting value allows some features to be more important, which is assigned to each observation value, is calculated by a distance decay function of observation i . Distances between grid data sets are calculated using grid centers in gridded data sets (Mennis, 2006). Distance decay functions can be modified by changing the bandwidth either manually or using optimized algorithms for minimizing cross-validation score as (2.10);

$$CV = \sum_{i=1}^n (y_i - \hat{y}_{i \neq i})^2 \quad (2.10)$$

where n is the number of observation. The other alternative of bandwidth is using the Akaike Information Criteria (AIC) score (2.11),

$$AIC_c = 2n \log_e(\hat{\sigma}) + n \log_e(2\pi) + n \left\{ \frac{n + \text{tr}(S)}{n - 2 - \text{tr}(S)} \right\} \quad (2.11)$$

where $\text{tr}(S)$ is the trace of the hat matrix. The AIC method has the advantage of assuming degrees of freedom belong to different observation points. Moreover, the user may use a fixed bandwidth for each observation or may change bandwidth size, which specifies the extent of the kernel should be determined, according to the density of the observation points (Charlton et al. no date).

GWR is used in several climate studies in which temperature and precipitation simulations are the main focus. Kamarianakis et al. (2008) studied satellite-based precipitation estimates in the Mediterranean region. The study compared observation values and satellite-based data on a local scale, and tested local stationary by using both observation values and satellite-based total precipitation data. Propastin (2012) used a satellite-based vegetation index (VI) in order to perform estimations of biomass in tropical rain forests. In this study, the common GWR was developed, as was an extended GWR model, geographically and altitudinal weighted regression (GAWR), which was used for applying the effects of horizontal and vertical differences to a spatial-weighting matrix. The authors compared the GAWR method with GWR and the global ordinary least squares (OLS) method and suggested that GAWR provides very important benefits. Li et al. (2010) investigated the relationships between urban land surface temperature and explanatory variables by using a spatial nonstationary method, GWR. The authors also used the OLS method and compared the performance of the models. In the study, it was claimed that GWR performance was better than OLS, and that it allowed the implementation of topographic and environmental conditions to the model.

2.5 Hydrological Model

In this study, runoff values were simulated by using the HBV (Hydrologiska Byråns Vattenbalansavdelning, HBV; Bergström, 1976, 1992). The HBV model is a numerical

rainfall-runoff model for simulating hydrological processes in a catchment scale. The water balance is described as (3.1):

$$P - E - Q = [SP + SM + UZ + LZ + \text{lakes}], \quad (3.1)$$

where:

P = precipitation

E = evapotranspiration

Q = runoff

SP = snow pack

SM = soil moisture

UZ = upper groundwater zone

LZ = lower groundwater zone

Lakes = lake volume (SMHI, 2014).

The HBV is a highly adaptable and challenging model because of its applicability across different countries that have different climates, such as Sweden, Zimbabwe, and India. Furthermore, it can be used in both very small and very large study areas, such as from lysimeter (Lindström and Rodhe, 1992) to the basin scale (Jia and Sun, 2012). The model can be used with daily temperature and precipitation values but only either daily or monthly potential evaporation. The HBV model has been used for runoff simulations (Chen et al. 2012; Talei et al. 2013; Gardner, 2009; Tahir et al. 2011; Menzel and Bürger, 2002; Fu et al. 2012) for different purposes all around the world. The HBV model uses daily rainfall, temperature, and potential evapotranspiration as input data. The HBV model works with daily values; however, it is possible to use for shorter time scales. The model usually utilizes monthly evaporation values, but it can also operate with daily values. Evaporation data already exist in the parameter file (param.dat) in the model; consequently, the model needs only precipitation and temperature data in order to perform runoff simulations. The model requires

temperature data in order to calculate snow melt, snow accumulation, and potential evaporation. The main features of the model include meteorological interpolation, snow melt and accumulation, evapotranspiration estimation, soil moisture calculation procedures, runoff generation, and routing procedures between sub basins (SMHI, 2014). Once the calibration is performed, the HBV model can be used in different basins with different climate characteristics. The structure (Figure 2.12) of the HBV model was first presented by Lindström et al. (1997).

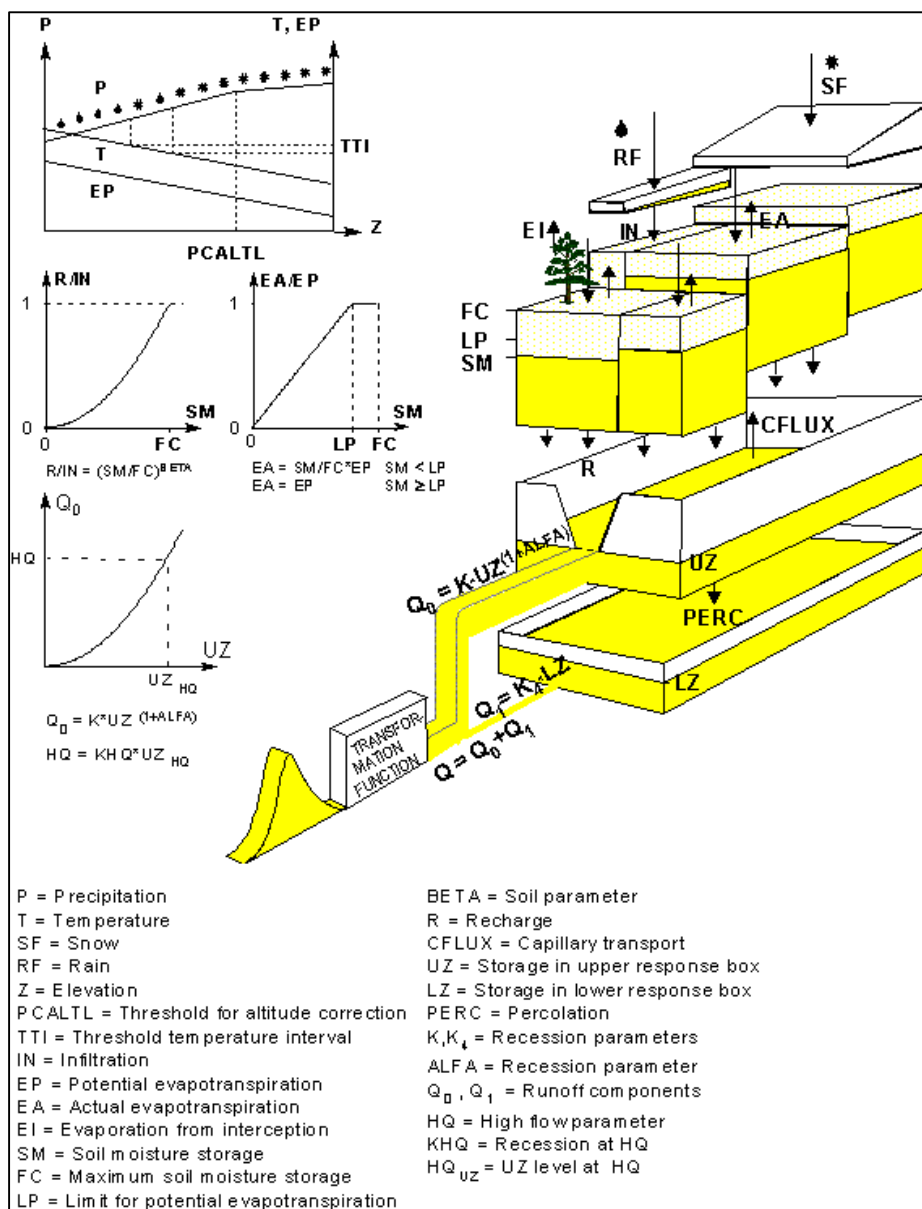


Figure 2.12 The HBV model structure (SMHI, 2014).

While the standard model uses weighting routines and a lapse rate, the HBV-96 model uses a geostatistical method similar to kriging to model areal temperature and precipitation (Daley, 1991). Air temperature and water-holding capacity of snow determine the snowmelt routines of the HBV. Additionally, the melting process is calculated according to temperature differences in distinctive land cover areas. Furthermore, a threshold value for temperature is used in order to discriminate precipitation from snowfall. The standard HBV model utilizes monthly potential evapotranspiration value-adjusted temperature anomalies (Lindström and Bergström, 1992). In this model, soil moisture content is calculated using bucket theory, which assumes statistical distributions of basin storage capacities. This is a necessary part of the model for controlling runoff. BETA, LP, and FC are the three parameters that the soil routine based on. The runoff generation routine is a reply function for the transformation of excess water to runoff. The division of the study area into sub basins may be very important for determining runoff, and pool routing should be applied in lakes for all sub basins. Rainfall to lakes is considered as raining to open space land areas with same altitudes, and is added to the current lake water volume directly. Evaporation from a lake is considered as potential evaporation with a modified parameter. After water routing runoff, transformation will take place according to a rating curve. If there is no specific rating curve for the lake, the model will assume a general rating curve (SMHI, 2014).

CHAPTER 3

DOWNSCALING RCM DATA WITH GWR

3.1 GWR Setting with Station Data

The GWR downscaling method was used to produce 1-km spatial resolution monthly precipitation and temperature data from 25-km spatial resolution RCM climate data. The GWR method uses station data of precipitation or temperature and their some explanatory data (variables) for simulation. Explanatory variables are the local characteristics of station points. The explanatory variables used in this study were altitude, aspect, slope, distance to sea, and surface roughness. The aim of using explanatory variables is to reflect the impact of topographical properties of stations in order to simulate results.

Explanatory variables of RCM grids, meteorology stations, and prediction points are determined by using ASTER GDEM data (Figures 3.4, 3.5, 3.6 for altitude, slope and aspect, respectively), a map of Istanbul in shapefile format, and classified LANDSAT 5 TM satellite images (Figure 3.7). Altitude, slope, aspect, and land cover values of meteorology stations were acquired from corresponding pixels after matching relevant maps with station points. The distances between station points and shorelines were calculated using an automatic function of ArcGIS 10.1 software.

The GWR method was calibrated by using explanatory variables from eight meteorology stations (Figure 2.1) located around the Omerli Basin in order to adjust the model for the local conditions of the Omerli Basin. Initially, a total of 31 explanatory variable combinations (table 3.1) was determined for calibration of the GWR method for the study area.

Table 3.1 Explanatory variables used in GWR calibration. (C = Combination, VAR = Variable)

	VAR. 1	VAR. 2	VAR. 3	VAR. 4	VAR. 5	WEIGHTS
C1	altitude	aspect	distancetosea	slope	surfaceroughness	
C2	altitude	aspect	distancetosea	slope	surfaceroughness	altitude
C3	altitude	aspect	distancetosea	slope	surfaceroughness	aspect
C4	altitude	aspect	distancetosea	slope	surfaceroughness	distancetosea
C5	altitude	aspect	distancetosea	slope	surfaceroughness	slope
C6	altitude	aspect	distancetosea	slope	surfaceroughness	surfaceroughness
C7	altitude	aspect	distancetosea	slope		
C8	altitude	aspect	distancetosea	slope		altitude
C9	altitude	aspect	distancetosea	slope		aspect
C10	altitude	aspect	distancetosea	slope		distancetosea
C11	altitude	aspect	distancetosea	slope		slope
C12	altitude	aspect	distancetosea		surfaceroughness	
C13	altitude	aspect	distancetosea		surfaceroughness	altitude
C14	altitude	aspect	distancetosea		surfaceroughness	aspect
C15	altitude	aspect	distancetosea		surfaceroughness	distancetosea
C16	altitude	aspect	distancetosea		surfaceroughness	surfaceroughness
C17	altitude	aspect		slope	surfaceroughness	
C18	altitude	aspect		slope	surfaceroughness	altitude
C19	altitude	aspect		slope	surfaceroughness	aspect
C20	altitude	aspect		slope	surfaceroughness	slope
C21	altitude	aspect		slope	surfaceroughness	surfaceroughness
C22	altitude		distancetosea	slope	surfaceroughness	
C23	altitude		distancetosea	slope	surfaceroughness	altitude
C24	altitude		distancetosea	slope	surfaceroughness	distancetosea
C25	altitude		distancetosea	slope	surfaceroughness	slope
C26	altitude		distancetosea	slope	surfaceroughness	surfaceroughness
C27		aspect	distancetosea	slope	surfaceroughness	
C28		aspect	distancetosea	slope	surfaceroughness	aspect
C29		aspect	distancetosea	slope	surfaceroughness	distancetosea
C30		aspect	distancetosea	slope	surfaceroughness	slope
C31		aspect	distancetosea	slope	surfaceroughness	surfaceroughness

However, 15 combinations were not functioned properly because of a lack of sufficient data, and the selection of the best combination for seasons was made from the 16 remaining combinations (bold in the table). For each simulation, seasonal precipitation data from seven of eight meteorology stations were used with GWR, and one of the stations was left free. Simulation results were compared with observed

seasonal precipitation values from the free station. Validation of the GWR developed for each combination is made at each free station by calculating the Root mean squared error (RMSE) and bias ratio values for all seasons and annually (Figure 3.1).

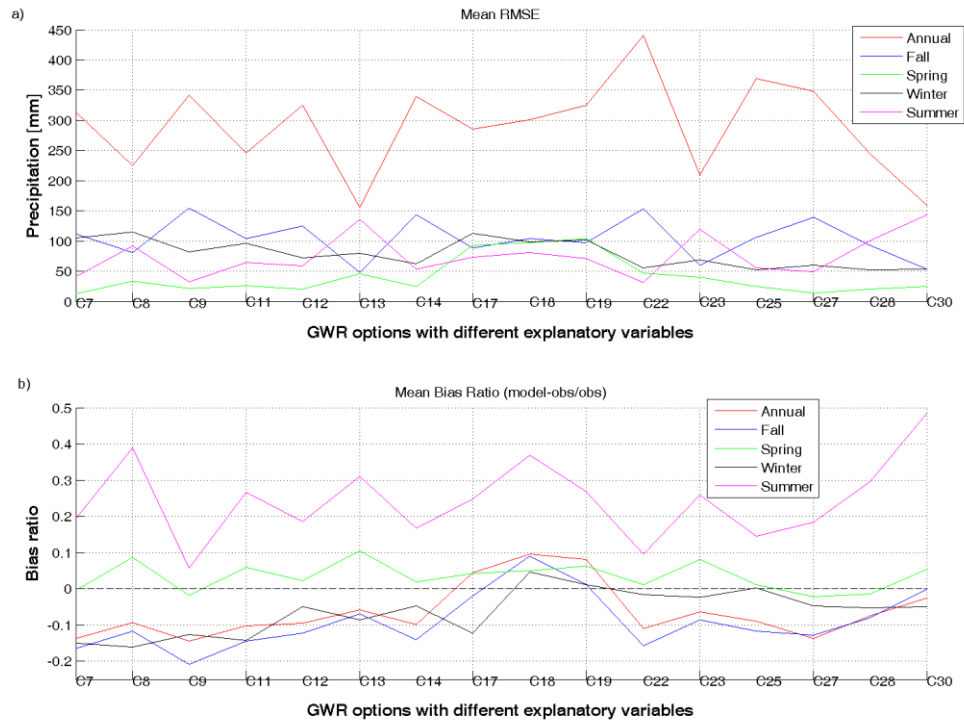


Figure 3.1 RMSE and Bias Ratio values between observations and simulations.

According to the lowest values of RMSE and bias ratio in Figure 3.1, the best GWR combination numbers given in Table 3.1 are 13 for annual, 7 for spring, 22 for summer, 30 for autumn, and 25 for winter. These best combinations are free from any RCM errors and thus, they are used in downscaling the 25-km RCM grid to 1-km as a function of representative explanatory variables of RCMs grid developed in the following section.

3.2 Determining Explanatory Variables for Grids

As it can be seen from the figure (3.2), four grids of RCMs cover both of the sub-catchments. Initially, an attempt was made to perform GWR with data belong to only these four grids. However, these data were not sufficient to perform GWR and

therefore, 12 more RCM grids were also selected around the Omerli Basin. One of the biggest deficiencies of spatial interpolation methods such as kriging, spline, and ordinary least square, is not making simulations where the number of stations is small (Bayraktar et al. 2005). Consequently, it is necessary to use climate data from 16 RCM grids as seen in Figure 3.2 when performing GWR simulations.

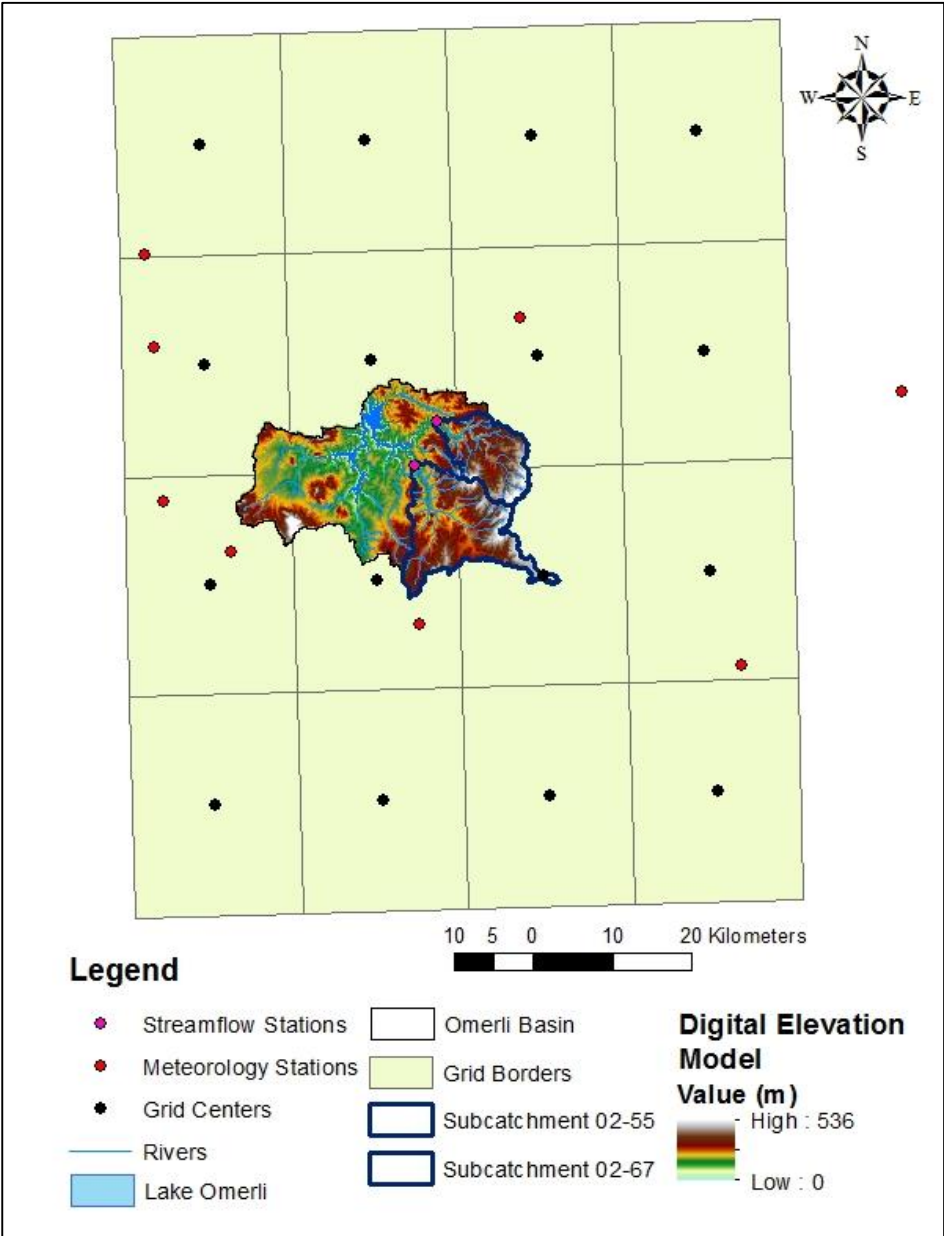


Figure 3.2 Study area and RCM grids around it.

Explanatory variables of the grids were determined using the metadata tool of ERDAS Imagine 2011 software (Figure 3.3). This tool calculates some statistics (mean and median) of displayed raster data; altitude, slope, and aspect information.

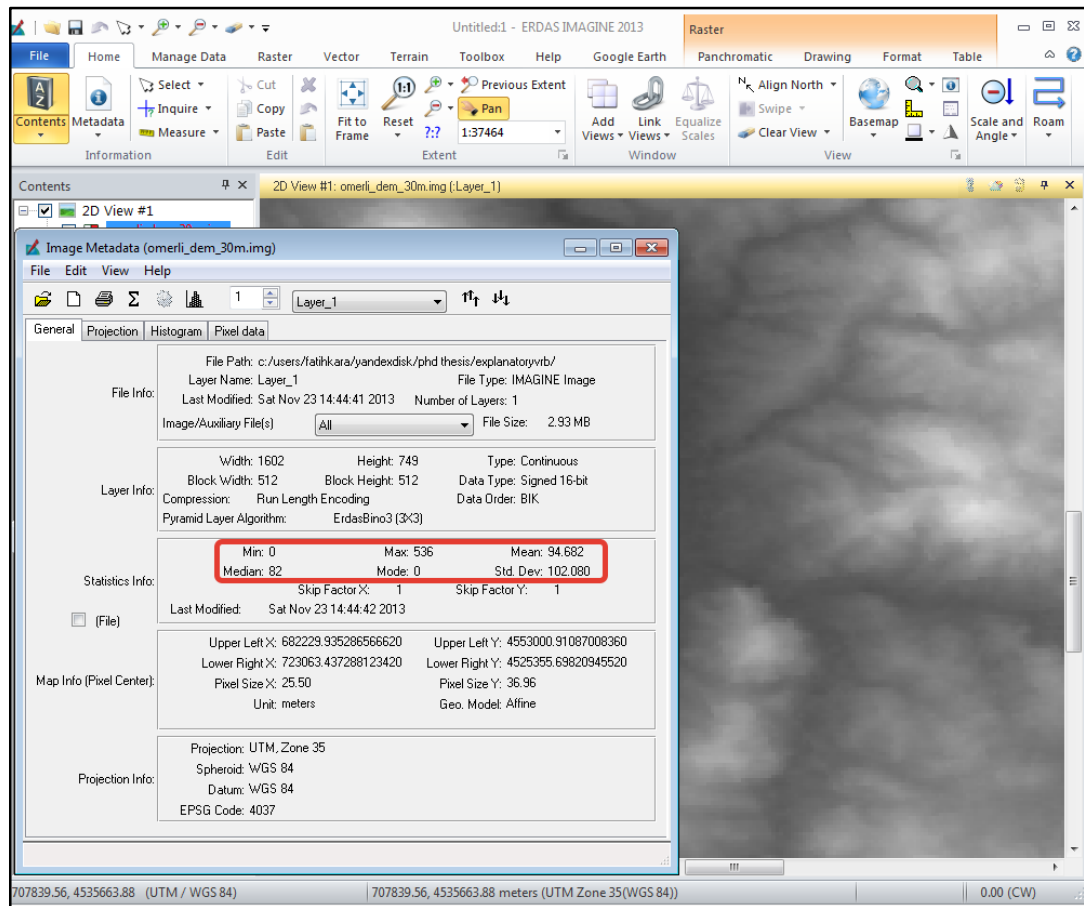


Figure 3.3 Automatic calculation of mean and median for altitude, slope, and aspect values of grids.

ASTER GDEM data were subset using grid borders and new 30 m spatial resolution DEM data were generated for the grids (Figure 3.4). Altitude information from 16 grids was taken from the new DEM data in mean and median. Following this, slope (Figure 3.5) and aspect maps (Figure 3.6) were produced from the DEM data using the terrain tool of ERDAS Imagine.

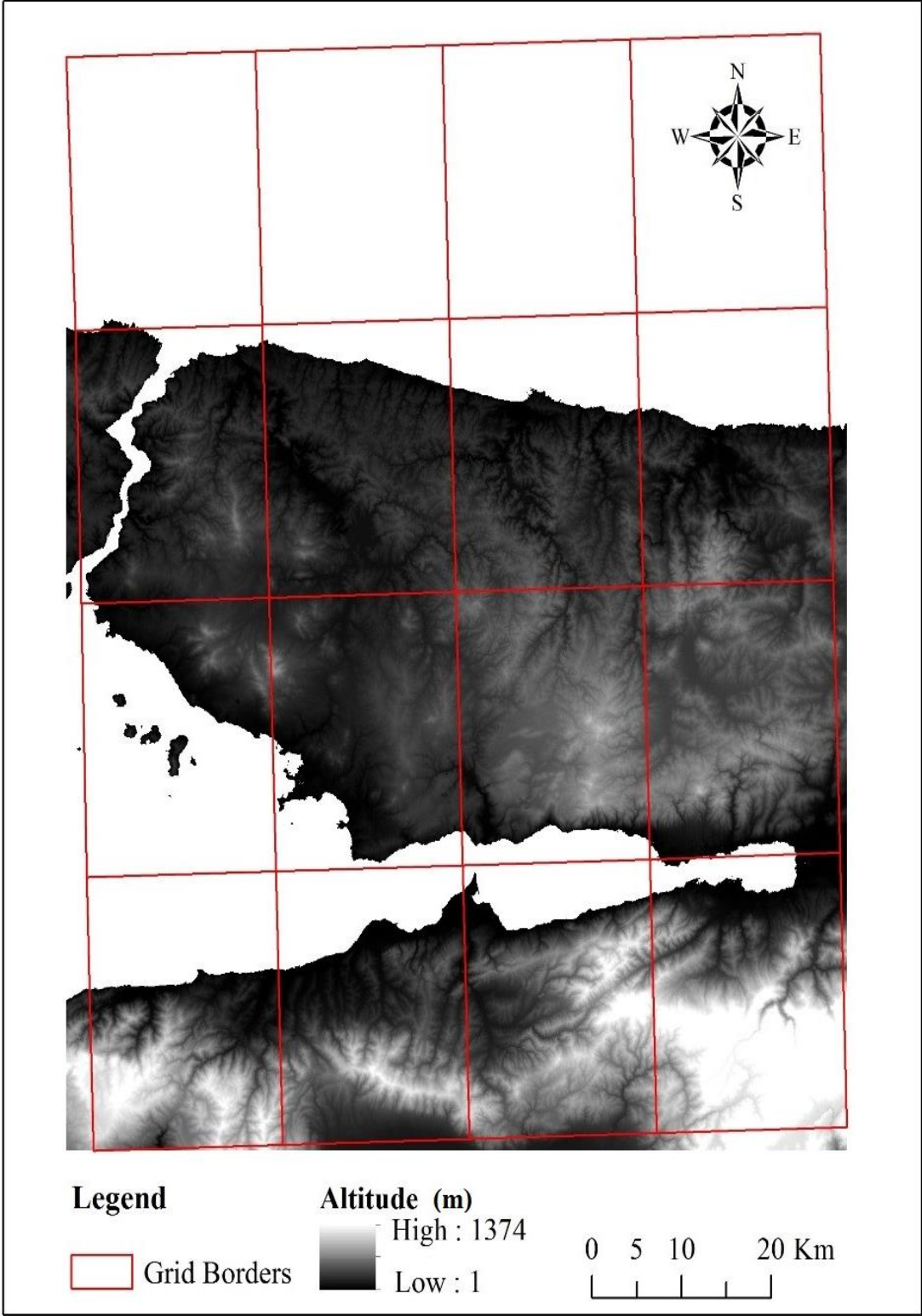


Figure 3.4 DEM map of RCM grids.

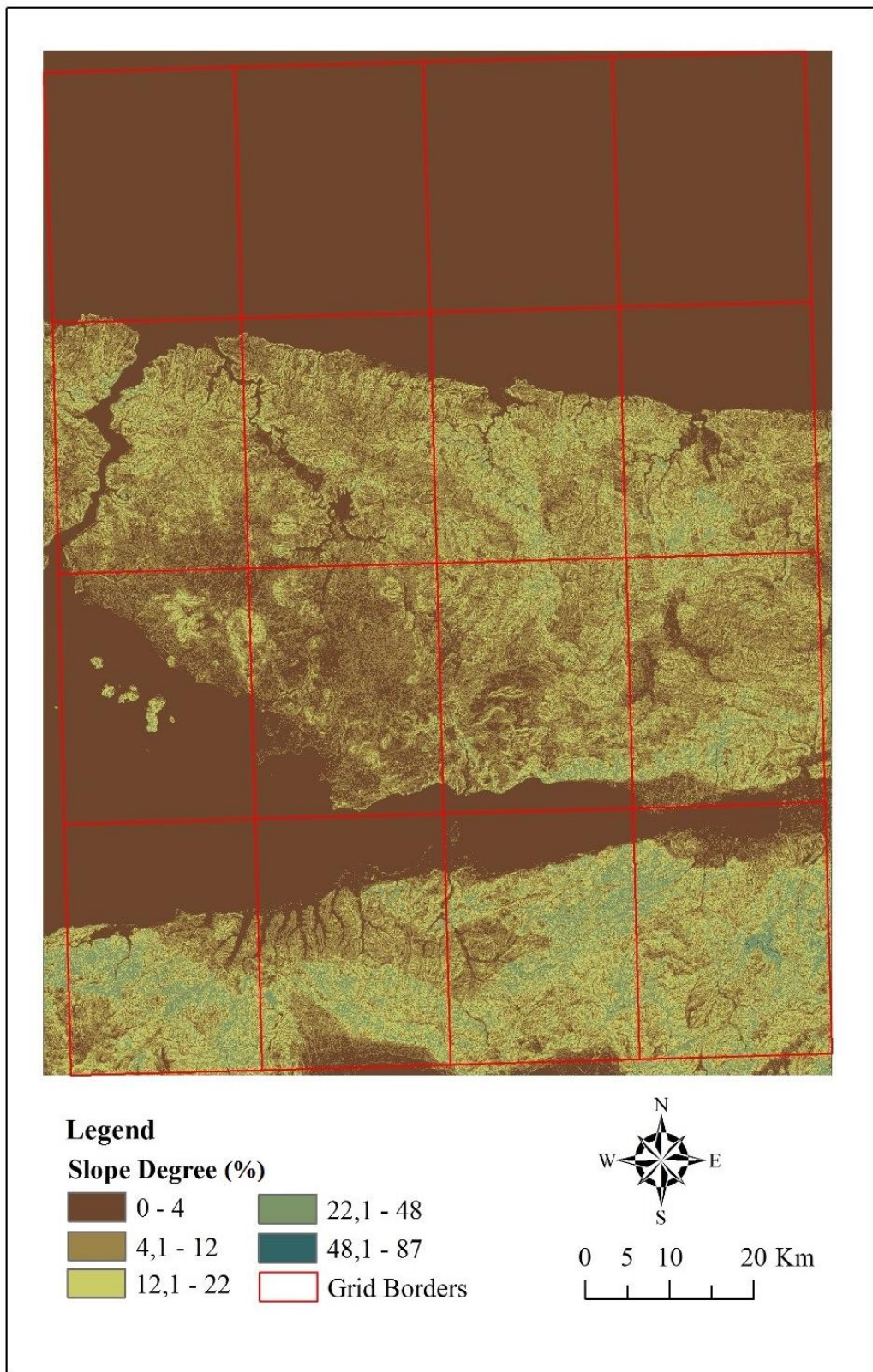


Figure 3.5 Slope map of RCM grids.

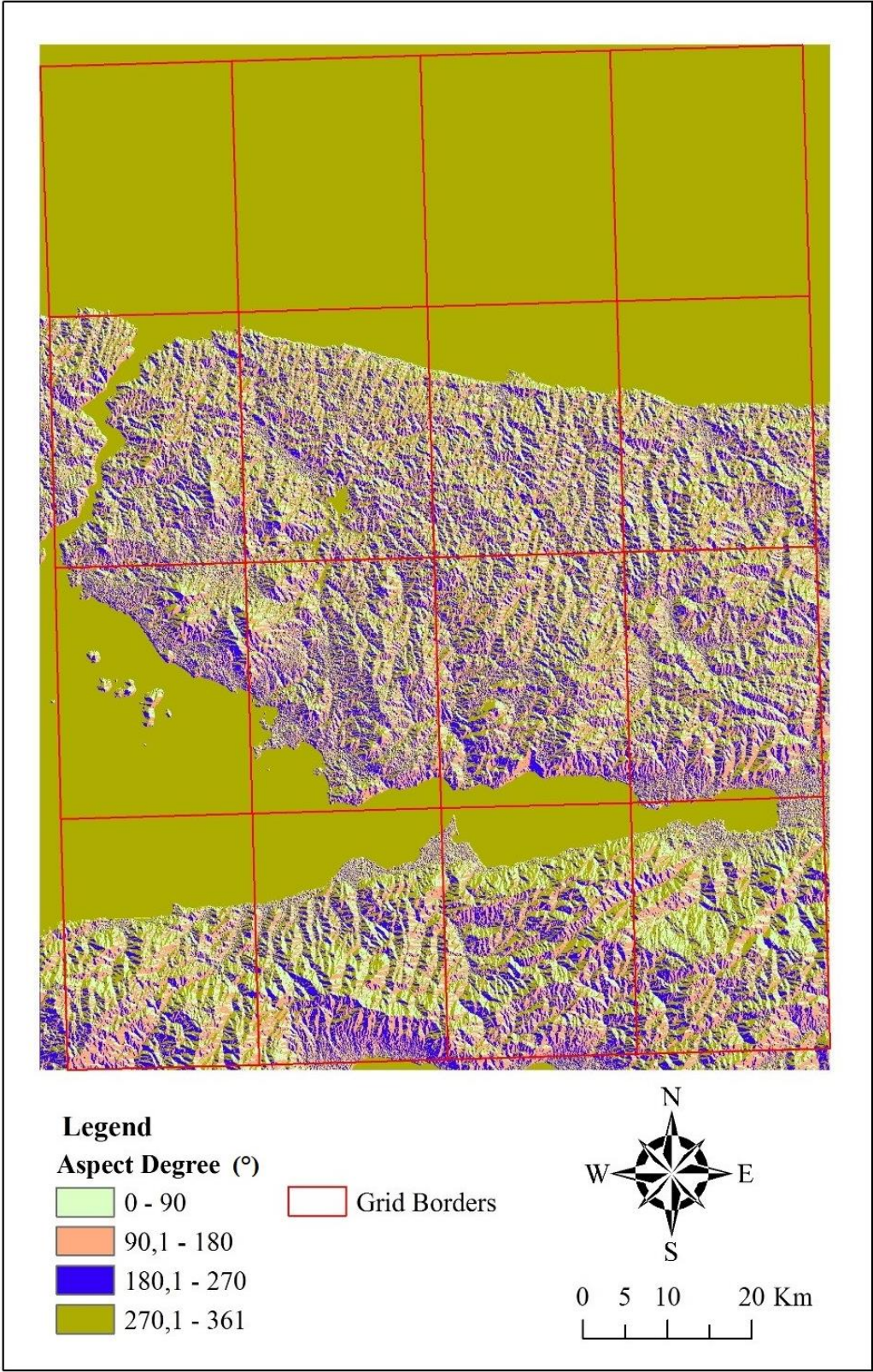


Figure 3.6 Aspect map of RCM grids.

A LANDSAT 5 TM satellite image was downloaded from the USGS (United States Geological Survey) website and was classified using the unsupervised classification technique. While using this technique, the maximum iteration, number of classes, and convergence threshold were selected as 25, 140, and 0.98, respectively (Figure 3.7).

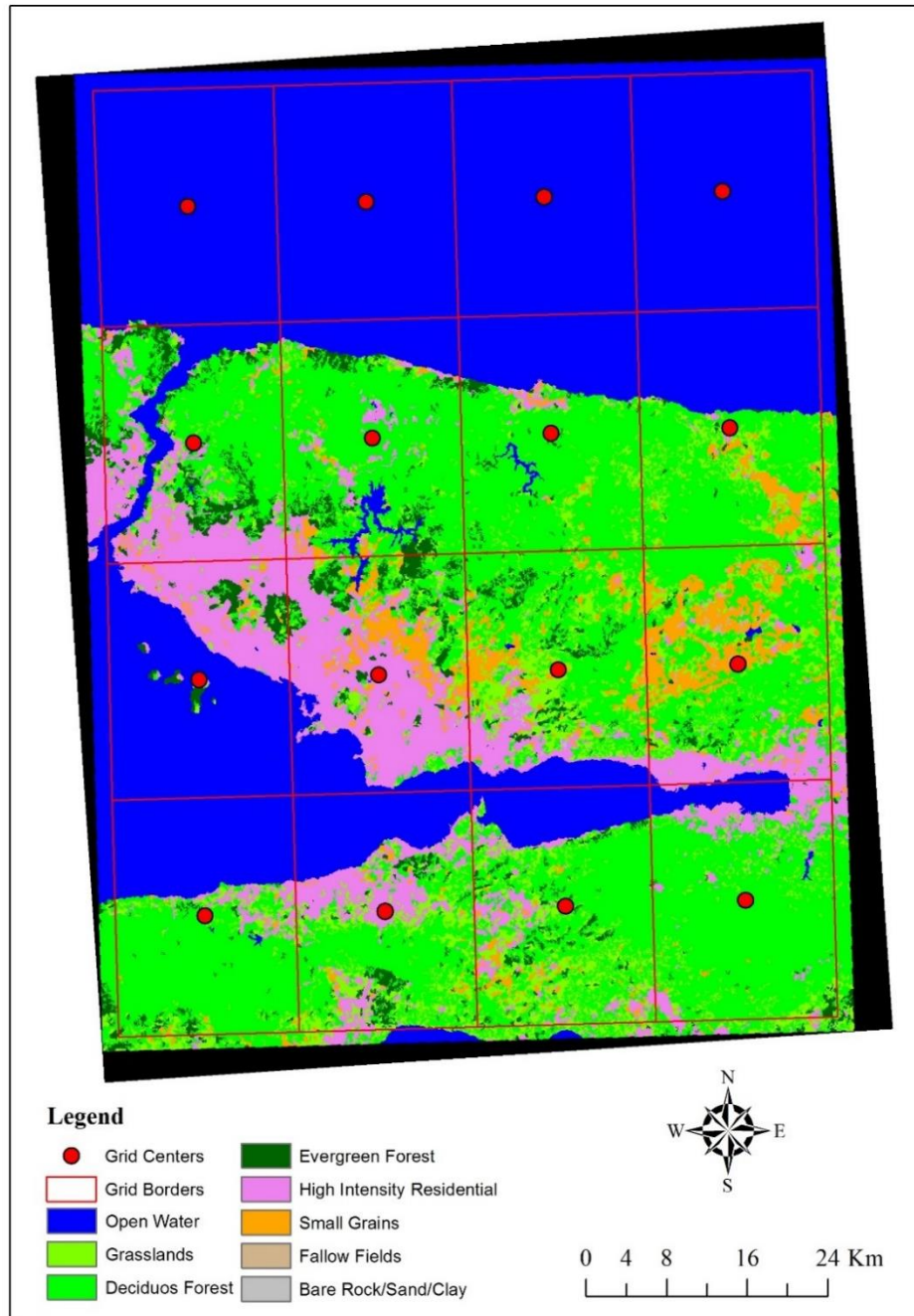


Figure 3.7 LU/LC types of RCM grids.

After the classification stage, pre-defined values of roughness length determined for USGS land cover types (table 3.2) are applied to each land cover class. Finally, the land cover map was matched with grid borders, and dominant and mean land cover values were determined for the grids. Table 3.2 was also used to determine surface roughness values of the station points explained in previous section.

Table 3.2 Surface roughness values of land cover types.

Land Cover Type	Surface Roughness Value (USGS)
Urban or Built-up Land	50
Dryland, Cropland and Pasture	10
Irrigated Cropland and Pasture	10
Mixed Dry/Irr Crop and Pasture	10
Grassland/Cropland Mosaic	10
Woodland/Cropland Mosaic	40
Grassland	7
Shrubland	20
Mixed Shrubland/Grassland	20
Savanna	20
Broadleaf Deciduous Forest	50
Deciduous Coniferous Forest	50
Evergreen Broadleaf Forest (Palm?)	40
Mixed Forest	50
Water	0,1
Herbaceous Wetland	15
Forested Wetland	45
Barren or Sparsely Vegetated	5
Herbaceous Tundra	10
Shrub and Brush Tundra	10

The Table 3.3 presents the mean and median explanatory variable values of the 16 RCM grids used in the production of the GWR data.

Table 3.3 Explanatory variable values of 16 grids around Omerli Basin.

Grids	Altitude (m)		Aspect (°)		Dist. to Sea (km)		Slope (%)		Surface Rough.	
	Median	Mean	Median	Mean	Median	Mean	Median	Mean	Dominant	Mean
1	110	107.86	21.54	145.72	7.6	6.47	4.42	5.44	50	34.45
2	268	244.33	51.15	157.58	10.48	10.34	7.43	9.03	50	32.45
3	89	84.84	10.27	140.18	9.27	9.41	6.37	7.45	50	37.34
4	80	89.4	361	114.25	6.39	5	5.9	7.73	50	31.11
5	68	237.38	361	102.62	5.67	5.74	4.72	8.73	50	28.05
6	111	170.15	361	127.28	7.96	6.64	5.67	8.26	50	29.5
7	288	296.89	7.46	145.56	9.31	8.4	9.78	11.69	50	30.73
8	527	509.27	44.1	159.56	11.24	10.96	11.46	13.18	50	42.24
9	0	33.92	361	56.02	3.91	3.09	0	2.28	0.1	15.08
10	258	240.43	73.67	165.02	11.63	12.39	8.97	10.33	50	34.04
11	97	94.51	32.82	148.78	4.3	2.95	7.09	8.26	50	39.87
12	30	78.18	361	96.29	4.68	2.37	3.22	6.47	0.1	22.29
13	0	0.09	361	361	0	0	0	0.03	0.1	1.12
14	0	0	361	361	0	0	0	0	0.1	0.1
15	0	0	361	361	0	0	0	0	0.1	0.1
16	0	0	361	361	0	0	0	0	0.1	0.1

Another test was applied to determine the effectiveness of the mean and median values of the explanatory variables. In this test, GWR was performed using both median and mean values, and the best results were obtained by using the median results. Consequently, monthly simulations of five selected RCMs are completed with median values of explanatory variables of RCM grids.

It was necessary to determine the explanatory variable values of the prediction points in order to run GWR. The explanatory variables of prediction points were determined by using the DEM data, which was resampled to 1 km and there was no need to calculate explanatory variables in mean and median separately owing to the equality of spatial resolution of the prediction points and DEM data.

3.3 Downcaling of Monthly Precipitation and Temperature Data

After determining the best combination and representative explanatory variables of RCM grids for GWR simulations, five best RCMs among 15 were selected and GWR was performed using monthly rainfall and temperature data from these RCMs. GWR

values were produced for 1-km spatial-resolution prediction points. The average values of the prediction points were calculated for each sub-catchment and monthly GWR-based temperature and precipitation values were produced. Consequently, monthly time series climate data were produced for both the reference and future time periods for both sub-catchment areas. Finally, 25-km RCM data were downscaled to 1 km spatial resolution for sub-catchments by performing the GWR method (Figure 3.8).

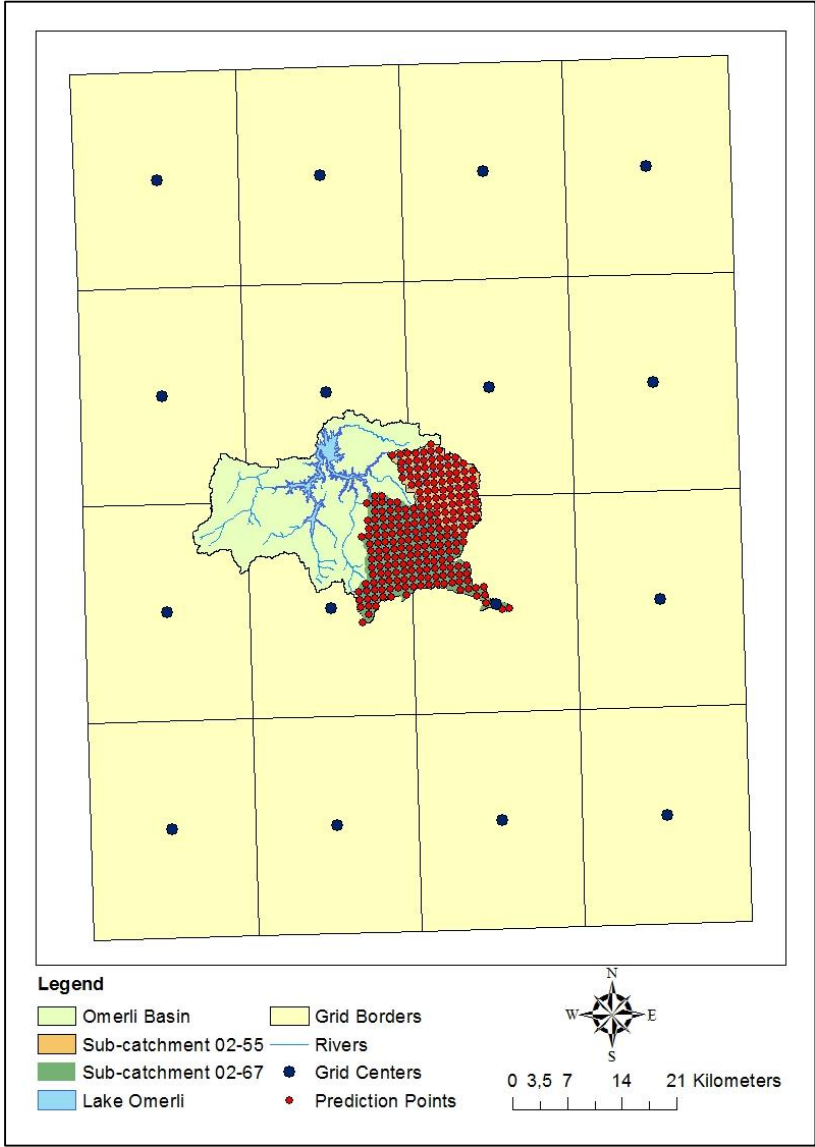


Figure 3.8 Grid centers and prediction points.

CHAPTER 4

THE HBV SETUP AND CALIBRATION

4.1 Introduction

It was necessary to calibrate the HBV model according to the catchment characteristics before performing the discharge simulations. The HBV model uses a parameter file (param.dat), which is necessary for running the model, and this file has values of some parameters (table 4.2). It was necessary to correct these parameters for each study area before running the model in order to perform accurate simulations.

The HBV model uses time series data as an input; these data were taken from meteorology stations or model simulations. Creating homogeneous temperature and precipitation data sets is a significant task for both the calibration and validation periods and the data sets used with this method must be long enough to calibrate the model (Lawrence et al. 2009). Input files with both time series daily precipitation and temperature values were generated for both of sub-catchments (02-55 and 02-67) for the period between 1978 and 2004 using the Thiessen polygons method. After the input files were generated, the calibration procedure was initiated, along with parameter estimation and minimal manual intervention.

Model calibration can be achieved both manually and automatically (Lawrence et al. 2009). For manual calibration, key parameters may be adjusted manually but this procedure is time consuming and requires the user to be experienced and skillful. Parameter selection can be computed automatically; this procedure is more efficient and may remove some potential subjectivity. Automatic parameter optimization and selection is a preferable method, as well as being more accessible and feasible. The

PEST parameter estimation routine (Doherty, 2004) has been used for the calibration of hydrological models, including the HBV. PEST refines five of the best fit models by using random sampling in order to establish feasible initial parameters. The existence of daily discharge time series data with sufficient length is another necessity for model calibration. The HBV is a runoff simulation model for forecasting purposes and it uses precipitation-temperature-discharge values (ptq.dta) as input data. In short, the HBV model has a simple structure and there are four storage components: snow, soil moisture, an upper runoff zone, and a lower runoff zone (Lawrence et al. 2009) (Figure 4.1).

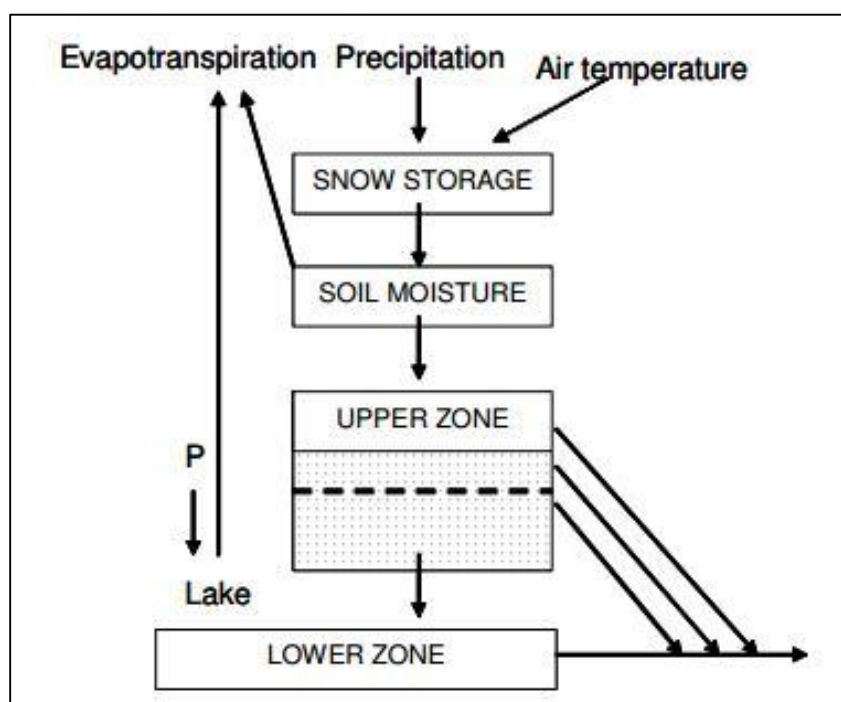


Figure 4.1 The HBV model structure: storage zones and main fluxes (Lawrence et al. 2009).

The processes within the model and the fluxes among the zones are represented by mathematical formulas that represent physical processes (Killingveit and Sælthun, 1995). These relationships are accepted to be linear and non-linear, and are controlled by selected parameters in the calibration process. The model simulates runoff values using input data that include daily precipitation and temperature values; these values

are compared with observed runoff values to acquire the best fit. The major physical properties of catchments used in the HBV model are total catchment area, hypsometric curve, and land cover types of the catchment area.

PEST is a parameter estimation procedure that uses a Gauss–Marquardt–Levenberg (GML) algorithm (Marquardt, 1963) for making an improved selection of best-fit parameters (Lawrence et al. 2009). PEST uses a Taylor expansion for defining the relationships between the parameters and simulation values in a model. PEST uses the same linear function in order to estimate new parameters and this is a superior method in comparison with determining simulation values. The linear function is used for estimating new parameters, tested by comparing newly simulated values with expected values. Comparing relative results of simulations improves the degree of convergence and more accurately determines the method of subsequent optimizations. This relative optimization is a strong benefit of PEST over the Monte-Carlo method, which utilizes random parameter selection.

4.2 Sub-catchment Properties

Some of the catchment properties that are needed for the HBV model calibration include:

- Total area
- Upper and lower limits of each of 10 elevation zones
- Altitudes of meteorology stations
- Lake areas for all elevation zones
- Glacier-covered areas
- First and secondary land cover types and land cover type of each altitude zone

Altitude and relevant information were acquired from 30-m spatial resolution ASTER GDEM data. A land-cover map of the Omerli Basin (Figure 4.2) was generated from a 30 m spatial resolution Landsat 5 TM satellite image taken in 2011.

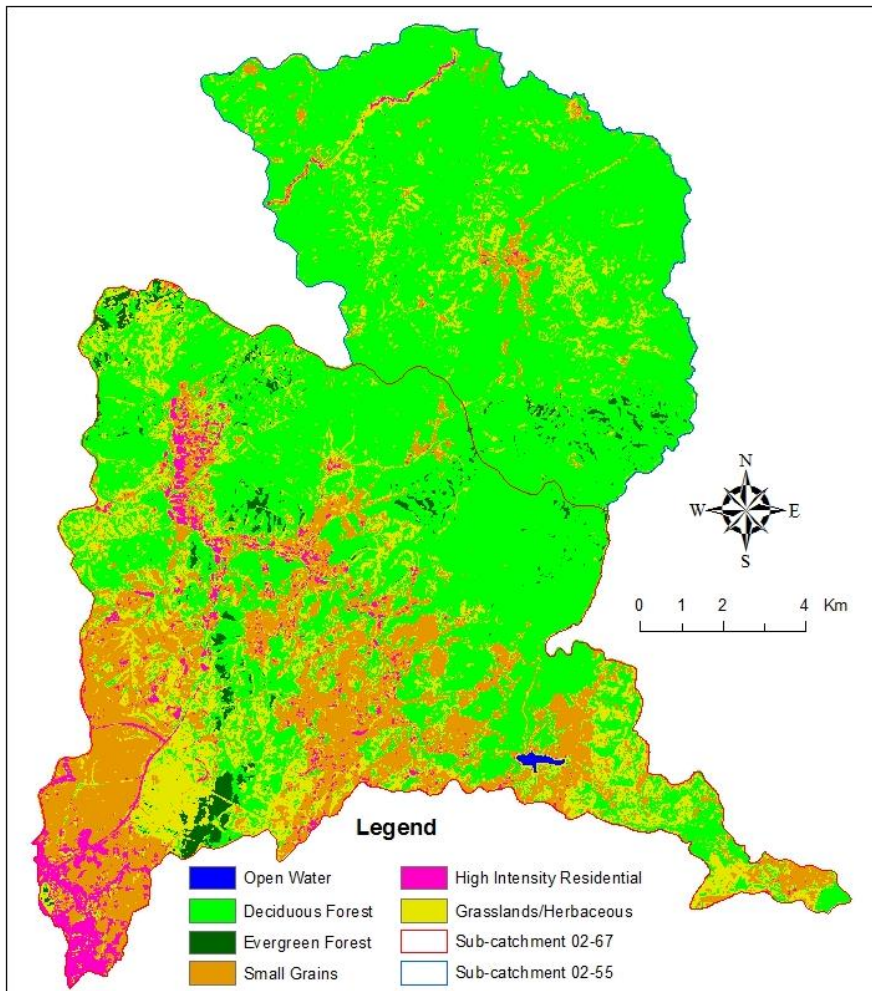


Figure 4.2 LU/LC types of sub-catchments of Omerli Basin.

Boundaries of the sub-catchments and the lake were digitized from ASTER GDEM, ArcGIS base maps, and ArcGIS 10.1 software; this process allowed the definition of the total area of the Omerli Basin and the sub-catchments. A hypsometric curve of the sub-catchments and related altitude zones (Figure 4.3 a,b) was extracted from ASTER GDEM data.

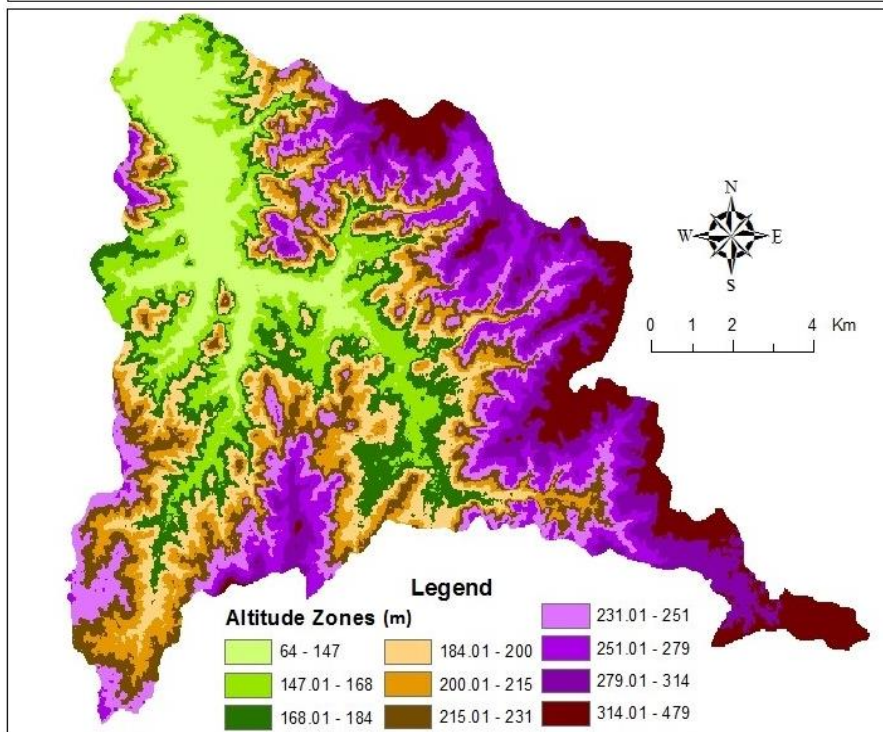
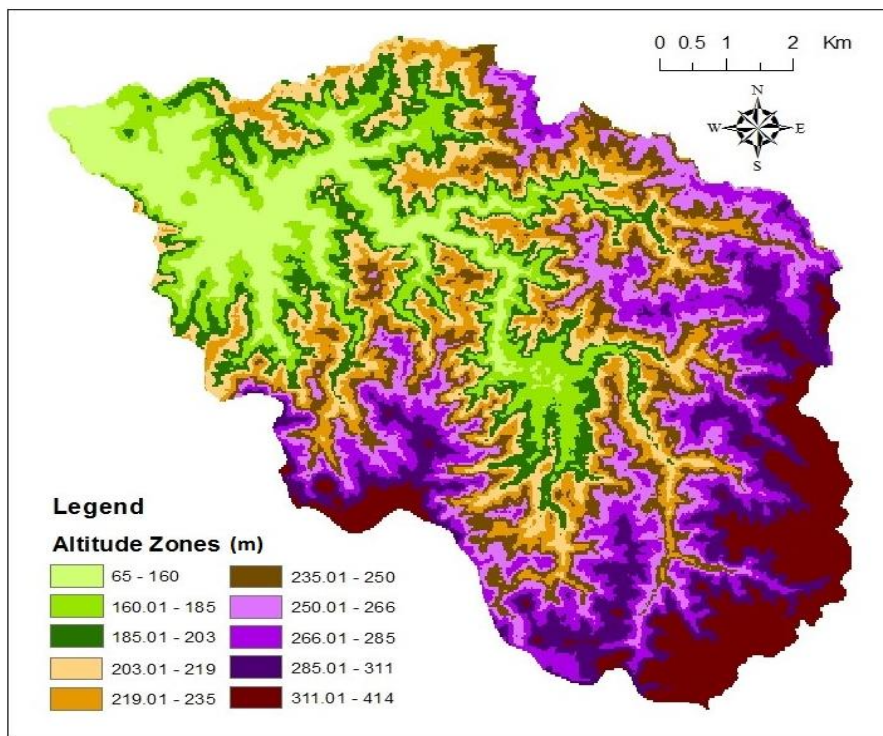


Figure 4.3 Equal area elevation zones of sub-catchment 02-55 (a-upper image) and sub-catchment 02-67 (b-lower image).

The land-cover map of the Omerli Basin was subset by each of 10 altitude zones, and primary and secondary land cover types were defined for the sub-catchments (table 4.1).

Table 4.1 Elevation zones, primary and secondary land cover types of sub-catchments

Sub-catchment 02-55			
Zone Number	Lower and Upper Limits (m)	Primary Land Cover Type	Secondary Land Cover Type
1	65-159	Deciduous Forest	Grasslands
2	160-184	Deciduous Forest	Grasslands
3	185-202	Deciduous Forest	Grasslands
4	203-218	Deciduous Forest	Grasslands
5	219-234	Deciduous Forest	Grasslands
6	235-249	Deciduous Forest	Grasslands
7	250-265	Deciduous Forest	Grasslands
8	266-284	Deciduous Forest	Grasslands
9	285-310	Deciduous Forest	Grasslands
10	311-414	Deciduous Forest	Grasslands
Sub-catchment 02-67			
Zone Number	Lower and Upper Limits (m)	Primary Land Cover Type	Secondary Land Cover Type
1	64-146	Deciduous Forest	Agricultural areas
2	147-167	Deciduous Forest	Agricultural areas
3	168-183	Deciduous Forest	Agricultural areas
4	184-199	Deciduous Forest	Agricultural areas
5	200-214	Deciduous Forest	Agricultural areas
6	215-230	Deciduous Forest	Agricultural areas
7	231-250	Deciduous Forest	Agricultural areas
8	251-278	Deciduous Forest	Grasslands
9	279-313	Deciduous Forest	Grasslands
10	314-479	Deciduous Forest	Grasslands

4.3 Calibration Procedure

The calibration and validation periods were defined and the data was divided into two parts in previous works. Initially, the HBV requires the user to input start and end dates for the simulation and these days must be arranged considering the calibration and

validation time periods. There are fifteen parameters that were used in optimization procedure and the parameter ranges were defined by Sælthun (1996) (table 4.2).

Table 4.2 The HBV parameter ranges for optimization (Recession constant: the rate of base flow decay) (Lawrence et al. 2009).

HBV Parameter	Description	Range
BETA	Soil moisture parameter	1.0 - 4.0
CX	Degree day correction factor	1.0 - 5.0
FC	Field capacity - soil zone	50.0 - 500.0
KLZ	Recession constant - lower zone	0.001 - 0.1
KUZ1	Recession constant - upper zone 1	0.01 - 1.0
KUZ2	Recession constant - upper zone 2	0.1 - 1.0
PERC	Percolation - upper to lower zone	0.5 - 2.0
PGRD	Precipitation lapse rate	0.0 - 0.1
PKORR	Rainfall correction factor	0.8 (0.4) - 3.0
SKORR	Snowfall correction factor	1.0 (0.6) - 3.0
TS	Threshold temperature for snowmelt	(-) 1.0 - 2.0
TX	Threshold temperature for rain/snow	(-) 1.0 - 2.0
TTGD	Temperature lapse rate - Clear days	(-) 1.0 - (-) 0.5
TVGD	Temperature lapse rate during precipitation	(-) 0.7 - (-) 0.3
UZ1	Threshold for quick runoff	10.0 - 100.0

PEST utilizes a local optimization procedure and it can incorporate more than one initial parameter. The initial parameters were tested by considering the Nash-Sutcliffe value, which it should be at least 0.25 for all parameters. Parameters with values are lower than 0.25 were discarded and new sets were created for testing. The Nash-Sutcliffe (N-S) value was acquired by means of a comparison of daily simulation and observation runoff values, and the total simulated and observed stream flows. After model runs were performed for the calibration period, the HBV was performed for the validation periods too. The models were ranked according to their performance in the validation period. Volumetric bias of the validation period is taken from another measurement of model performance (Lawrence et al. 2009). Finally;

- N – S value for validation period
- Volumetric bias of validation period

- N – S values for the entire simulation period (daily and weekly)
- Seasonal distribution of runoff
- Snow storage
- Cumulative distribution functions for all levels were taken into account in the selection of the final model.

Daily precipitation and discharge values were acquired for the sub-catchments for the period 1978–2004 and calibration procedure was performed for both sub-catchments. The HBV model calibration was not completed for sub-catchment 02-55 owing to inconsistencies between the daily discharge and daily precipitation values (Figure 4.4 a). For example, in this figure some constant low flow values that are not consistent with precipitation input are seen for 02-55 sub-basin. The division of the data for calibration and validation purposes for both catchments is also shown in this figure. The N–S value was negative (–) for sub-catchment 02-55. The range of N–S values lies between 1 and $-\infty$. An efficiency value of “1” states perfect matching of model values with observed data. An efficiency of “0” claims equality of model predictions with observation data. Negative values (–) mean that values of observed time series would have been a better predictor than the model (Krause *et al.* 2005). As mentioned above, precipitation–discharge consistency was better in the 02-67 sub-catchment (see Fig. 4.4b) and therefore, calibration procedure was applied successfully for this catchment. The N–S calibration value was 0.63 for sub-catchment 02-67 and this value lies within the acceptable range of PEST which is between 0.60 and 1. Finally, it was not possible to generate a parameter file for sub-catchment 02-55 and the subsequent work focused on only sub-catchment 02-67.

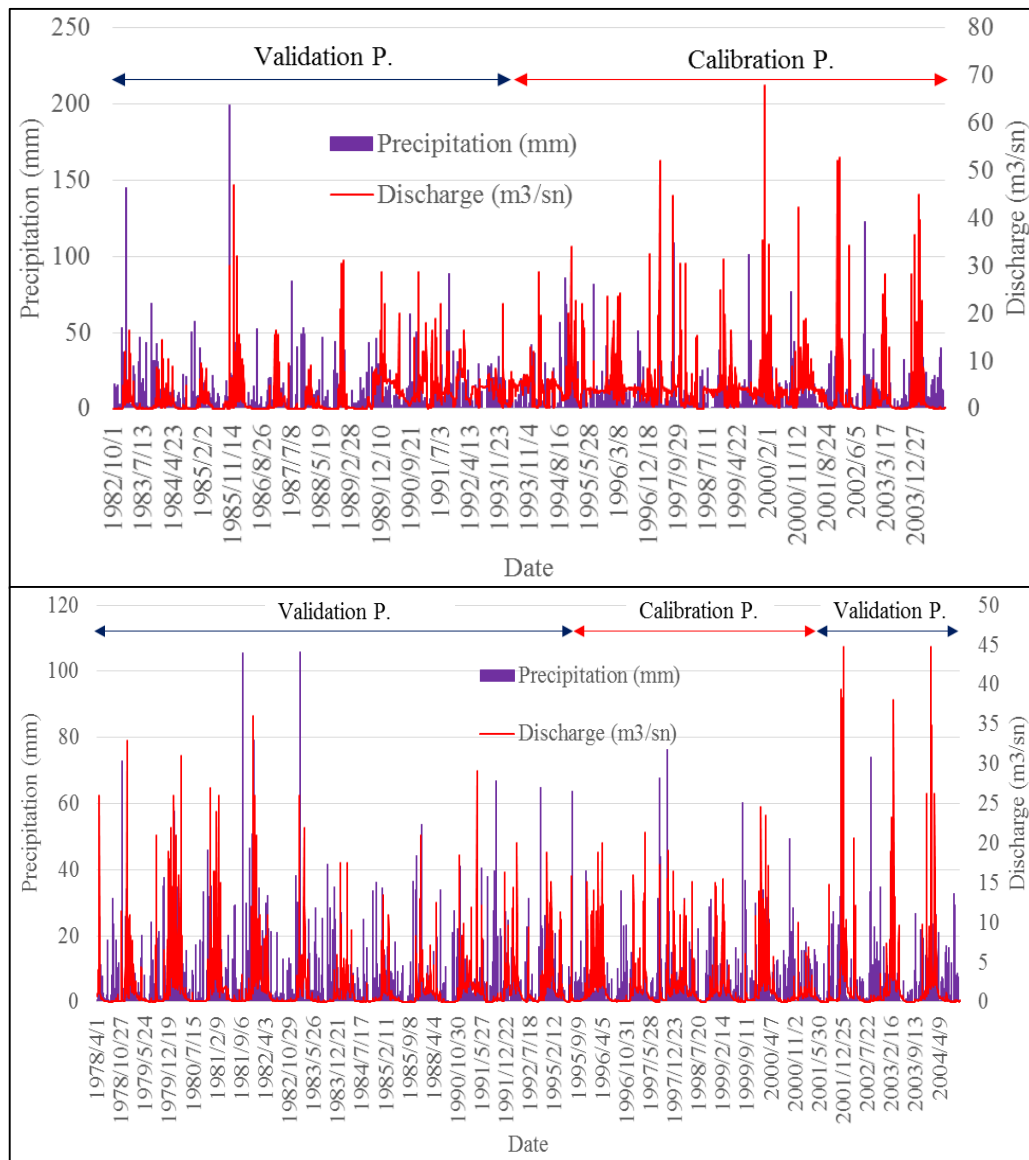


Figure 4.4 Daily precipitation and discharge values of sub-catchment 02-55 (a-upper image) and sub-catchment 02-67 (b-lower image).

The calibration process using two different segments of observed climate and discharge data sets in 02-67 basin is applied. The generated parameter files (param1.dat and param2.dat) are used to run the HBV model for validation. Figure 4.5 shows scatter plots between simulated and observed daily discharges for two calibration processes and their validation results. As it appears, the second calibration and validation results release better statistics in RMSE and correlation coefficient values than the first calibration. This better behavior with observed discharges from

the second calibration is also seen on monthly time series of simulated and observed discharges during calibration and validation periods (see Fig. 4.6 for first calibration and 4.7 for second calibration).

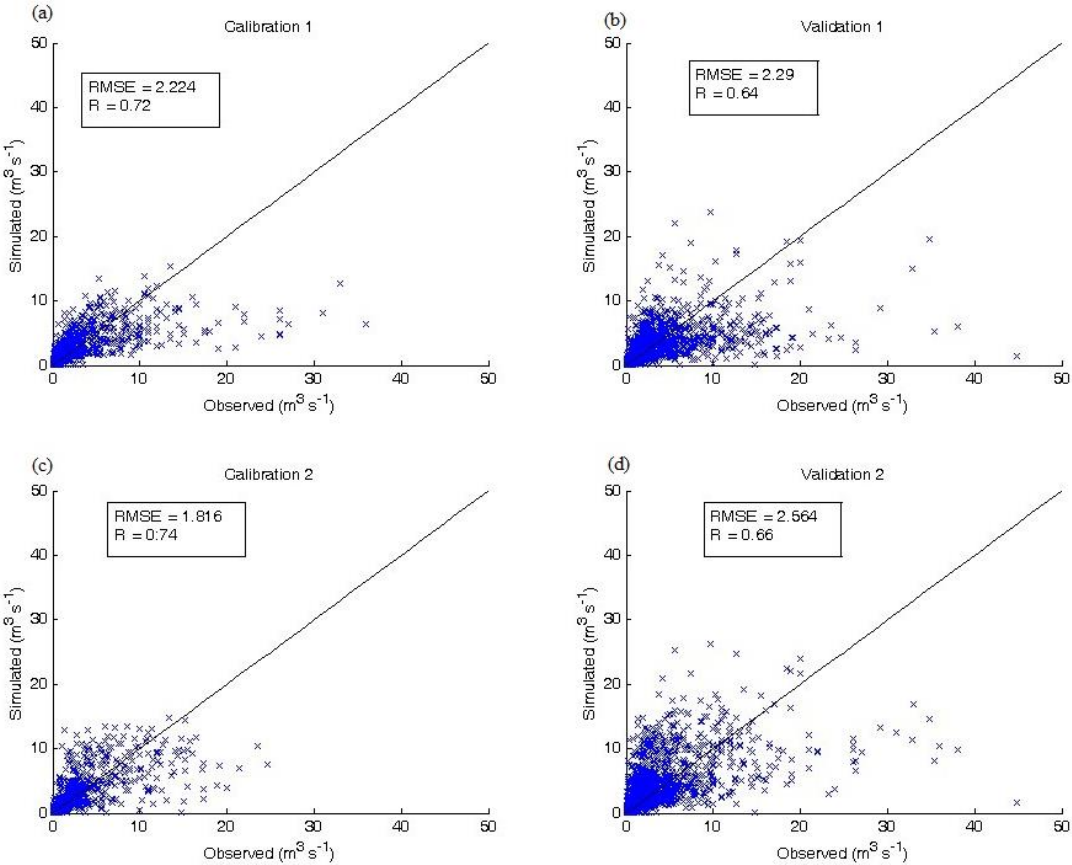


Figure 4.5 Scatterplots created by param1.dat (a, b) and param2.dat (c,d) files.

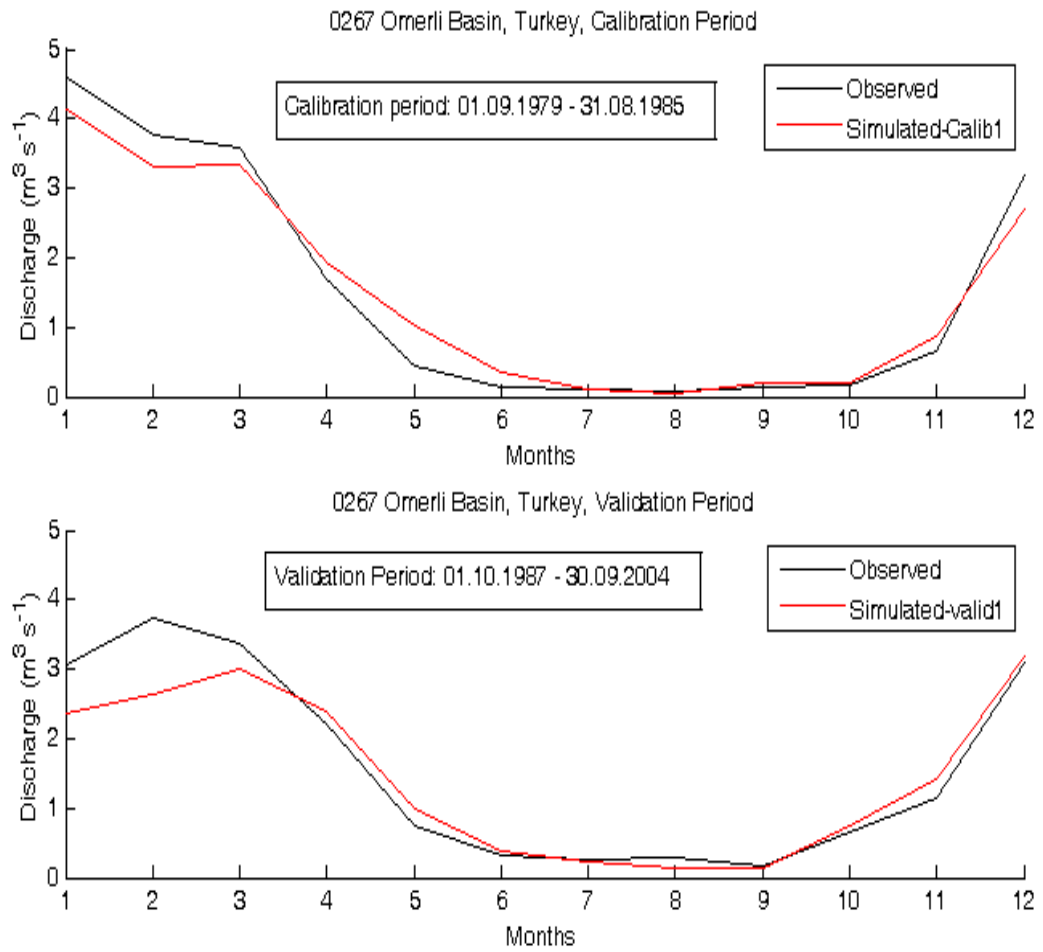


Figure 4.6 The HBV Calibration Results by Param1.dat file for Sub-catchment 02-67.

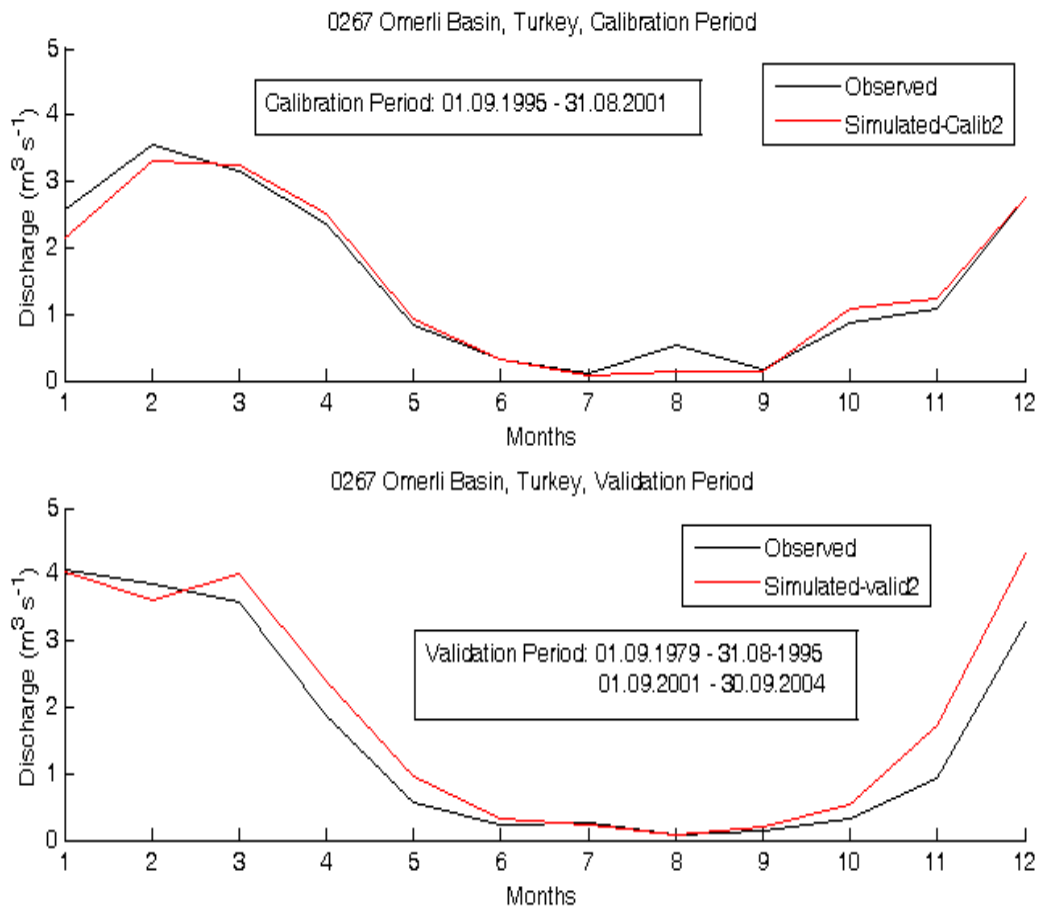


Figure 4.7 The HBV Calibration Results by Param2.dat file for Sub-catchment 02-67.

Following calibration, the HBV model was applied with the daily observed precipitation and temperature values in order to test the performance of the model. The HBV model demonstrated a very good performance in simulating the discharge, and the actual observed discharge values were very close to simulated values. The HBV performance was good in simulating the cumulative runoff values and there were only some small underestimations due to underestimating high flows (Figure 4.8).

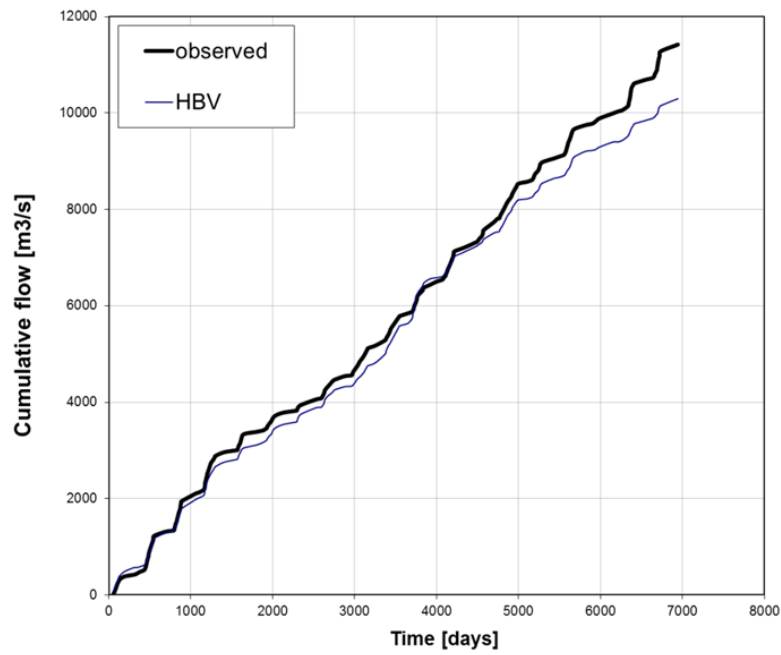


Figure 4.8 Simulated versus observed cumulative volumes.

The HBV displayed a weak performance in simulating extreme values and demonstrated a strong systematic underestimation of peak flow quantiles in the frequency distribution (Figure 4.9).

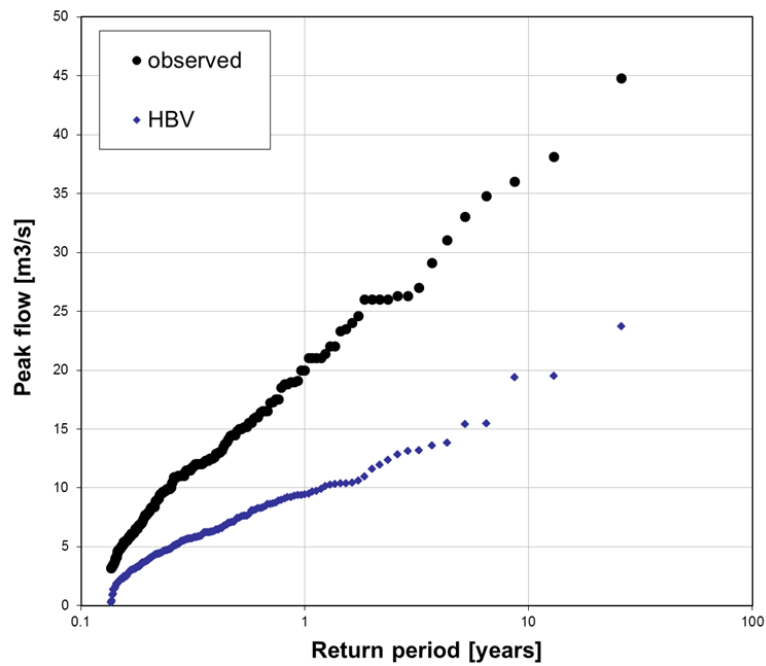


Figure 4.9 Simulated versus observed empirical peak flow distribution.

CHAPTER 5

PRECIPITATION ANALYSIS

Precipitation analyses were conducted by comparison of three types of data: (a) daily RCMs simulations, (b) monthly RCMs simulations, and (c) monthly GWR-based interpolation results in sub-catchment 02-67. As it is mentioned in Chapter 4 the HBV model is poorly calibrated for sub-catchment 02-55 and therefore, precipitation and discharge analyses were only conducted for sub-catchment 02-67 in Omerli Basin.

5.1 General Precipitation Evaluation for RCMs and GWR

General performance of RCMs and downscaled technique is evaluated for the reference period (1961-1990) in daily and monthly timesteps in order to check their skills and deficiencies. This assessment helps us to know how reliable the future (2071-2100) projections obtained from each GCM/RCM system.

Figure 5.1 and 5.2 displays time series of averaged daily precipitation from observation (bold-blue line) and 15 RCM models for reference period (1961-1990) and future period (2071-2100), respectively. According to Figure 5.1, simulation values of RCMs are usually below observations in reference period. In addition, there are also some occasions especially during spring period RCM simulations show overestimation feature. During summer, there is a distinct feature that only one model (SMHIRCA ECHAM5) significantly overestimates precipitation probably due to its convective scheme that is very sensitive to produce unstable boundary layer.

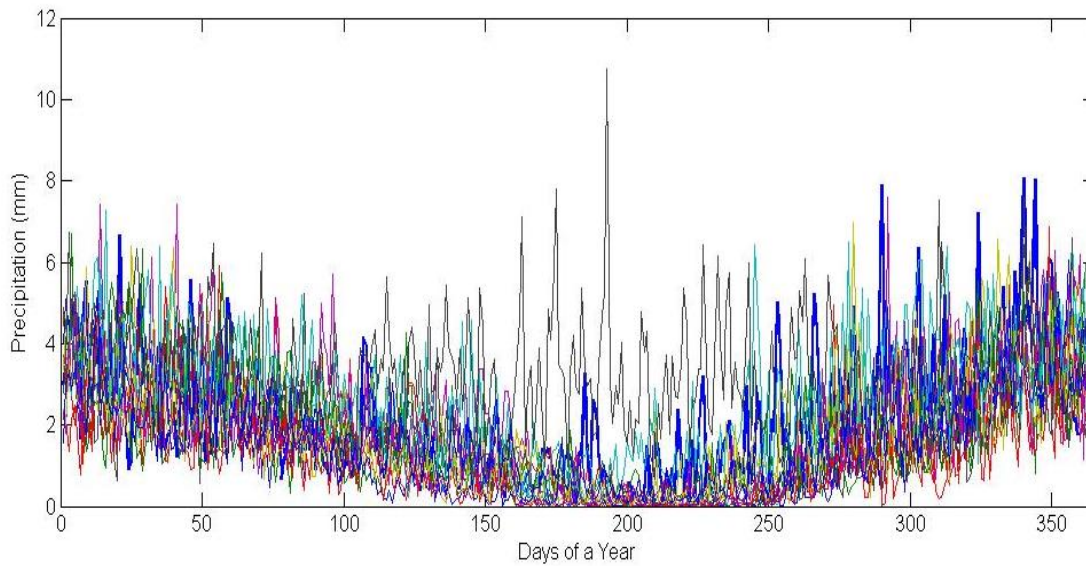


Figure 5.1 Comparison of observed (bold-blue line) and modelled precipitation values for sub-catchment 02-67 between 1961 and 1990.

The variability in producing precipitation among RCMs is smaller and more compact especially during winter and spring periods in future period (Figure 5.2) and there is no isolated feature from any RCMs along with the year. In this figure, as a reference or to observe the deviations of simulations from the reference line observed precipitation is also shown.

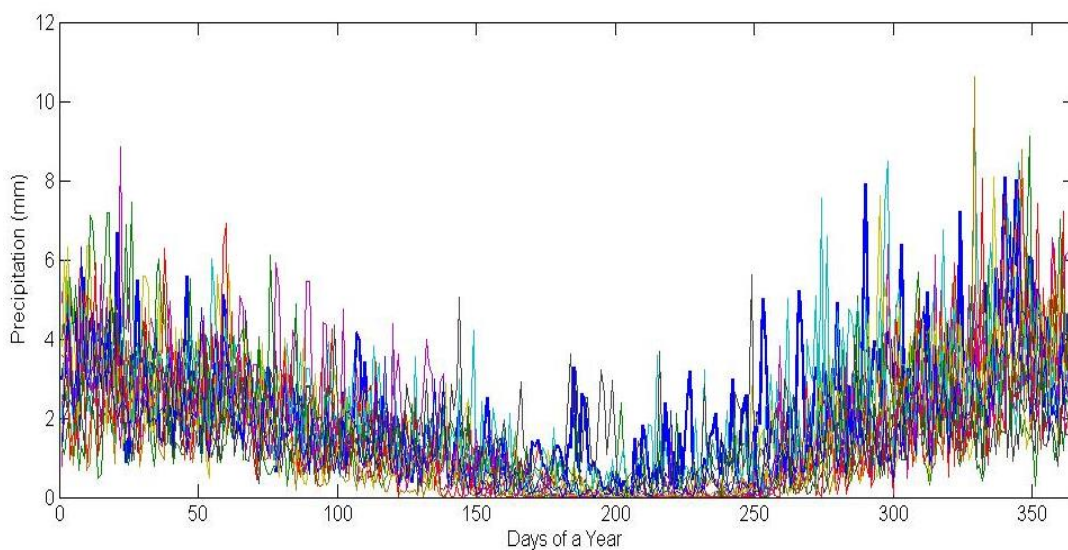


Figure 5.2 Comparison of observed (bold-blue line) and modelled precipitation values for sub-catchment 02-67 between 2071 and 2100. Observation values belong to years between 1961 and 1990.

Along reference period using 30 years data, daily precipitation of 15 RCMs are averaged to show the general trend with respect to observed precipitation in Figure 5.3. In this figure, standard deviations of 15 RCMs as error bars (standard deviation values (SD)) are also shown. Average observed precipitation generally lies within the range of RCMs but the model values generally show weak performance on following the extreme rainfall peaks. This weakness is more pronounced during fall season toward winter.

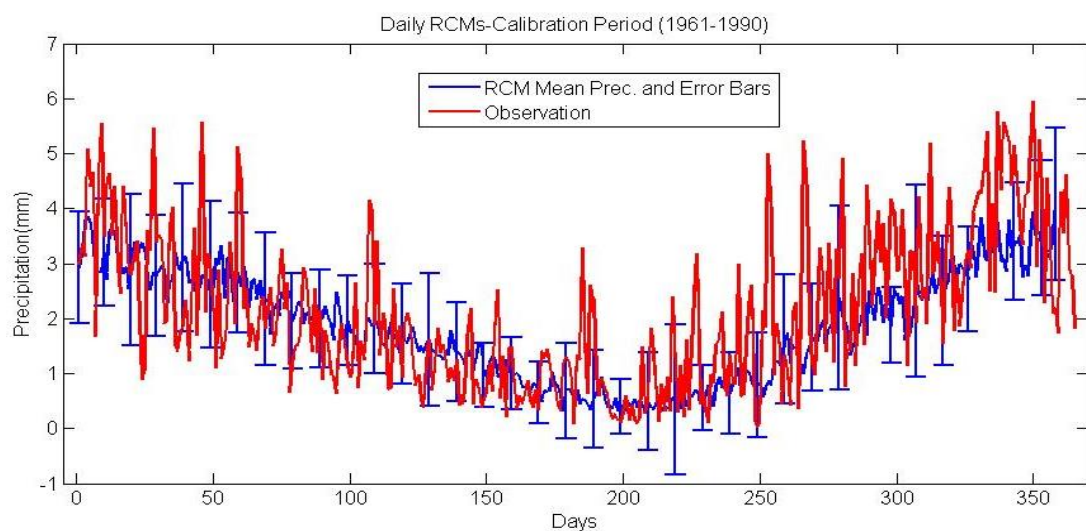


Figure 5.3 Comparison of observed precipitations and RCM mean precipitations.

Figure 5.4 show comparisons of averaged monthly precipitation from 15 RCMs and observation averaged over reference period in (a) for original RCMs and in (b) for GWR downscaled RCM precipitation. RCM values are very similar to observations in monthly mean precipitation from February to June in the year but there is some discrepancy between observed and model-derived monthly mean precipitation in other months with and without application of GWR. However, with GWR such discrepancy is almost removed except summer. This explains that some of the downscaled RCMs are matching well with observation. Another improvement from GWR is that SD values of downscaled RCMs up to fall season are substantially lower than those of original RCMs and this indicates a similar performance from all RCMs in capturing the observed winter and spring precipitation. From February to May, RCMs slightly

overestimate monthly precipitation while they underestimate it from June to January. GWR tries to correct these features of estimation during spring and fall seasons along which there is a great match with observation.

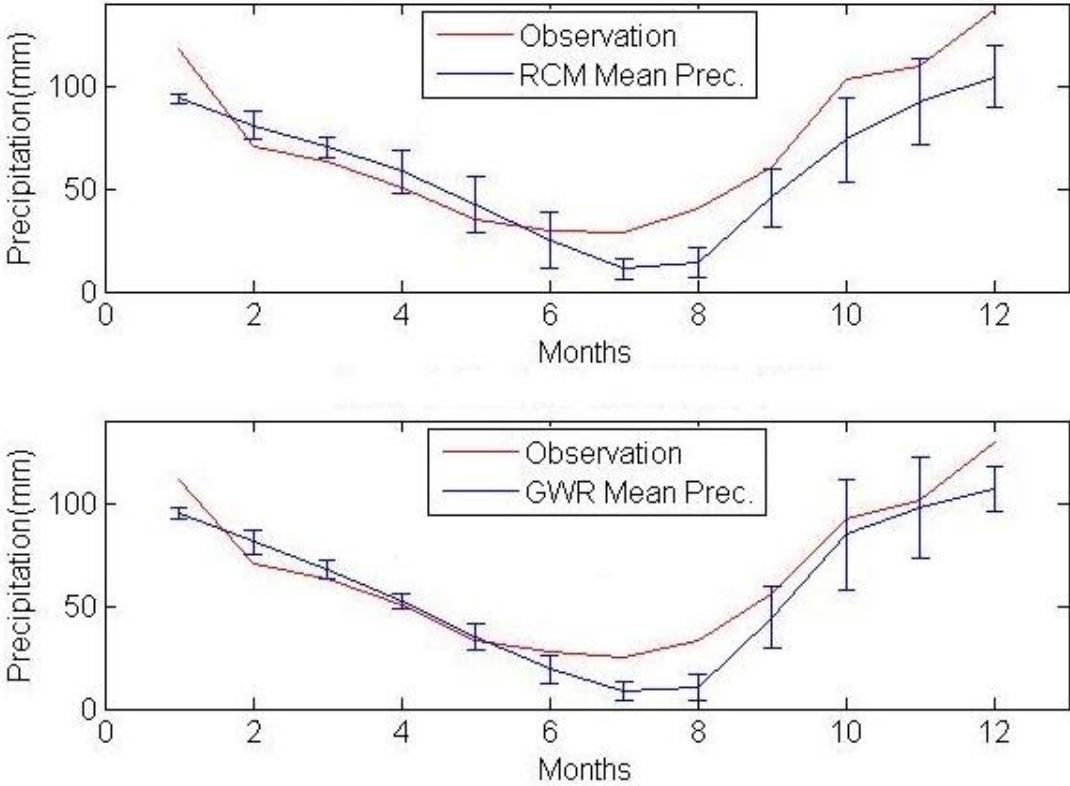


Figure 5.4 Comparison of RCMs averages and observation values for reference period. Standard deviation values are also imposed to the figures.

Figure 5.5 shows scatterplots between observation and mean of 5 RCMs for monthly mean precipitation with and without GWR method for reference period (1961-1990). It appears that data pairs with GWR method are more scattered but the underestimation behavior of RCMs is slightly reduced. Downscaling method enhances the extreme precipitation that is poorly resolved by coarse RCM grid. This is another example of goodness of GWR method over RCMs averages. Moreover, with more scattered distribution from GWR the general statistics of bias and correlation coefficient values are better than those from RCMs without GWR method. RMSE values are 20.12 mm and 14.3 mm for RCM and GWR; bias values are 0.27 mm and 0.14 mm for RCM and GWR; and correlation coefficient values are 0.94 for both RCM and GWR.

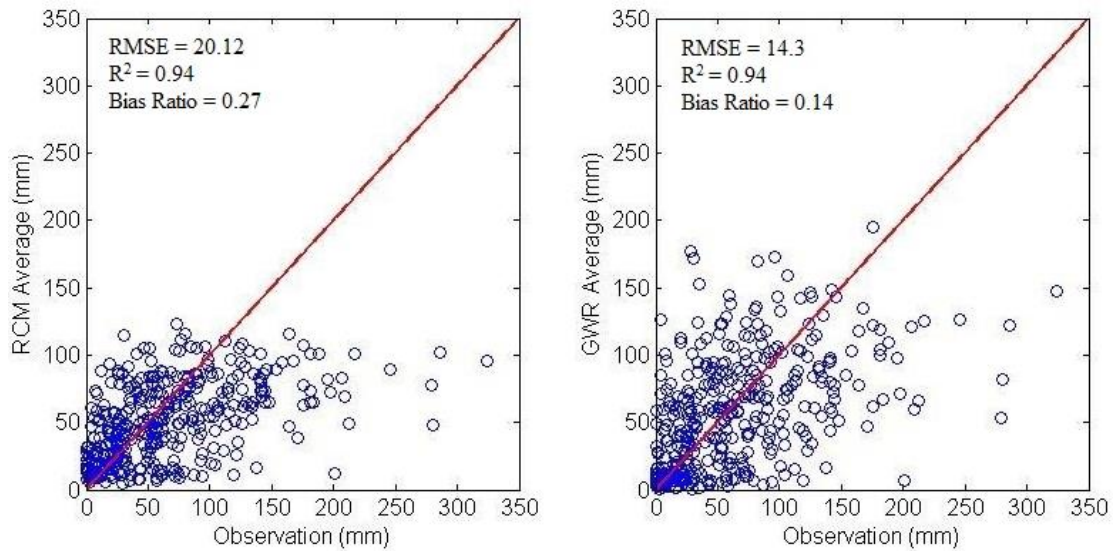


Figure 5.5 Comparison of observed and modeled precipitation values in scatterplots for reference period.

5.2. Extreme Precipitation Index Calculation

Extreme weather events are defined as “the occurrence of a value of a weather or climate variable above (or below) a threshold value near the upper (or lower) ends of the range of observed values of the variables” (IPCC, 2012). Characteristics of precipitation extremes with respect to seasons and all year are also evaluated to assess the changes in extreme precipitation in Omerli catchment using RCMs with and without downscaling GWR method. Both model performance and future changes in extreme precipitation events are assessed by calculating the extreme precipitation index (EPI). The outputs from following two subsections are analysed using EPI.

EPI is defined as the average change in extreme precipitation higher than a defined return period. In this study, the return period is set equal to 1 and 5 yrs. EPI is estimated separately for each GWR, RCM, threshold return period, season and temporal aggregation for Omerli sub-catchment of 02-67. Four seasons are considered: winter (December to February), spring (March to May), summer (June to August), and autumn (September to November). Additionally, the index is estimated considering the whole time series, i.e. without dividing in seasons. The temporal aggregations

considered are 1, 2, 5, 10, and 30 days. These are estimated using a moving average from the daily time series.

The first step in the calculation of EPI is to extract the extreme value series from the precipitation time series. The Peak Over Threshold (POT) method is used for this purpose. Peaks are extracted by using the 1- and 5-yr threshold return periods. For example, with a 30-yr record, the 30 and 6 most extreme events are included in the extreme series for the 1- and 5-yr threshold levels, respectively. An independence criterion based on the inter-event time is applied to make sure that extreme values are independent, i.e. only values separated by more than Δt days are considered. Δt is set equal to the temporal aggregation, i.e. for an aggregation time of 1 day, events must be separated by more than one day. EPI is then estimated as:

$$EPI = \frac{\overline{POT}_2}{\overline{POT}_1} \quad (1)$$

where \overline{POT}_1 and \overline{POT}_2 are the averages of the selected POT values used as reference (observation) and scenario (referenced RCMs), respectively. EPI takes the value of 1 if no change is estimated from reference to scenario and greater (less) than 1 if the average extreme precipitation is higher (lower) in the scenario time series.

5.2.1 Extreme precipitation evaluation for RCMs and GWR

In this section, the performance of RCMs with and without downscaling method in extreme precipitation events during four seasons and yearly period is investigated. For this analysis, EPI value is calculated between observation and original RCMs and observation and downscaled RCMs for the reference period. With these analyses, we measure the error of the GWR method in downscaling the RCM outputs for extreme precipitation and evaluate the performance of the RCMs in simulating extreme precipitation, and thus they allow us to assess whether the error in the downscaled time series is smaller than in the RCMs.

Figure 5.6 shows box plots of extreme precipitation index values for 5 RCMs along with 5 different time aggregation periods, four seasons, and full year for 1-yr and 5 – yr threshold return periods while Figure 5.7 shows equivalent plots for downscaled RCM precipitation with GWR method. In all seasons, RCMs underestimate the extreme precipitation as index values stay below 1 for both return periods (see Figure 5.6). The highest errors in extreme precipitation occur with spring and fall season while the lowest errors first appear with winter and then summer periods. As aggregation time (search window for moving average) increases from 1 day to 30 days the error decreases or the median value approaches the index value of 1 for all seasons and full year data. With the application of GWR method in Figure 5.7, the errors in extreme precipitation series are greatly reduced in all seasons for both return periods. Underestimation behavior of RCMs is largely reduced for all seasons and full year by approaching the boxes and median values to index value 1 with the application of GWR method. For example, all median values of boxes in winter period show index values greater than 1 and this means that downscaled RCMs overestimate the observed extreme precipitation series.

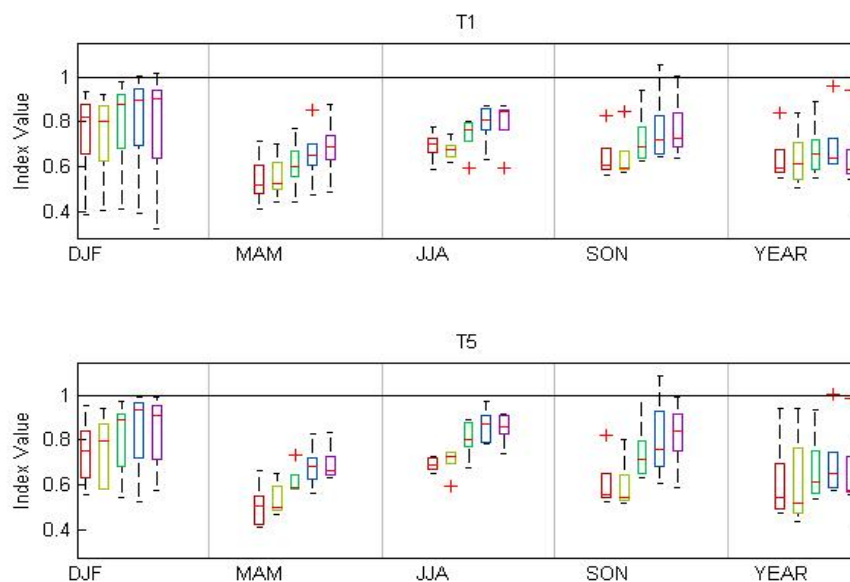


Figure 5.6 Performance test of 5 RCMs in index value calculation for 1 year and 5 year analysis time. Each boxes are representing different search window such as red box (1.) 1 day, yellow box (2.) 2 days, green box (3.) 5 days, blue box (4.) 10 days, and purple box (5.) 30 days.

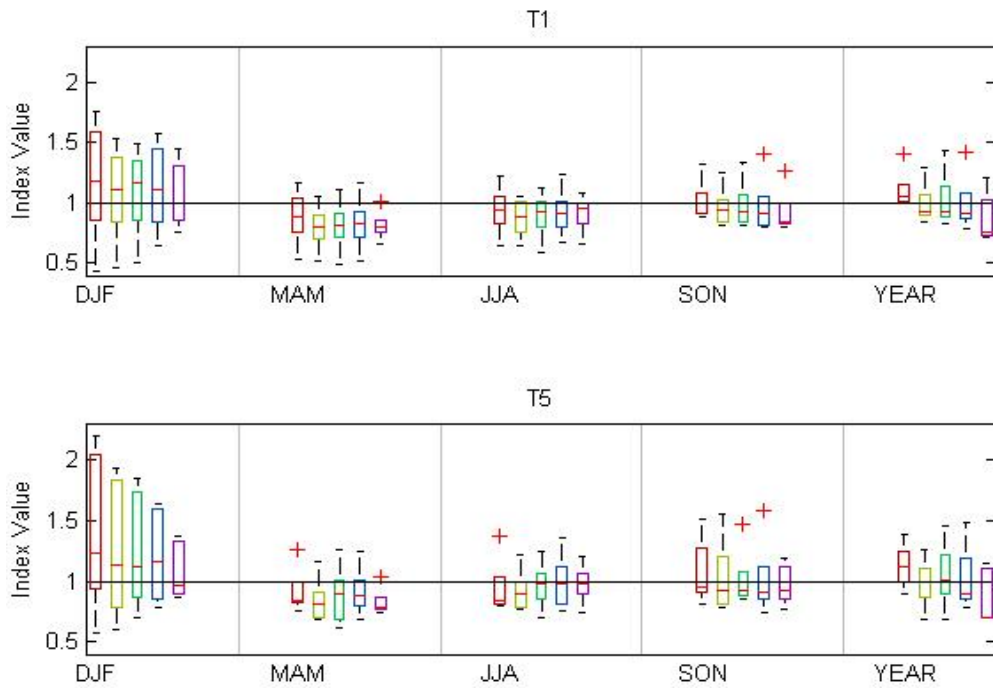


Figure 5.7 Performance test of 5 GWRs in index value calculation for 1 year and 5 year analysis time.

5.2.2 Changes in extreme precipitation

In this section, EPI is used to compare the changes in the original RCMs and the downscaled RCMs time series from reference to future. This allows us to compare the changes estimated from the downscaled precipitation through GWR to the changes projected by the RCMs.

Figure 5.8 shows box plots of EPI values representing 15 RCMs for 1-yr and 5-yr threshold return periods for 1, 2, 5, 10, and 30 days of aggregation time along with seasons and all year. In general, winter, spring, and summer periods show an increase in extreme precipitation at all time aggregation periods (search window) because median values of 15 RCMs always stay above index value of 1 during these seasons. Among these seasons the highest increase in extreme precipitation is obtained with summer period particularly with 10 and 30 days search windows. For example, median value of index is greater than 1.5 for summer while with other seasons (winter and spring) its index values are around 1.1. Only decrease in extreme precipitation is

obtained with 1 and 2 days search windows in fall season but other search windows in this season also show an increase in extreme precipitation according to their median index values. Therefore, the trend of the change in extreme precipitation is not consistent with fall season. When evaluating the yearly index values, the change in extreme precipitation from reference to future does not appear for 5, 10, and 30 search windows as their median index values are almost 1 with very small box sizes. However, 1 and 2 days search windows indicate an important decrease in extreme precipitation that is mostly influenced by precipitation decrease in fall season with the same search windows. Nevertheless, yearly extreme precipitation analyses do not reflect important increases in extreme precipitation especially with summer. With 5-yr threshold return period these behaviors are more pronounced as extreme precipitation events become more significant.

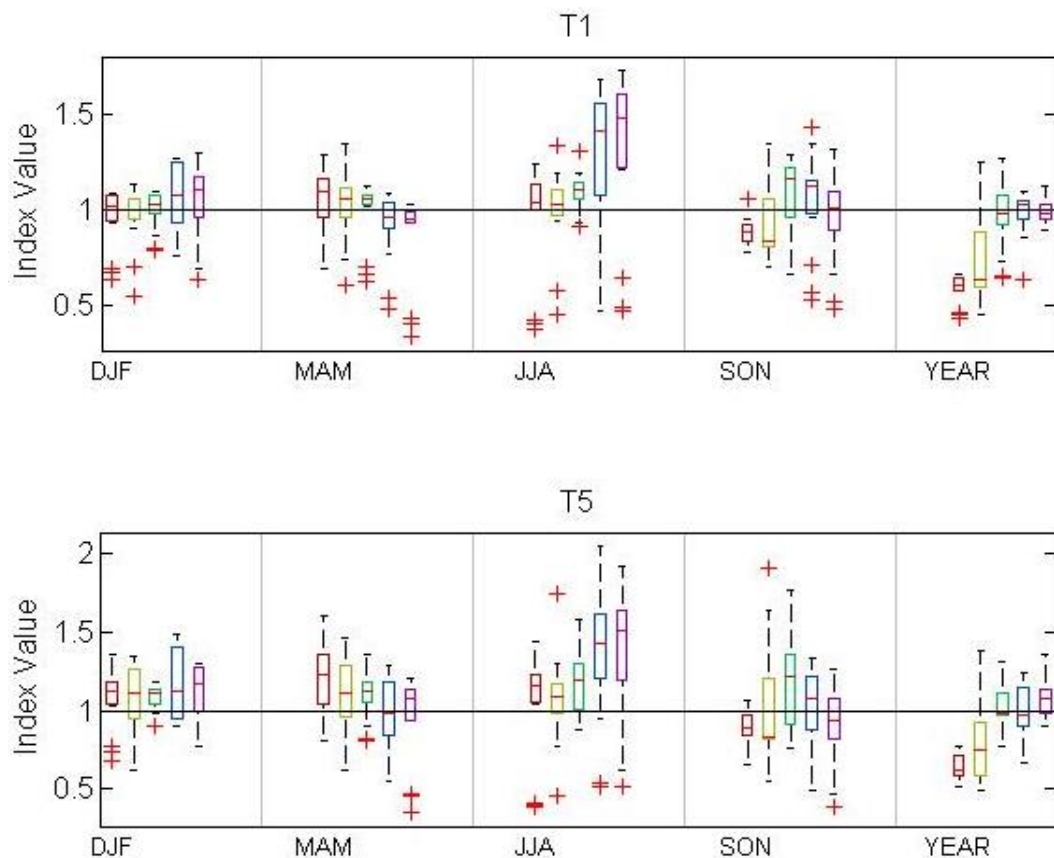


Figure 5.8 Index values of extreme precipitations of daily RCMs for 1 and 5 year time periods. Each boxes are representing different search window such as red box (1.) 1 day, yellow box (2.) 2 days, green box (3.) 5 days, blue box (4.) 10 days, and purple box (5.) 30 days.

Since GWR is applied for monthly precipitation data daily extreme value analyses are performed by distributing the monthly precipitation totals into daily using distribution derived from 30 years of observed precipitation. Figure 5.9 shows box plots of extreme index values from GWR derived precipitation using 5 RCMs models within each box for 1-yr and 5-yr threshold return periods. With 1-yr threshold, median values of each box for all search windows extreme index values are always greater than 1 for winter, spring, and summer periods while they are always lower than 1 for fall season and all year analyses. The seasonal extreme precipitation trend such as increase in winter, spring, and summer and decrease in fall is more consistent but small in magnitude when they are compared with original RCMs (see Figure 5.6). Yearly analyses only show decrease in extreme precipitation from reference to future period. When extreme events are represented with 5-yr return period the variability among downscaled 5 RCMs (box size increases) increases. Thus, the consistency of extreme index change along with search windows loses. For all search windows, only the fall season analyses still show important decrease in extreme precipitation for 5-yr return value.

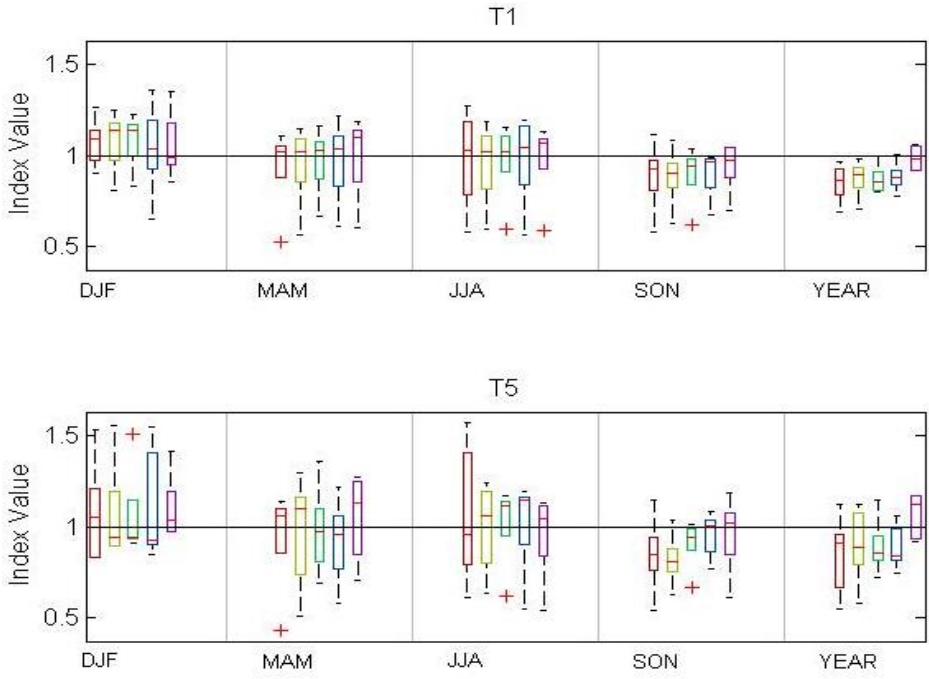


Figure 5.9 Index values of extreme precipitations of daily GWRs for 1 and 5 year time period. Each boxes are representing different search window such as red box (1.) 1 day, yellow box (2.) 2 days, green box (3.) 5 days, blue box (4.) 10 days, and purple box (5.) 30 days.

5.3 Frequency Analysis

Frequency analyses are conducted using data series of maximum daily peak and maximum monthly peak precipitations in the year for observed and RCM-derived precipitation with and without GWR method during reference and future periods. According to our test maximum precipitation data is best represented by log-normal distribution such frequency analyses are performed by this distribution function. Figure 5.10 shows probability of non-exceedance versus daily precipitation peaks from observation and 15 RCMs during calibration and future periods. For lowest precipitation amounts (10-25 mm) in general all RCMs show close probability of exceedance with observation but for higher precipitation amounts such skill is lost among RCMs with substantial underestimation tendency. Only one of 15 RCMs' (SMHIRCA-BCM) indicates overestimation for a given exceedance probability along with the range of maximum daily precipitation in reference period (1961-1990). There is great variability among RCMs in estimating the probability of exceedance values towards higher maximum precipitation amounts. SMHIRCA ECHAM5 model follows the observed frequency curve better than other models. In future period, the variability in estimating exceedance probability for higher precipitation amounts is smaller comparing to reference period. This explains that almost all models tend to estimate higher precipitation amount for a given probability of exceedance in future period. SMHIRCA-BCM that was the only model showed overestimation behavior during reference period shows now lower estimates for a given same exceedance probability in future period. Furthermore, two of 15 models (METO-HADRM3Q3 and SMHIRCA-HadCM3Q16) show no frequency curve for the future period (Figure 5.10).

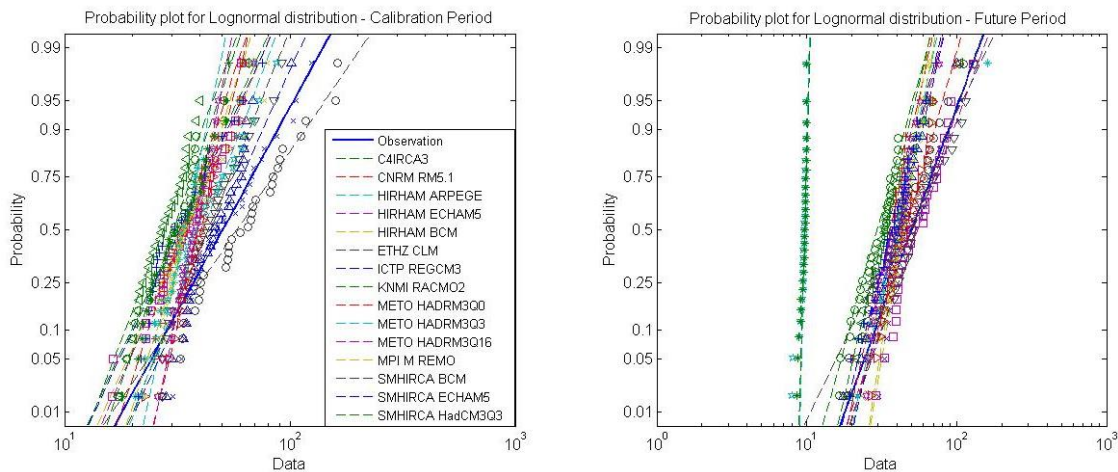


Figure 5.10 Probability of extreme precipitations of observation and modeled daily RCMs for reference and future period.

The impact of downscaling on frequency curves is investigated for maximum monthly precipitation in annual series during reference and future periods. Figure 5.11 shows frequency curves of maximum monthly precipitation for observation and 5 RCMs during reference and future periods while Figure 5.12 shows equivalent plots for downscaled RCM precipitation obtained through GWR method. The skill of following observed frequency curve from all RCMs is improved for all exceedance probability values with the application of GWR method (see Figure 5.11). The underestimation behavior of original RCMs towards higher precipitation magnitudes is reduced with downscaling method so that the magnitudes of extreme monthly precipitation is increased for a given exceedance probability or return period. For example, with GWR method ETHZ CLM model overestimates precipitation amount for all range of probability values. With and without GWR method MPI M REMO model releases the best performance in following the observed frequency curve. In future period, with the exception of SMHIRCA HADCM3Q3 all RCMs provide higher monthly precipitation amounts for given exceedance probability than those in reference period. This feature is more developed when downscaling method is applied to RCMs precipitation.

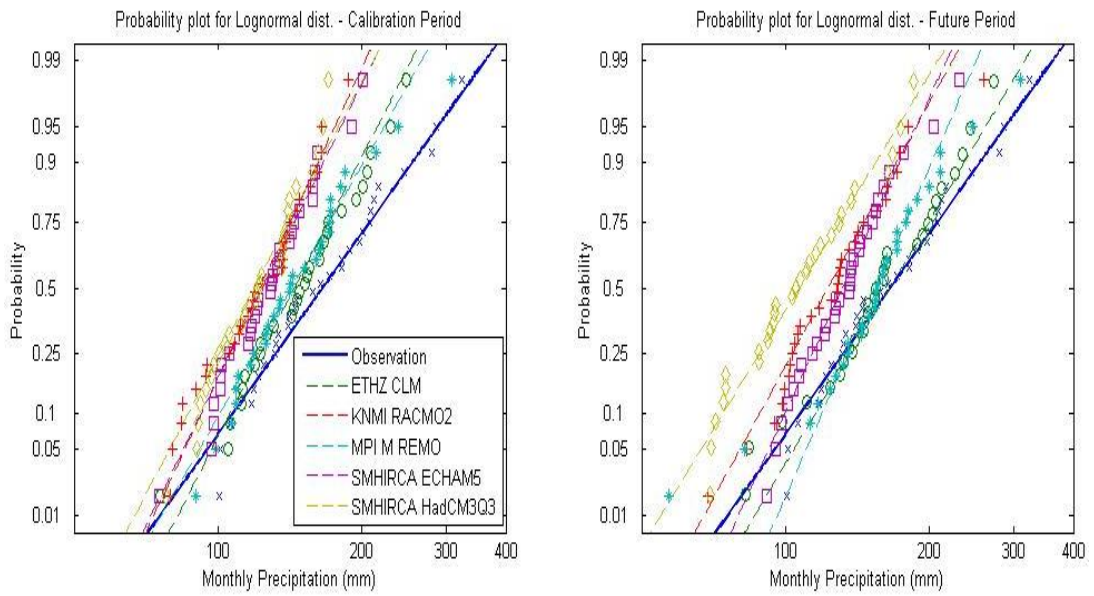


Figure 5.11 Probability of extreme precipitations of observation and modeled monthly RCMs for reference and future period.

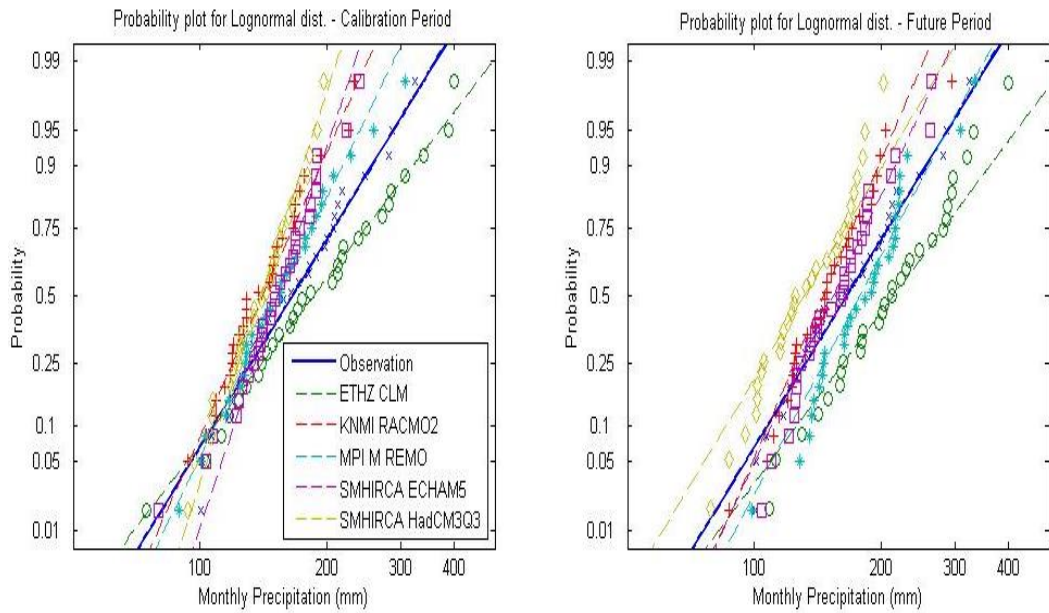


Figure 5.12 Probability of extreme precipitations of observation and modeled monthly GWRs for reference and future period.

CHAPTER 6

DISCHARGE ANALYSIS

The HBV Model requires daily precipitation and temperature as input. The model has been calibrated and validated using observed daily climate and river discharge data available in the sub-catchment (02-67) of Omerli Basin. The calibrated HBV Model is applied with inputs of daily precipitation and temperature from RCMs with and without GWR method for reference and future periods.

6.1 Model Performance Evaluation

Daily discharges derived from HBV model using RCM data with and without downscaling method are evaluated by making comparison with observed discharges available during reference period (1961-1990). Figure 6.1 shows comparison of time series between observed and HBV-derived daily discharges using input from each of 15 RCMs in (a) and input from each of downscaled 5 RCMs results in (b) during reference period. Since we used only 5 RCMs in GWR method these 5 RCMs are represented with the same legend in 15 RCMs. Hydrologic regime of Omerli Basin shows that observed discharges with frequent extreme events occur during winter, spring and fall seasons depending on existence of frontal and convective weather systems in the region. Summer months are usually dry and therefore, hydrologic regime in this season is dominated by base flows. Depending on precipitation input to the HBV model, simulated discharges are well underestimated during the calendar year (Fig 6.1 a and b). During wet season, dominantly winter season fluctuations in observed discharges are somehow followed by several RCMs with the significant underestimation tendency. However, some RCMs do not show any skill at all in capturing these observed trends. During dry season (summer) simulated discharges

match with observation as no important precipitation events are available from RCMs input. With using downscaled RCM input in HBV, still significant underestimation tendency exist in simulations but there are some increases in the magnitude of extreme discharges particularly events seen towards the end of the year (see Fig 6.1b).

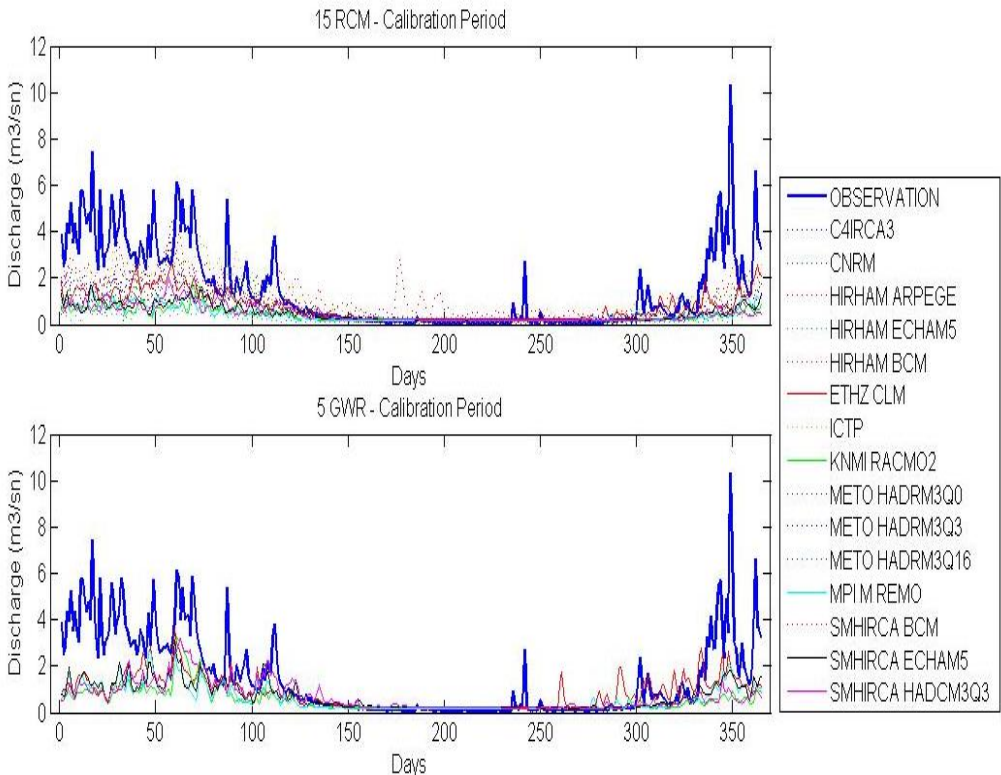


Figure 6.1 Comparison of RCMs and GWRs with observed discharge values for reference (1961-1990) period.

Figure 6.2 shows the similar comparison between observed (1961-1990) and simulated discharges for future period (2071-2100). Depending on the variability of RCMs input there is generally decrease in future discharge values in Ömerli Basin. That is visible both from RCMs and downscaled RCMs inputs.

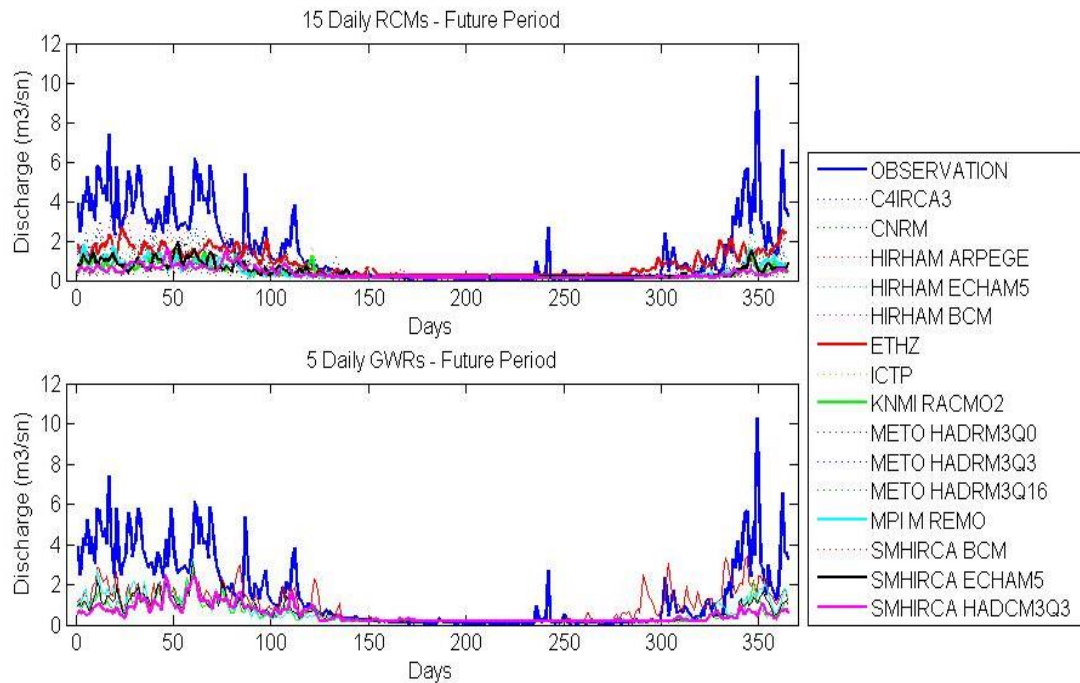


Figure 6.2 Comparison of daily discharges derived using RCMs and GWRs input values for future (2071-2100) period. As a reference observed daily discharges from reference period are also shown.

Overall skill of RCM-derived HBV model with and without GWR downscaling method is also tested with the mean discharge simulations of 5 RCMs inputs that are used in GWR method. Figure 6.3 shows comparison of mean discharges from 5 RCMs, downscaled 5 RCMs and observation. In this plot, corresponding mean precipitation data sets are also shown. Fluctuations in observed discharges are better matched with downscaled GWR data. However, there is still substantial discrepancy between observed discharge and modeled discharge with and without downscaling method. Overall, there is a positive performance in discharge simulations provided by GWR method as the downscaling corrects the magnitude of extreme precipitation values by considering the geophysical parameters in the method. However, its sensitivity on correcting precipitation values is substantially lower than the sensitivity related to RCMs physics and dynamics. Therefore, the improvements remain relatively small in the analyses.

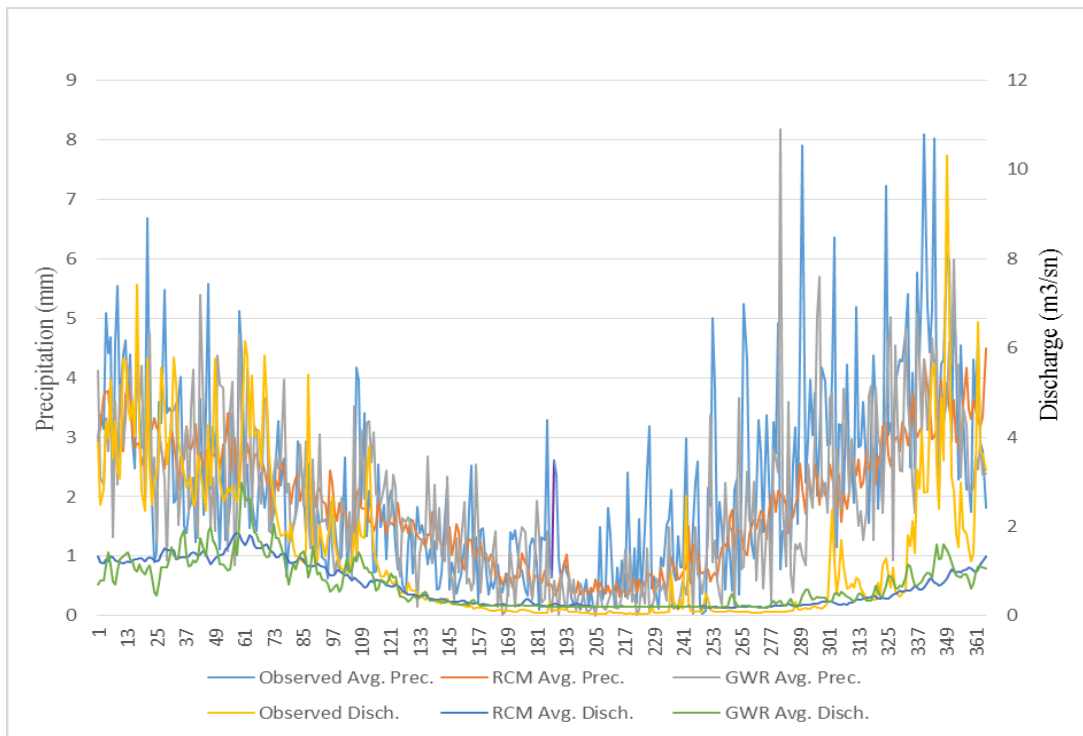


Figure 6.3 Comparison of precipitation and discharge values of observation, mean RCMs, and mean GWR simulations.

Figure 6.4 shows scatter plots between daily mean observed and modeled discharges over reference period for RCMs in (a) and downscaled RCMs in (b). The most significant feature from these plots is that downscaled precipitation inputs makes the discharge distribution slightly more scattered but improves the underestimation behavior of discharges using RCM input without GWR method. Volumetric improvements in discharge hydrograph with GWR are also seen with statistics of RMSE and bias ratio values while temporal trend with GWR is slightly worse as indicated by correlation coefficient values.

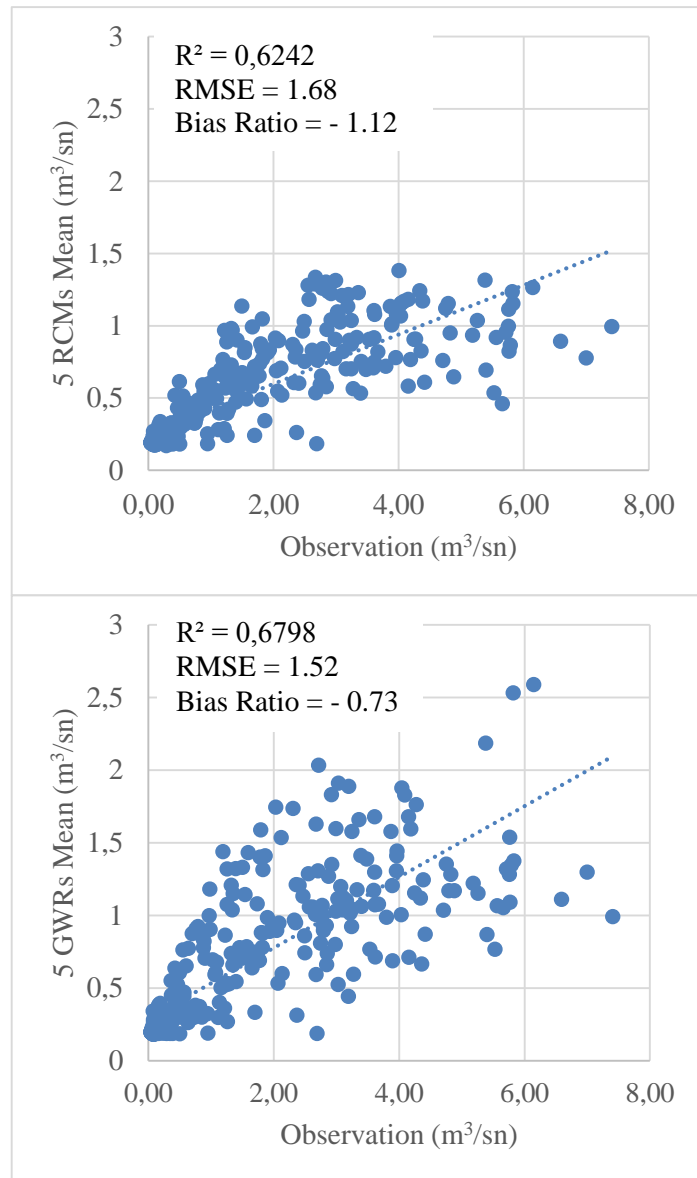


Figure 6.4 Scatterplots of RCM via Observed discharges and GWR via Observed discharges.

6.2 Extreme Flow Index Calculation

For the evaluation of the effects of the downscaling method on the projection of changes in the extreme flows, extreme flow index (EFI) is used. As the significant feature of extreme flow, the index is defined to calculate the magnitude of the peak flow.

In order to compute the index, a time series of extreme flows is first defined and extracted from the simulated daily discharge data. The extremes are selected using the peaks-over-threshold (POT) approach as used in extreme precipitation analyses. Two threshold levels used in precipitation index calculation are also considered in this analysis to evaluate the impact of the implemented downscaling method on changes in the extreme flows of different severity levels: the 1-year and 5-year flood levels. In order to assure independence of the selected peaks over a given threshold level, two independence criteria were implemented. The first criterion is that the inter-event time (k_s) should exceed a minimum time that is estimated based on the recession constant of a typical discharge hydrograph for the catchment. The second criterion is that the minimum discharge between two events recesses. This is estimated as a certain fraction (f) of the smaller of the two events. More details on the approach are presented in Willems (2009). According to WETSPRO program (Willems, 2009) that is applied to Omerli Basin, parameters, k_s and f used for separation in quick flow periods and peak flow selection are 4 days and 0.7, respectively.

The extreme flow index highlights the magnitude of the extreme discharge and is defined as the mean of the extracted POT values of the discharge time series over the given period (reference or scenario period). The changes in the extreme index between the reference (observation) and scenario (control) period are then estimated as the ratio of the index between the scenario (control) and the reference (observation) period.

6.2.1 Extreme flow evaluation

In this section, the performance of HBV model forced by RCM precipitation with and without downscaling method in extreme flow events during four seasons and yearly period is investigated. For this analysis, EFI value is calculated between observed discharge and simulated discharges from original RCMs and observed discharge and simulated discharge from downscaled RCMs for the reference period. With these

analyses, we assess whether the error in the downscaled time series is smaller than in the RCMs in simulating extreme flow events.

Figure 6.5 shows box plots of extreme flow index values for 5 RCMs in (a) and for 5 downscaled RCMs in (b) along with 1-yr and 5-yr return periods for four seasons and full year. In all seasons and year, both RCMs and GWR underestimates the extreme flow as index values stay below 1 for both return periods (see Figure 6.5). Comparing to precipitation extremes the errors are much higher for extreme flow as the underestimation tendency is more pronounced with extreme flows. The highest errors in extreme flow occur with summer and fall season while the lowest errors first appear with spring and then winter periods. However, with the application of GWR method, the errors in extreme flow series are importantly reduced in all seasons for both return periods. Such error reduction was the highest for spring period with 5-yr return value. With error reduction only the median value of 5-yr return period for spring exceeds 0.5 index value and all other median values of boxes belong to other seasons and year still remain below 0.5 index value. Overall the errors in extreme flows with 5-yr return flood are slightly smaller (closer to index value 1) than 1-yr return period for both RCMs and GWR.

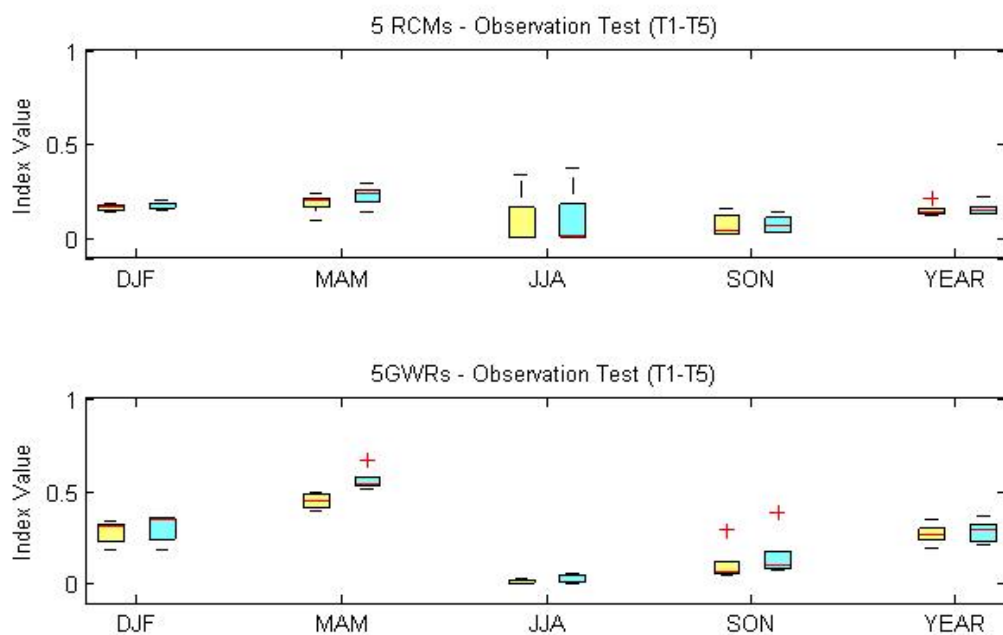


Figure 6.5 Performance test of 5 RCMs and 5 GWRs in index value calculation.

6.2.2 Changes in extreme flow

In this section, EFI is used to compare the changes in the flows derived by original RCMs and the flows derived by downscaled RCMs from reference to future. Figure 6.6 shows box plots of EFI values representing 5 RCMs-derived flows in (a) and 5 downscaled RCMs-derived flows in (b) for 1-yr and 5-yr threshold return periods for four seasons and all year. Winter and spring periods show an increase in extreme flow from reference to future period as their median values are above 1 of index value. Fall season shows decrease in extreme flow in this evaluation period. These results are consistent with extreme precipitation changes (see Fig. 5.6) seen during reference to future period. However, strong increase in extreme precipitation during summer is reversed for extreme flows (see Fig 6.6). Strong low flow condition in Omerli Basin during summer may attribute this as precipitation is partitioned for infiltration and evapotranspiration process by the model. When downscaled precipitation is used in HBV as input these pronounced seasonal decrease or increases from reference to future period are more enhanced for both return periods. Also, downscaled precipitation is greatly decreased RCMs variability by reducing the box sizes for spring and fall seasons.

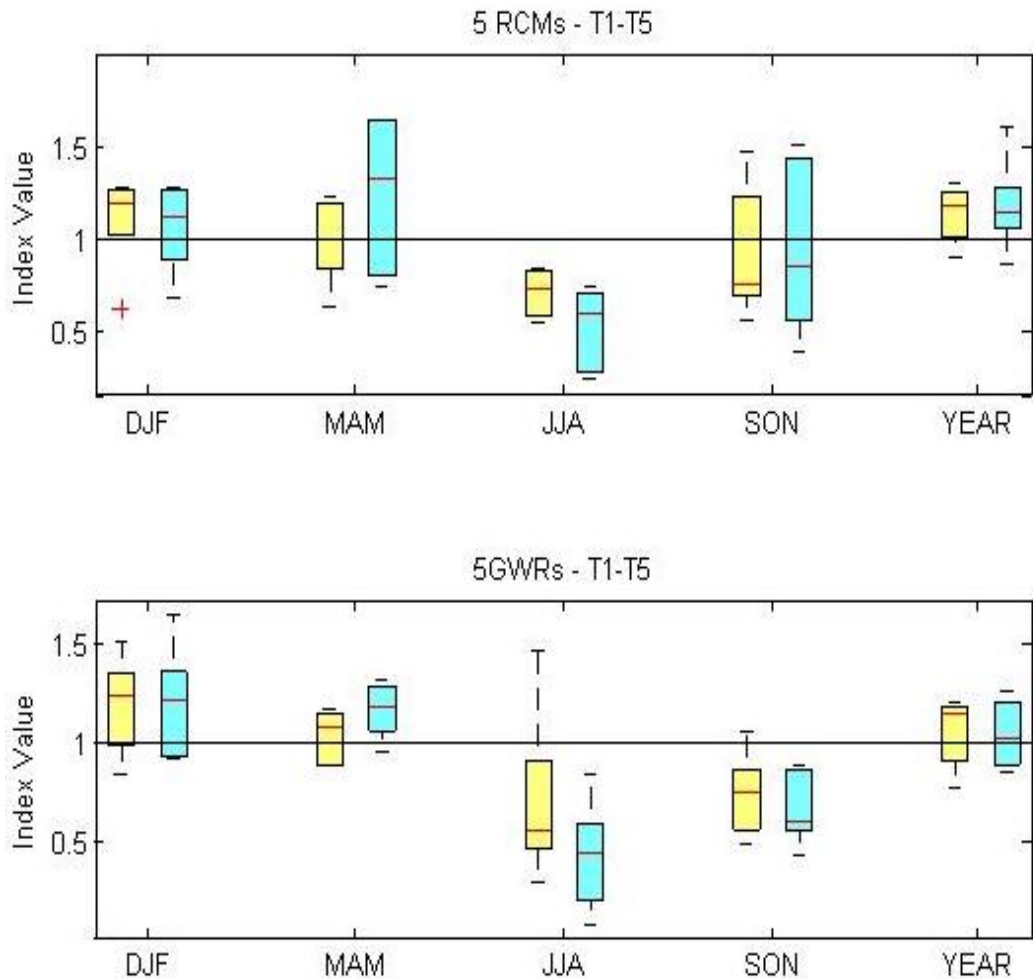


Figure 6.6 Index values of 5 RCMs and 5 GWRs.

6.2.3 Changes in extreme flow volume

The second index is a measure of the flood volume. For each extreme event identified using the POT method, this is computed by moving backward and forward from the time of peak and computing the volume above the selected threshold level (1 or 5 years). The mean of this volume over the given period is defined as the extreme volume index. Note that this index is not a measure of the total flood volume, but rather the volume above the threshold flood level. The threshold value used to derive the volume index in the scenario period is the same value defined for the reference period. Events identified in the scenario period that have a peak value less than this threshold are excluded in the computation of the volume index. In case none of the events has a peak

exceeding the threshold, the volume index is set to zero. The changes in the extreme indices between the control and scenario period are then estimated as the ratio of the indices between the scenario and the control period. If the volume index is zero in the scenario period due to the absence of an event whose peak exceeds the threshold, the change is also set to zero.

Figure 6.7 shows box plots of flow volume indexes representing 5 RCMs input for 1 and 5 years thresholds for winter, spring, summer, fall, and annual periods for RCMs with no GWR and RCMs with GWR method. With original RCMs extreme flow volumes in future period increase for summer and fall seasons but there is no significant change for winter and spring periods. Yearly values also show some increase in flow volume for both thresholds. With GWR method, while there is increase in flow volume for winter and spring, fall season shows decrease. Similarly, yearly flow volumes also increase in future period with GWR. Especially, increase in flow volume during winter for future period is important for the management of water supply available in Omerli Basin. In fall season according to median value of boxes, original RCMs show 2 to 3 times higher flow volumes in future period comparing to reference. However, this significant increase is not followed by GWR application and reversely, GWR decreases the flow volume during fall season. The impact of climate change on the seasonality of flow volume is reflected differently from RCMs when they are evaluated with and without downscaling.

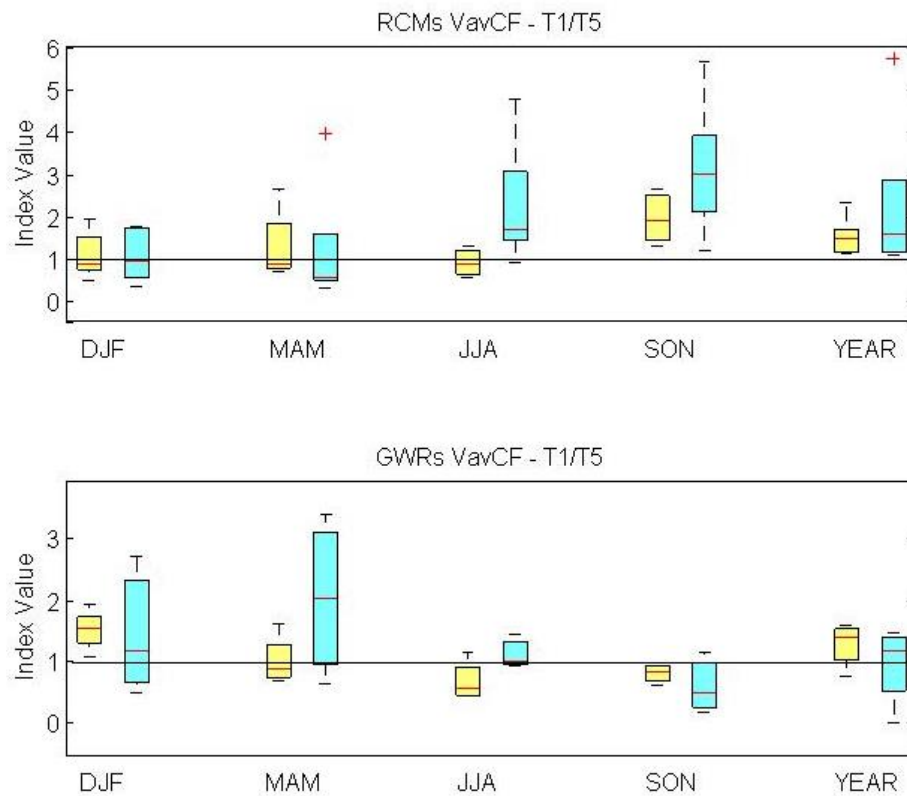


Figure 6.7 Index values of flow volume for 5 RCMs and 5 GWRs.

6.3 Frequency Analysis

Frequency analyses are conducted using data series of annual maximum daily peak flows for observed and simulated discharges from HBV forced by 5 RCMs with and without downscaling method during reference and future periods. As in annual daily maximum precipitation, annual daily peak flows are represented best by the the log-normal distribution function. Figure 6.8 shows probability of non-exceedance as function of annual daily peak flows from observation and HBV derived by 5 RCMs during reference and future periods while Figure 6.9 shows equivalent diagrams for downscaled 5 RCMs inputs. For a given probability of exceedance the magnitudes of flows are lower than observation for original RCM inputs for all data range (see Fig. 6.8). The variability among RCMs inputs in estimating flood frequencies is relatively high while the closest match to observed frequency curve is obtained by ETHZ CLM model. For future period ETHZ CLM and MPIM REMO models increase their flood

frequency estimates while other models especially SMHIRCA HADCM3Q3 model decreases their frequency estimates (see Fig 6.8b). Models behave differently in flood frequency analyses between reference and future periods.

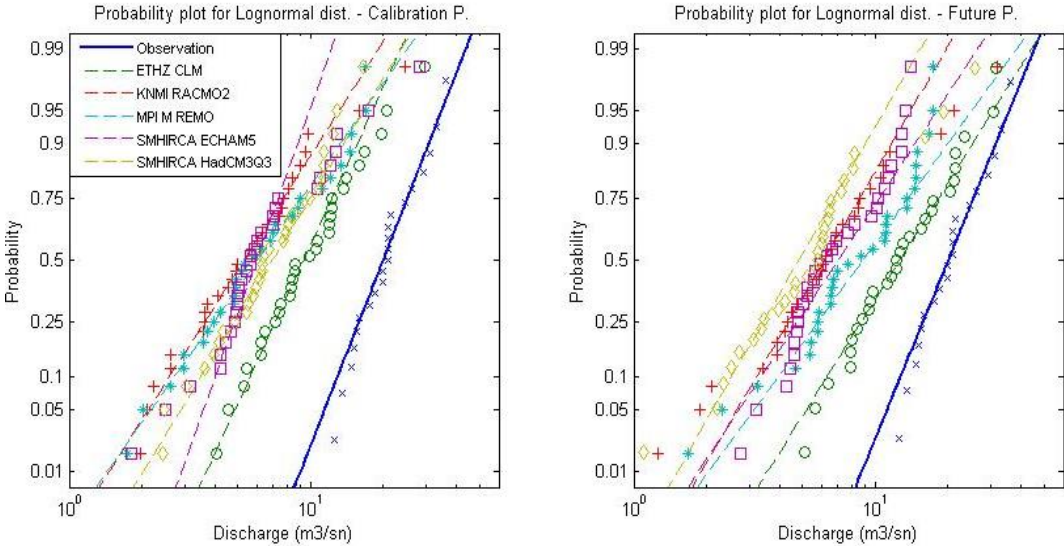


Figure 6.8 Frequency analysis of extreme discharge events of 5 RCMs that are used in GWR method.

The accuracy of estimating flood frequency values by each RCM is improved with the use of downscaling precipitation inputs in the HBV model (see Fig. 6.9). For both low and high flow values, frequencies are improved through the use of downscaled data. In addition, GWR method has no effect in altering the decreasing or increasing frequency behavior for a given flood value from reference to future period.

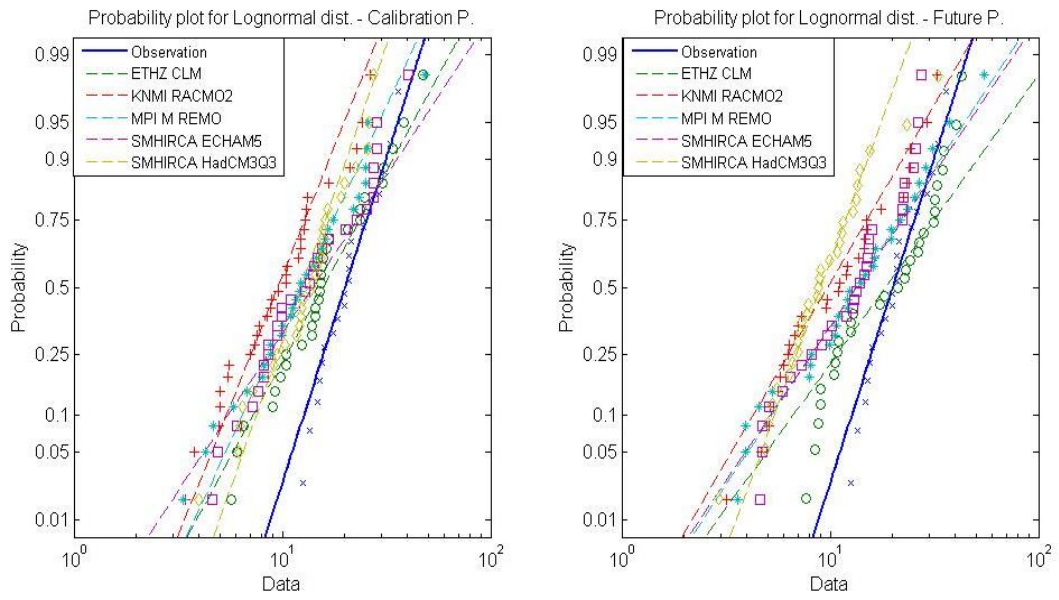


Figure 6.9 Frequency analysis of extreme discharge events of 5 GWRs.

CHAPTER 7

SUMMARY, CONCLUSIONS, AND RECOMMENDATIONS

7.1 Summary

This thesis describes research in which hydrological impact assessment of climate change on the Omerli Basin of Istanbul, Turkey is carried out to investigate the changes in precipitation and streamflow from past (1960-1990) to the end of 21st century (2070-2100). In order to use daily and monthly precipitation and temperature data from the fifteen different GCM/RCM combinations based on A1 carbon emission scenario from EU-ENSEMBLES project 25-km RCM grids that are collocating the study area are extracted for the reference and projected periods. Simulations from multi model scenarios are used in this study because many studies highlight that the ensemble approach improves forecast accuracy and decreases uncertainties. Moreover, a single GCM/RCM might perform well for some variables in some regions but not for other variables.

The grid scale obtained from RCMs is relatively coarse when it is compared to conceptual streamflow scale and stays poor in representing extreme precipitation in catchment scale. Therefore, finer resolution downscaling technique is necessary prior to practical hydro meteorological applications. A GIS based downscaling method, GWR that relies on local geo-physical (explanatory) parameters of roughness, altitude, slope, aspect, and distance to sea representing meteorology stations is first developed and validated. Then, it is executed for RCM grids, which are represented by explanatory variables found as median values using 1-km resampled ASTER data to downscale the monthly precipitation to 1-km resolution. Since the developed method

requires high computational run time during application it is only applied to five best RCM results among 15.

Hydrologic response of the Omerli Basin using the RCM precipitation input with and without downscaling method was determined by the application of HBV hydrologic model in daily time step. The model was calibrated automatically for N-S index and due to the availability and reliability of observed streamflow data the calibration/validation was only performed at the 02-67 sub-catchment of the Omerli Basin.

Comparisons were made between modeled variables (precipitation and streamflow) and observed data from climate stations for precipitation and DSI for discharge for model simulations (both RCM and HBV) with and without downscaling method to investigate the improvement (or otherwise) in RCMs' and HBV's abilities to describe the mean, extreme, and frequency values of surface precipitation and streamflow fields. The extreme value series were extracted using POT method for 1-yr and 5-yr threshold return periods. POT precipitation series were analyzed with temporal aggregations of 1, 2, 5, 10, and 30 days. As expected, precipitation downscaling was found to greatly improve the simulated precipitation and streamflow values versus no downscaling method during winter, spring, summer, and fall seasons, and annually. The most striking improvement was in the accuracy with which models (RCMs and HBV) calculates the magnitude and frequency of extreme precipitation and streamflow events. However, there was a strong underestimation tendency from all RCMs in estimating daily precipitation for all seasons and this also appeared with simulated discharges.

Extreme index values described as ratio between mean extreme series for reference (1960-1990) and mean extreme series for scenario (2070-2100) periods were calculated for each season to determine the changes from past to future period for the magnitudes of precipitation and streamflow under the influence of downscaling technique. Similarly, extreme flow volume index values were also calculated to

monitor the flow volume changes produced by the extremes. Frequency behaviors of simulated extreme daily precipitation and streamflow were shown to assess whether the extreme magnitude increases or decreases for a given return period for future period and how that influenced with downscaling for different RCMs. Generally, seasonal and annual changes either decrease or increase in extreme variables were more enhanced with downscaling method for both threshold return periods. Also, with downscaling the variability in producing precipitation amount from RCMs was reduced especially for spring and fall seasons. Majority of RCMs regardless of downscaling method showed that magnitudes of extremes will increase for a given return period and the frequency (return period) will decrease (increase) for a magnitude in future.

7.2 Conclusions

The primary conclusions that can be drawn on the basis of the research described in this thesis are as follows:

- It was clearly demonstrated that a GIS based downscaling method considering the local geo-psychical parameters was successfully developed and applied to RCMs grids. It was shown that downscaling had a strong influence on precipitation extremes.
- All RCMs with varying magnitude showed underestimation tendency in mean and extreme precipitation.
- Errors in simulating extremes were found to vary with the seasons. The lowest errors in predicting extreme precipitations were obtained in the winter season and the highest errors were obtained for the spring season.

- GWR improves the underestimation tendency of RCMs in precipitation; this improvement was found to be significantly better with extreme values. For example, precipitation extremes with GWR in winter were overestimated.
- Changes in extreme precipitation from the reference to the future increased for the winter, spring, and summer seasons, and decreased for the fall season and annually. These changes became more significant with downscaling. Seasonality in extreme precipitation became important. The fall season has a strong effect on annual extreme precipitation as it was attributable to decrease in annual precipitation.
- The changes obtained for different temporal aggregations also depend on the physical geographical characteristics of the catchment and season analysed, i.e. there is no general tendency for an increase or decrease in the extreme precipitation index with increasing temporal aggregation.
- All RCMs without GWR underestimated the observed precipitation frequency curve but this underestimation was significantly improved with downscaling application.
- From reference to future period, magnitude of the extreme precipitation for all range of probability of occurrences increased for four RCMs while it only decreased for SMHIRCA HadCM3Q3 model. Again, these behaviors were more distinctive with GWR.
- Depending on precipitation input, the HBV significantly underestimated daily mean runoff and extreme runoff events. Downscaled precipitation inputs provided improvements in runoff simulations particularly with extreme values. However, an appreciable underestimation tendency still existed.

- Spring extreme runoffs produced the smallest errors in comparison with the other seasons.
- Projections showed that the magnitudes of extreme discharges increased in the winter and spring while they decreased in the fall and summer from reference to future periods. Annually there was also a slight increase. GWR decreased the variability among the RCMs for simulating extreme magnitudes during the spring and fall seasons.
- Annual extreme flow volumes increased with and without downscaled precipitation input for future period. This was mostly attributed to increase in winter flow volumes according to the GWR results. Fall season flow volumes showed important increase with original RCMs input while they exhibited decrease with downscaled input.
- For all five RCMs downscaled precipitation input provided much better frequency distribution for extreme discharges than RCMs with no downscaling input. For a given probability of occurrence the underestimation problem was significantly improved.
- As in precipitation frequency, magnitude of extreme discharges for all range of probability occurrences increased for four RCMs in the future period but it decreased with the SMHIRCA HadCM3Q3 model. This feature was more obvious with GWR input.

7.3 Recommendations

In the ensemble approach the fifteen RCMs are driven by six GCMs. For all seasons, the RCM–GCM projections are the main source of variability in the precipitation results additionally, the RCMs represent a larger percentage of the total variability than the GCMs, especially in summer. This is attributable to the sensitivity of different

convective schemes used in each RCM because precipitation extremes occur mostly from local convections during summer in the Omerli Basin. For example, ETHZ CLM model provided the best results for frequency distributions of precipitation and discharge among 15 RCMs in this study area. However, this model may not give the same accuracy for other study regions depending on the geographical conditions and climate system that affect the performance of the physics used in these models. Therefore, as stated in the literature (e.g. Sunyer et al. 2014) the multi model ensemble method instead of a single model is recommended to use in climate change impact studies. RCMs with and without downscaling method suggest that both extreme flows and the corresponding volumes of the extreme flows are expected to increase by the end of the 21st century in annual series under the SRES A1B emission scenario. Seasonal increases in winter and spring are responsible for these annual increases. The extreme flows and corresponding volumes are generally projected to decrease in summer and fall seasons. The general tendency in the expected changes in the extreme flows is that the extreme flows tend to increase in the Omerli Basin with rainfall-dominated precipitation regimes during winter period. These projected seasonal changes (increase in winter and decrease in fall) in extreme precipitation and discharge should be considered in planning of Omerli dam reservoir in order to sustain the effective storage and effective use of water. As consistent with the studies from Aksoy et al. (2008, 2009), frequency distribution analyses suggested that Omerli Basin can be under water stress in the future as return periods of the events show increasing tendency. These results should be used in Omerli Dam's water management policies to be followed in the future and could provide support for research and decision making in the science and policy-making arenas.

REFERENCES

- Adam, J.C., Hamlet, A.F., and Lettenmaier, D.P. (2009). Implications of global climate change for snowmelt hydrology in the twenty-first century. *Hydrological Processes*, 23(7): 962-972.
- Aguilera, H. and Murillo, J.M. (2009). The effect of possible climate change on natural groundwater recharge based on a simple model: a study of four karstic aquifers in SE Spain. *Environmental Geology*, 57(5): 963-974.
- Aksoy, Hafzullah, N., Unal, E., Alexandrov, V., Dakova, S., and Yoon, J. (2008). Hydrometeorological analysis of northwestern Turkey with links to climate change. *International Journal of Climatology*, 28: 1047-1060.
- Akyürek, Z., Sürer, S., and Beşer, O. (2011). Investigation of the snow-cover dynamics in the Upper Euphrates Basin of Turkey using remotely sensed snow-cover products and hydrometeorological data. *Hydrological Processes*, 25: 3637-3648.
- Alexander, C., Moeslund, J.E., Bocher, P.K., Arge, L., and Svenning, J.C. (2013). Airborne laser scanner (LiDAR) proxies for understory light conditions. *Remote Sensing of Environment*, 134: 152–161.
- Anderson, J.B., Wallace, D.J., Simms, A.R., Rodriguez, A.B., and Milliken, K.T. (2014). Variable response of coastal environments of the northwestern Gulf of Mexico to sea-level rise and climate change: Implications for future change. *Marine Geology*, 352: 348-366.
- Aniya, M. (1999). Recent glacier variations of the Hielos Patagónicos, South America, and their contribution to sea-level change. *Arctic, Antarctic, and Alpine Research*, 31: 165-173.
- Arndt, D.S., Baringer, M.O., and Johnson, M.R. (2010). State of the Climate in 2009. *Bulletin of the American Meteorological Society*, 91(7): 1-224.
- Aubrecht, C., Steinnocher, K., Hollaus, M., and Wagner, W. (2009). Integrating earth observation and GIScience for high resolution spatial and functional modeling of urban land use. *Computers, Environment and Urban Systems*, 33: 15–25.
- Baban, A., Goktas, O.C., Hocaoglu, S.M., Atasoy, E., Akalin, N.G., Donertas, A., Erdem, I.C., Magarzo, C., Hernandez, M., and Tobella, J. (2011). Integrated Urban Water Management and Investigation of New Water Resources . *Nieuwegein* : European Comission 7th Framework Programme.

- Bavay, M., Grünewald, T., and Lehning, M. (2013). Response of snow cover and runoff to climate change in high Alpine catchments of Eastern Switzerland. *Advances in Water Resources*, 55: 4-16.
- Bayraktar, H. and Turalioglu, F.S. (2005). Average areal sulphur dioxide concentration estimation by percentage weighting polygon method in Erzurum urban centre, Turkey. *Atmospheric Environment*, 39: 5991–5999.
- Bayraktar, H., Turalioglu, F. S., and Sen, Z. (2005). The estimation of average areal rainfall by percentage weighting polygon method in Southeastern Anatolia Region, Turkey. *Atmospheric Research*, 73: 149-160.
- Beare, S., and Heaney, A. (2002). Climate change and water resources in the Murray Darling Basin, Australia. *World Congress of Environmental and Resource Economists*, (s. 1-33). Monterey, California.
- Beck, L. and Bernauer, T., (2011). How will combined changes in water demand and climate affect water availability in the Zambezi river basin? *Global Environmental Change*, 21: 1061-1072.
- Bergström, S. (1976). Development and application of a conceptual runoff model for Scandinavian catchments. Ph.D. Thesis. SMHI Reports RHO No. 7, Norrköping.
- Bergström, S. (1992). The HBV model - its structure and applications. SMHI Reports RH, No. 4, Norrköping.
- Bijma, J., Pörtner, H.O., Yesson, C., and Rogers, A.D. (2013). Climate change and the oceans – What does the future hold? *Marine Pollution Bulletin*, 74: 495-505.
- Boon, S., Sharp, M., and Nienow, P. (2003). Impact of extreme melt event on the runoff and hydrology of a high Arctic glacier. *Hydrological Processes*, 17: 1051-1072.
- Bozkurt, D. and Sen, O.L. (2013). Climate change impacts in the Euphrates–Tigris Basin based on different model and scenario simulations. *Journal of Hydrology*, 480 149-161.
- Brunnabend, S.E., Schröter, J., Timmerman, R., Rietbroek, R., and Kusche, J. (2012). Modeled steric and mass-driven sea level change caused by Greenland Ice Sheet melting. *Journal of Geodynamics*, 59–60: 219-225.
- Burke, E.J., Perry, R.H.J., and Brown, S.J. (2010). An extreme value analysis of UK drought and projections of change in the future. *Journal of Hydrology*, 388: 131–143.

- Burrough, P.A. and McDonnell, R.A. (1998). Principles of Geographical Information Systems. *Oxford University Press*, Oxford.
- Bussi, G., X. Rodríguez-Lloveras, F. Francés, G. Benito, Y. Sánchez-Moya, and A. Sopeña, (2013). Sediment yield model implementation based on check dam infill stratigraphy in a semiarid Mediterranean catchment. *Hydrology and Earth System Sciences*, 17: 3339-3354.
- Butler, B.J., Hewes, J.H., Liknes, G.C., Nelson, M.D., and Snyder, S.A. (2014). A comparison of techniques for generating forest ownership spatial products. *Applied Geography*, 46: 21-34.
- CACC (Canada's Action on Climate Change). (2013). *Causes of Climate Change*. 10 December. Accessed: September 05, 2014.
<http://www.climatechange.gc.ca/default.asp?lang=en&n=65CD73F4-1>.
- CACC (Canada's Action on Climate Change). (2014). *Impacts of Climate Change*. 03 July. Accessed: September 06, 2014.
<http://www.climatechange.gc.ca/default.asp?lang=en&n=036D9756-1>.
- Chaouche, K., Neppel, L., Dieulin, C., Pujol, N., Ladouche, B., Martin, E., Salas, D., and Caballero, Y. (2010). Analyses of precipitation, temperature and evapotranspiration in a French Mediterranean region in the context of climate change. *C. R. Geoscience* 342: 234–243.
- Charlton, M., Fotheringham, S. and Brunson, C. (no date). Geographically Weighted Regression Version 2.x, User's Manual and Installation Guide.
- Chattopadhyay, N., and Hulme, M. (1997). Evaporation and potential evapotranspiration in India under conditions of recent and future climate change. *Agricultural and Forest Meteorology*, 87: 55-73.
- Chen, H., Xu, C.Y., and Guo, S. (2012). Comparison and evaluation of multiple GCMs, statistical downscaling and hydrological models in the study of climate change impacts on runoff. *Journal of Hydrology*, 434–435: 36-45.
- Clow, D.W. (2010). Changes in the timing of snowmelt and streamflow in Colorado: a response to recent warming. *Journal of Climate*, 23(9): 2293-2306.
- Dai, A. (2013). Increasing drought under global warming in observations and models. *Nature Climate Change*, 3: 52-58.
- Dai, A., Qian, T., Trenberth, K.E., and Milliman, J.D. (2009). Changes in continental freshwater discharge from 1948 to 2004. *Journal of Climate*, 22(10): 2773-2792.

- Dai, S.B., Lu, X.X., Yang, S.L., and Cai, A.M. (2008). A preliminary estimate of human and natural contributions to the decline in sediment flux from the Yangtze River to the East China Sea. *Quaternary International*, 186: 43-54.
- Daley, R. (1991). Atmospheric Data Analysis. *Cambridge University Press*.
- Dalfes, H.N., Karaca, M., and Sen, O.L. (2007). Climate change scenarios for Turkey in "Climate Change & Turkey: Impact, Sectoral Analyses, Socio-Economic Dimensions. Ankara: United Nations Development Programme (UNDP) Turkey Office.
- Dankers, R., Arnell, N.W., Clark, D.B., Clark, D.B., Falloon, P.D., Fekete, B.M., Gosling, S.N., Heinke, J., Kim, H., Masaki, Y., Satoh, Y., Stacke, T., Wada, Y., and Wisser, D. (2013). First look at changes in flood hazard in the Inter-Sectoral Impact Model Intercomparison Project ensemble. *Proceedings of the National Academy of Sciences*, 1: 1-5.
- DeMers, M.N. (2003). Fundamentals of Geographic Information Systems, Second Edition. *Wiley*, NJ.
- Demir, İ., Kılıç, G., Coşkun, M., and Sümer, U.M. (2008). Türkiye’de Maksimum, Minimum ve Ortalama Hava Sıcaklıkları ile Yağış Dizilerinde Gözlenen Değişiklikler ve Eğilimler. *TMMOB İklim Değişimi Sempozyumu*. Ankara: TMMOB adına TMMOB Meteoroloji Mühendisleri Odası. 69-84.
- Derakshan, H. and Talebbeydokhti. N. (2011). Rainfall disaggregation in non-recording gauge stations using space-time information system. *Scientia Iranica A*, 18(5): 995–1001.
- Di Piazza, A., Lo Conti, F., Noto, L.V., Viola, F., and La Loggia, G. (2011). Comparative analysis of different techniques for spatial interpolation of rainfall data to create a serially complete monthly time series of precipitation for Sicily, Italy. *International Journal of Applied Earth Observation and Geoinformation*, 13: 396–408.
- Dikici, M. (2009). İstanbul yağışlarının kurak dönem analizi. *Master Thesis*. Istanbul Technical University, Graduate School of Science, Engineering, and Technology.
- Dobbertin, M., Baltensweiler, A., and Rigling, D. (2001). Tree mortality in an unmanaged mountain pine (*Pinus mugo* var. *uncinata*) stand in the Swiss National Park impacted by root rot fungi. *Forest Ecology and Management*, 145: 79-89.
- Doherty, J. (2004). PEST: Model Independent Parameter Estimation. Fifth edition of user manual. *Watermark Numerical Computing*, Brisbane, Australia.

- Dowdeswell, J.A., Hagen, J.O., Björnsson, H., Glazovsky, A.F., Harrison, W.D., Holmlund, P., Jania, J. (1997). The Mass Balance of Circum-Arctic Glaciers and Recent Climate Change. *Quaternary Research*, 48: 1-14.
- Earman, S., Campbell, A.R., Phillips, F.M., and Newman, B.D. (2006). Isotopic exchange between snow and atmospheric water vapor: Estimation of the snowmelt component of groundwater recharge in the southwestern United States. *Journal of Geophysical Research-Atmospheres*, 111(D9): D09302.
- EPA (Environmental Protection Agency). 2014. *Climate Change: Basic Information*. 18 March. Accessed: September 05, 2014. <http://www.epa.gov/climatechange/basics/>.
- Ertürk, A., Ekdal, A., Gürel, M., Karakaya, N., Guzel, C., and Gönenç, E. (2014). Evaluating the impact of climate change on groundwater resources in a small Mediterranean watershed. *Science of the Total Environment*, xxx xxx-xxx (Article in Press).
- ESRI (Environmental Systems Research Institute) (2014). ArcGIS Help 10.1. ArcGIS Resources: http://resources.arcgis.com/en/help/main/10.1/index.html#/What_are_geostatistical_interpolation_techniques/003100000031000000/. Accessed: June 24, 2014.
- EU-CC (European Union – Climate Change). (2014). Consequences of climate change. 05 September. Accessed: September 06, 2014. http://ec.europa.eu/clima/policies/brief/consequences/index_en.htm.
- Ezber, Y., Sen, O.L., Kindap, T., and Karaca, M. (2007). Climatic effects of urbanization in Istanbul: a statistical and modeling analysis. *International Journal of Climatology*, 27: 667-679.
- Fischer, T., C. Menz, B. Su, and T. Scholten. (2013). Simulated and projected climate extremes in the Zhujiang River Basin, South China, using the regional climate model COSMO-CLM. *International Journal of Climatology*, 33(14): 2988-3001.
- Fotheringham, A. S., Brunson, C., and Charlton, M.E. (2002). Geographically Weighted Regression: The Analysis of Spatially Varying Relationships, *Wiley*, Chichester.
- Fowler, H. J. and Ekström, M. (2009). Multi-model ensemble estimates of climate change impacts on UK seasonal precipitation extremes. *Int. J. Climatol.*, 29: 385–416.

- Fowler, H. J., Blenkinsop, S., and Tebaldi, C. (2007). Linking climate change modelling to impacts studies: recent advances in downscaling techniques for hydrological modelling. *Int. J. Climatol.*, 27: 1547–1578.
- Fu, C., Chen, J., Dong, L., and Jiang, H. (2012). Field investigation and modeling of runoff generation in a granitic catchment in Zhuhai, China. *Journal of Hydrology*, 458–459: 87-102.
- Fujihara, Y., Tanaka, K., Watanabe, T., Nagano, T., and Kojiri, T. (2008). Assessing the impacts of climate change on the water resources of the Seyhan River Basin in Turkey: Use of dynamically downscaled data for hydrologic simulations. *Journal of Hydrology*, 353: 33-48.
- Gardner, A.S., Moholdt, G., Cogley, J.G., Wouters, B., Arendt, A.A., Wahr, J., Berthier, E., Hock, R., Pfeffer, W.T., Kaser, G., Ligtenberg, S.R.M., Bolch, T., Sharp, M.J., Hagen, J.O., van den Broeke, M.R., and Paul, F., (2013). A reconciled estimate of glacier contributions to sea level rise: 2003 to 2009. *Science*, 340(6134): 852-857.
- Gardner, L.R. (2009). Assessing the effect of climate change on mean annual. *Journal of Hydrology*, 379: 351-359.
- Gething, P.W., Noor, A.M., Zurovac, D., Atkinson, P.M., Hay, S.I., Nixon, M.S., and Snow, R.W. (2004). Empirical modelling of government health service use by children with fevers in Kenya. *Acta Tropica*, 91: 227–237.
- Giuntoli, I., Renard, B., and Lang, M. (2012). Floods in France. In: Changes in Flood Risk in Europe [Kundzewicz, Z.W. (eds.)]. *CRC Press*, Wallingford, UK, pp. 199-211.
- Givati, A., and Rosenfeld, D. (2013). The Arctic Oscillation, climate change and the effects on precipitation in Israel. *Atmospheric Research*, 132-133: 114-124.
- Gobiet, A., Kotlarski, S., Beniston, M., Heinrich, G., Rajczak, J., Stoffel, M. (2014). 21st century climate change in the European Alps—A review. *Science of the Total Environment*, 493: 1138-1151.
- Grant, R.H., Hollinger, S.E., Hubbard, K.G., Hoogenboom, G., and Vanderlip, R.L. (2004). Ability to predict daily solar radiation values from interpolated climate records for use in crop simulation models. *Agricultural and Forest Meteorology*, 127: 65–75.
- Guang, Y. and Weili, J. (2011). Research on Impact of Ground Control Point Distribution on Image Geometric Rectification Based on Voronoi Diagram. *Procedia Environmental Sciences*, 11: 365 – 371.

- Haerberli, W. and Burn, C.R. (2002). Natural hazards in forests: glacier and permafrost effects as related to climate change. In: *Environmental Change and Geomorphic Hazards in Forests* [Sidle, R.C. (ed.)]. IUFRO Research Series 9, CABI Publishing, Wallingford and New York, pp. 167–202.
- Handmer, J., Honda, Y., Kundzewicz, Z.W., Arnell, N., Benito, G., Hatfield, J., Mohamed, I.F., Peduzzi, P., Wu, S., Sherstyukov, B., Takahashi, K., and Yan, Z. (2012). Changes in impacts of climate extremes: human systems and ecosystems. In: *Managing the Risks of Extreme Events and Disasters to Advance Climate Change Adaptation* [Field, C.B., V. Barros, T.F. Stocker, D. Qin, D.J. Dokken, K.L. Ebi, M.D. Mastrandrea, K.J. Mach, G.-K. Plattner, S.K. Allen, M. Tignor, and P.M. Midgley (eds.)]. A Special Report of Working Groups I and II of the Intergovernmental Panel on Climate Change, *Cambridge University Press*, Cambridge, UK, and New York, US, pp. 231-290.
- Hanel, M. and Buishand, T.A. (2012). Multi-model analysis of RCM simulated 1-day to 30-day seasonal precipitation extremes in the Czech Republic. *Journal of Hydrology*, 412–413, 141–150.
- Hao, X., Chen, Y., Xu, C., and Li, W. (2008). Impacts of Climate Change and Human Activities on the Surface Runoff in the Tarim River Basin over the Last Fifty Years. *Water Resources Management*, 22: 1159-1171.
- Harmancıoğlu, N.B., Özkul, S., Fıstıkoğlu, O., Barbaros, F., Onuşluel, G., Çetinkaya, C.P., and Dalkılıç, Y. (2007). Modeling for climate change effects in the Gediz and Büyük Menderes river basins in "Climate Change & Turkey: Impacts, Sectoral Analyses, Socio-Economic Dimensions". *Ankara: United Nations Development Programme*.
- Hattermann, F.F., Kundzewicz, Z.W., Huang, S., Vetter, T., Kron, W., Burghoff, O., Merz, B., Bronstert, A., Krysanova, V., Gerstengarbe, F.-W., Werner, P., and Hauf, Y. (2012). Flood risk from a holistic perspective -observed changes in Germany. In: *Changes in Flood Risk in Europe* [Kundzewicz, Z.W. (eds.)]. *CRC Press*, Wallingford, UK, pp. 212-237.
- Hirabayashi, Y., Mahendran, R., Koirala, S., Konoshima, L., Yamazaki, D., Watanabe, S., and Kanae, S. (2013). Global flood risk under climate change. *Nature Climate Change*, 3: 816-821.
- Hirschi, M., Seneviratne, S.I., Alexandrov, V., Boberg, F., Boroneant, C., Christensen, O.B., Formayer, H., Orłowsky, B., and Stepanek, P. (2011). Observational evidence for soil-moisture impact on hot extremes in southeastern Europe. *Nature Geoscience*, 4(1): 17-21.

- Hoelze, M., Chinn, T., Stumm, D., Paul, F., Zemp, M., and Haeberli, W. (2007). The application of glacier inventory data for estimating past climate change effects on mountain glaciers: A comparison between the European Alps and the Southern Alps of New. *Global and Planetary Change*, 56: 69-82.
- Hühn, M. (2000). Non-regular spatial patterns of plants and their effect on several agronomic traits per area. *European Journal of Agronomy*, 12: 1–12.
- Huss, M. (2011). Present and future contribution of glacier storage change to runoff from macroscale drainage basins in Europe. *Water Resources Research*, 47: W07511.
- IMM (Istanbul Metropolitan Municipality), (2014). *İstanbul İl ve İlçe Alan Bilgileri*. June 15. Accessed September 08, 2014. <http://www.ibb.gov.tr/tr-tr/kurumsal/pages/ilceveilkademe.aspx>.
- IPCC (2000). IPCC special report: emission scenarios. *Cambridge University Press*, Cambridge, United Kingdom and New York, NY, USA.
- IPCC (2012). Glossary of terms. In: *Managing the Risks of Extreme Events and Disasters to Advance Climate Change Adaptation* [Field, C.B., V. Barros, T.F. Stocker, D. Qin, D.J. Dokken, K.L. Ebi, M.D. Mastrandrea, K.J. Mach, G.-K. Plattner, S.K. Allen, M. Tignor, and P.M. Midgley (eds.)]. A Special Report of Working Groups I and II of the Intergovernmental Panel on Climate Change (IPCC). *Cambridge University Press*, Cambridge, UK, and New York, NY, USA, pp. 555-564.
- IPCC (2013). *Climate Change 2013: The Physical Science Basis. Contribution of Working Group I to the Fifth Assessment Report of the Intergovernmental Panel on Climate Change* [Stocker, T.F., D. Qin, G.-K. Plattner, M. Tignor, S.K. Allen, J. Boschung, A. Nauels, Y. Xia, V. Bex and P.M. Midgley (eds.)]. *Cambridge University Press*, Cambridge, United Kingdom and New York, NY, USA, 1535 pp.
- IPCC (2014). *Climate Change 2014: Impact, Adaptation, and Vulnerability. Contribution of Working Group II to the Fifth Assessment Report of the Intergovernmental Panel on Climate Change*. *Cambridge University Press*, Cambridge, United Kingdom and New York, NY, USA.
- Ishak, E.H., Rahman, A., Westra, S., Sharma, A., and Kuczera, G. (2010). Preliminary analysis of trends in Australian flood data. In: *World Environmental and Water Resources Congress 2010: Challenges of Change* [Palmer, R.N. (eds.)]. *Proceedings of the congress, American Society of Civil Engineers*, Reston, USA, pp. 115-124.

- IWSA (Istanbul Water and Sewerage Administration) (2009). Geçmişten günümüze İstanbul'da suyun yönetimi. Rapor, İstanbul: İSKİ.
- IWSA (Istanbul Water and Sewerage Administration) (2010). *İklim değişikliğinin İstanbul ve Türkiye su kaynakları geleceğine tesirleri projesi nihai raporu*. Rapor, İstanbul: İSKİ.
- Jarvis, D., Stoeckl, N., and Chaiechi, T. (2013). Applying econometric techniques to hydrological problems in a large basin: Quantifying the rainfall–discharge relationship in the Burdekin, Queensland, Australia. *Journal of Hydrology*, 496: 107–121.
- Jeelani, G. (2008). Aquifer response to regional climate variability in a part of Kashmir Himalaya in India. *Hydrogeology Journal*, 16(8): 1625-1633.
- Jia, Q.Y. and Sun, F.H. (2012). Modeling and forecasting process using the HBV model in Liao river delta. *Procedia Environmental Sciences*, 13: 122-128.
- Jóhannesson, T., Aðalgeirsdóttir, G., Ahlstrøm, A., Andreassen, L.M., Beldring, S., Björnsson, H., Crochet, P., Einarsson, B., Elvehøy, H., Guðmundsson, S., Hock, R., Machguth, H., Melvold, K., Pálsson, F., Radić, V., Sigurðsson, O., and Thorsteinsson, T. (2012). Hydropower, snow and ice. In: *Climate Change and Energy Systems: Impacts, Risks and Adaptation in the Nordic and Baltic Countries* [Thorsteinsson, T. and H. Björnsson (eds.)]. *Nordic Council of Ministers*, Copenhagen, Denmark, pp.91-111.
- Juen, I., Kaser, G., and Georges, C. (2007). Modelling observed and future runoff from a glacierized tropical catchment. *Global and Planetary Change*, 59: 37-48.
- Kadıoğlu, M. (1997). Trends in surface air temperature data over Turkey. *International Journal of Climatology*, 17: 511-520.
- Kahya, E. and Kalaycı, S. (2004). Trend analysis of streamflow in Turkey. *Journal of Hydrology*, 289: 128-144.
- Kamarianakis, Y., Feidas, H., Kokolatos, G., Chrysoulakis, N., and Karatzias, V. (2008). Evaluating remotely sensed rainfall estimates using nonlinear mixed models and geographically weighted regression. *Environmental Modelling and Software*, 23: 1438–1447.
- Karl, T.R., Ya Groisman, P., Knight, R.W., and Heim Jr, R.R. (1993). Recent Variations of Snow Cover and Snowfall in North America and Their Relation to Precipitation and Temperature Variations. *Journal of Climate*, 6: 1327-1344.

- Katul, G. and Novick, K. (2009). Evapotranspiration. In: Encyclopedia of Inland Waters [Likens, G.E. (eds.)]. *Academic Press*, Massachusetts, USA, pp. 661-667.
- Kay, J.E., Raeder, K., Gettelman, A., and Anderson, J. (2011). The boundary layer response to recent Arctic sea ice loss and implications for high-latitude climate feedbacks. *Journal of Climatology*, 24: 428–447.
- Killingveit, Å. and Sælthun, N.R. (1995). Hydrological models. In *Hydropower Development 7: Hydrology*. *Trondheim: Norwegian Institute of Technology*, pp. 99-128.
- Knutson, T.R., McBride, J.L., Chan, J., Emanuel, K., Holland, G., Landsea, C., Held, I., Kossin, J.P., Srivastava, A.K., and Sugi, M. (2010). Tropical cyclones and climate change. *Nature Geoscience*, 3(3): 157-163.
- Korhonen, J. and Kuusisto, E. (2010). Long-term changes in the discharge regime in Finland. *Hydrology Research*, 41(3-4): 253-268.
- Koutroulis, A.G., Tsanis, I.K., Daliakapoulos, I.N., and Jacob, D. (2013). Impact of climate change on water resources status: A case study for Crete Island, Greece. *Journal of Hydrology*, 479: 146–158.
- Krause, P., Boyle, D.P., and Base, F. (2005). Comparison of different efficiency criteria for hydrological model assessment. *Advances in Geosciences*, 5: 89–97.
- Kristensen, L., Olsen, J., Weiner, J., Griepentrog, H.W., and Norremark, M. (2006). Describing the spatial pattern of crop plants with special reference to crop-weed competition studies. *Field Crops Research*, 96: 207–215.
- Kum, G. and Çelik, M.A. (2014). Impacts of global climate change on the Mediterranean Region: Adana as a case study. *Procedia - Social and Behavioral Sciences*, 120: 600-608.
- Kundzewicz, Z.W., Kanae, S., Seneviratne, S.I., Handmer, J., Nicholls, N., Peduzzi, P., Mechler, R., Bouwer, L.M., Arnell, N., Mach, K., Muir-Wood, R., Brakenridge, G.R., Kron, W., Benito, G., Honda, Y., Takahashi, K., and Sherstyukov, B. (2013). Flood risk and climate change -global and regional perspectives. *Hydrological Sciences Journal*, 59(1): 1-28.
- Kusangaya, S., Warburton, M., van Garderen, E.A., and Jewitt, G.P.W. (2014). Impacts of climate change on water resources in southern Africa: A review. *Physics and Chemistry of the Earth, Parts A/B/C*, 67-69: 47-54.

- Kysely, J., Begueria, S., Beranova, R., Gaal, L., and Lopez-Moreno, J.I. (2012). Different patterns of climate change scenarios for short-term and multi-day precipitation extremes in the Mediterranean. *Global and Planetary Change*, 98–99: 63–72.
- Lawrence, D., Haddeland, I., and Langsholt, E. (2009). Calibration of HBV hydrological models using PEST parameter estimation. OSLO: *Norwegian Water Resources and Energy Directorate*.
- Lespinas, F., Ludwig, W., and Heussner, S. (2014). Hydrological and climatic uncertainties associated with modeling the impact of climate change on water resources of small Mediterranean coastal rivers. *Journal of Hydrology*, 511: 403-422.
- Li, F., Zhang, Y., Xu, Z., Teng, J., Liu, C., Liu, W., and Mpelasoka, F. (2013). The impact of climate change on runoff in the southeastern Tibetan Plateau. *Journal of Hydrology*, 505: 188-201.
- Li, S., Zhao, Z., Miaomiao, X., and Wang, Y. (2010). Investigating spatial non-stationary and scale-dependent relationships between urban surface temperature and environmental factors using geographically weighted regression. *Environmental Modelling and Software*, 25: 1789-1800.
- Lindström, G. and Bergström, S. (1992). Improving the HBV and PULSE-models by use of temperature anomalies. *Vannet i Norden*, 25(1): 16-23.
- Lindström, G. and Rodhe, A. (1992). Transit times of water in soil lysimeters from modelling of oxygen-18. *Water, Air and Soil Pollution*, 65: 83-100.
- Lindström, G., Johansson, B., Persson, M., Gardelin, M., and Bergström, S. (1997). Development and test of the distributed HBV-96 hydrological model. *Journal of Hydrology*, 201:272-288.
- Linnenluecke, M.K., Stathakis, A., and Griffiths, A. (2011). Firm relocation as adaptive response to climate change and weather extremes. *Global Environmental Change*, 21: 123-133.
- Lu, X.X., Zhang, S., and Xu, J. (2010). Climate change and sediment flux from the Roof of the World. *Earth Surface Processes and Landforms*, 35(6): 732-735.
- Lu, X. and Cheng, G. (2009). Climate change effects on soil carbon dynamics and greenhouse gas emissions in *Abies fabri* forest of subalpine, southwest China. *Soil Biology and Biochemistry*, 41: 1015-1021.
- Ludwig, R., Roson, R., Zografos, C., and Kallis, G. (2011). Towards an interdisciplinary research agenda on climate change, water and security in

Southern Europe and neighboring countries. *Environmental Science & Policy*, 14: 794-803.

Marquardt, D. (1963). An algorithm for Least-Squares Estimation of Nonlinear Parameters. *SIAM Journal on Applied Mathematics*, 11: 431-441.

Masterson, J.P. and Garabedian, S.P. (2007). Effects of sea-level rise on ground water flow in a coastal aquifer system. *Ground Water*, 45(2): 209-217.

McDonald, R.I. and Girvetz, E.H. (2013). Two challenges for U. S. irrigation due to climate change: increasing irrigated area in wet states and increasing irrigation rates in dry states. *Plos One*, 8(6): e65589.

Mennis, J. (2006). Mapping the Results of Geographically Weighted Regression. *The Cartographic Journal*, 43: 171-179.

Menzel, L. and Bürger, G. (2002). Climate change scenarios and runoff response in the Mulde catchment (Southern Elbe, Germany). *Journal of Hydrology*, 267: 53-64.

Miao, C., J. Ni, Borthwick, A.G.L., and Yang, L. (2011). A preliminary estimate of human and natural contributions to the changes in water discharge and sediment load in the Yellow River. *Global and Planetary Change*, 76(3-4): 196-205.

Mirza, M.M.Q. (2003). Climate change and extreme weather events: can developing countries adapt? *Climate Policy*, 3: 233-248.

Mori, N., Shimura, T., Yasuda, T., and Mase, H. (2013). Multi-model climate projections of ocean surface variables under different climate scenarios—Future change of waves, sea level and wind. *Ocean Engineering*, 71: 122-129.

NASA. (National Aeronautics and Space Administration) (2014). *What Is Climate Change?* May 14. Accessed: September 05, 2014.
http://www.nasa.gov/audience/forstudents/k-4/stories/what-is-climate-change-k4.html#.VAIpS_mSx8E.

Okkonen, J. and Klove, B. (2010). A conceptual and statistical approach for the analysis of climate impact on ground water table fluctuation patterns in cold conditions. *Journal of Hydrology*, 388: 1-12.

Omstedt, A. and Hansson, D. (2006). The Baltic Sea ocean climate system memory and response to changes in the water and heat balance components. *Continental Shelf Research*, 26: 236-251.

Paerl, H.W. and Huisman, J. (2008). Climate - Blooms like it hot. *Science*, 320: 57-58.

- Partal, T. and Kahya, E. (2006). Trend analysis in Turkish precipitation data. *Hydrological Processes*, 20: 2011-2026.
- Pednekar, A.M., Grant, S.B., Jeong, Y., Poon, Y., and Oancea, C. (2005). Influence of climate change, tidal mixing, and watershed urbanization on historical water quality in Newport Bay, a saltwater wetland and tidal embayment in southern California. *Environmental Science and Technology*, 39(23): 9071-9082.
- Petrow, T. and Merz, B. (2009). Trends in flood magnitude, frequency and seasonality in Germany in the period 1951-2002. *Journal of Hydrology*, 371(1-4): 129-141.
- Portmann, F.T., Döll, P., Eisner, S., and Flörke, M. (2013). Impact of climate change on renewable groundwater resources: assessing the benefits of avoided greenhouse gas emissions using selected CMIP5 climate projections. *Environmental Research Letters*, 8(2): 024023.
- Prasad, S., Witt, A., Kienel, U., Dulski, P., Bauer, E., and Yancheva, G. (2009). "The 8.2 ka event: Evidence for seasonal differences and the rate of climate change in western Europe." *Global and Planetary Change*, 67: 218-226.
- Propastin, P. (2012). Modifying geographically weighted regression for estimating aboveground biomass in tropical rainforests by multispectral remote sensing data. *International Journal of Applied Earth Observation and Geoinformation*, 18: 82–90.
- Rabassa, J. (2009). Impact of global climate change on glaciers and permafrost of South America, with emphasis on Patagonia, Tierra del Fuego, and the Antarctic Peninsula. *Developments in Earth Surface Processes*, 13: 415-438.
- Ruelland, D., Ardoin-Bardin, S., Billen, G., and Servat, E. (2008). Sensitivity of a lumped and semi-distributed hydrological model to several methods of rainfall interpolation on a large basin in West Africa. *Journal of Hydrology*, 361: 96–117.
- Sælthun, N.S. (1996). The Nordic HBV Model. *NVE Publication* no. 07, 26 pp.
- Salvati, L., Sateriano, A., and Zitti, M. (2013). Long-term land cover changes and climate variations – A country-scale approach for a new policy target. *Land Use Policy*, 30: 401-407.
- Schewe, J., Heinke, J., Gerten, D., Haddeland, I., Arnell, N.W., Clark, D.B., Dankers, R., Eisner, S., Fekete, B., Colón-González, F.J., Gosling, S.N., Kim, H., Liu, X., Masaki, Y., Portmann, F.T., Satoh, Y., Stacke, T., Tang, Q., Wada, Y., Wisser, D., Albrecht, T., Frieler, K., Piontek, F., Warszawski, L., and Kabat, P. (2013). Multi-model assessment of water scarcity under climate change.

Proceedings of the National Academy of Sciences of the United States of America, in press.

- Seaby, L.P., Refsgaard, J.C., Sonnenborg, T.O., Stisen, S., Christensen, J.H., and Jensen, K.H. (2013). Assessment of robustness and significance of climate change signals for an ensemble of distribution-based scaled climate projections. *Journal of Hydrology*, 486: 479–493.
- Seneviratne, S.I., Corti, T., Davin, E.L., Hirschi, M., Jaeger, E.B., Lehner, I., Orlowsky, B., and Teuling, A.J. (2010). Investigating soil moisture–climate interactions in a changing climate: A review. *Earth-Science Reviews*, 99(3-4): 125-161.
- Seneviratne, S.I., Nicholls, N., Easterling, D., Goodess, C.M., Kanae, S., Kossin, J., Luo, Y., Marengo, J., McInnes, K., Rahimi, M., Reichstein, M., Sorteberg, A., Vera, C., and Zhang, X. (2012). Changes in climate extremes and their impacts on the natural physical environment. In: *Managing the Risks of Extreme Events and Disasters to Advance Climate Change Adaptation* [Field, C.B., V. Barros, T.F. Stocker, D. Qin, D.J. Dokken, K.L. Ebi, M.D. Mastrandrea, K.J. Mach, G.-K. Plattner, S.K. Allen, M. Tignor, and P.M. Midgley (eds.)]. A Special Report of Working Groups I and II of the Intergovernmental Panel on Climate Change (IPCC). *Cambridge University Press*, Cambridge, UK, and New York, NY, USA, pp. 109-230.
- Shi, C., Zhou, Y., Fan, X., and Shao, W. (2013). A study on the annual runoff change and its relationship with water and soil conservation practices and climate change in the middle Yellow River basin. *CATENA*, 100: 31-41.
- SMHI (2014). The HBV Model. Swedish Meteorological and Hydrological Institute: <http://www.smhi.se/sgn0106/if/hydrologi/hbv.htm>, Accessed July 14, 2014.
- Stahl, K., Hisdal, H., Hannaford, J., Tallaksen, L.M., van Lanen, H.A.J., Sauquet, E., Demuth, S., Fendekova, M., and Jodar, J. (2010). Streamflow trends in Europe: evidence from a dataset of near-natural catchments. *Hydrology and Earth System Sciences*, 14(12): 2367-2382.
- Statham, P.J. (2012). Nutrients in estuaries — an overview and the potential impacts of climate change. *Science of the Total Environment*, 434: 213-227.
- Stoffel, M., Tiranti, D., and Huggel, C. (2014). Climate change impacts on mass movements — Case studies from the European Alps. *Science of The Total Environment*, 493: 1255-1266.
- Tahir, A.A., Chevallier, P., Arnaud, Y., Neppel, L., and Ahmad, B. (2011). Modeling snowmelt-runoff under climate scenarios in the Hunza River basin, Karakoram Range, Northern Pakistan. *Journal of Hydrology*, 409: 104-117.

- Takala, M., Pulliainen, J., Metsamäki, S.J., and Koskinen, J.T. (2009). Detection of snowmelt using spaceborne microwave radiometer data in Eurasia from 1979 to 2007. *IEEE Transactions on Geoscience and Remote Sensing*, 47(9): 2996-3007.
- Talei, A., Chua, L.H.C., Quek, C., and Jansson, P.E. (2013). Runoff forecasting using a Takagi–Sugeno neuro-fuzzy model with online learning. *Journal of Hydrology*, 488: 17-32.
- Tan, A., Adam, J.C., and Lettenmaier, D.P. (2011). Change in spring snowmelt timing in Eurasian Arctic Rivers. *Journal of Geophysical Research-Atmospheres*, 116: D03101.
- Tao, F. and Zhang, Z. (2013). Climate change, wheat productivity and water use in the North China Plain: A new super-ensemble-based probabilistic projection. *Agricultural and Forest Meteorology*, 170: 146–165.
- Tayanç, M., İm, U., Doğruel, M., and Karaca, M. (2009). Climate change in Turkey for the last half century. *Climatic Change*, 94: 483-502.
- Taylor, I.H., Burke, E., McColl, L., Falloon, P.D., Harris, G.R., and McNeall, D. (2013). The impact of climate mitigation on projections of future drought. *Hydrology and Earth System Sciences*, 17(6): 2339-2358.
- Taylor, R.G., Scanlon, B., Döll, P., Rodell, M., van Beek, R., Wada, Y., Longuevergne, L., Leblanc, M., Famiglietti, J.S., Edmunds, M., Konikow, L., Green, T.R., Chen, J., Taniguchi, M., Bierkens, M.F.P., MacDonald, A., Fan, Y., Maxwell, R.M., Yechieli, Y., Gurdak, J.J., Allen, D.M., Shamsudduha, M., Hiscock, K., Yeh, P.J.-F., Holman, I., and Treidel, H. (2013). Ground water and climate change. *Nature Climate Change*, 3(4): 322-329.
- Teutschbein, C. and Siebert, J. (2012). Bias correction of regional climate model simulations for hydrological climate-change impact studies: Review and evaluation of different methods. *Journal of Hydrology*, 456–457: 12–29.
- Thodsen, H., Hasholt, B., and Kjærsgaard, J.H. (2008). The influence of climate change on suspended sediment transport in Danish rivers. *Hydrological Processes*, 22(6): 764-774.
- Tibby, J. and Tiller, D. (2007). Climate-water quality relationships in three Western Victorian (Australia) lakes 1984-2000. *Hydrobiologia*, 591(1): 219-234.
- Toan, T. (2014). 9 – Climate Change and Sea Level Rise in the Mekong Delta: Flood, Tidal Inundation, Salinity Intrusion, and Irrigation Adaptation Methods. *Engineering and Planning Perspectives*, 199-218.

- Tramblay, Y., Badi, W., Driouech, F., El Adlouni, S., Neppel, L., and Servat, E. (2012). Climate change impacts on extreme precipitation in Morocco. *Global and Planetary Change*, 82-83: 104–114.
- Türkeş, M., Koç, T., and Sariş, F. (2009). Spatiotemporal variability of precipitation total series over Turkey. *International Journal of Climatology*, 29: 1056-1074.
- Türkeş, M., Sümer, U.M., and Demir, İ. (2002). Re-evaluation of trends and changes in mean, maximum, and minimum temperatures of Turkey for the period 1929-1999. *International Journal of Climatology*, 22: 947-977.
- Türkeş, M. (1996). Spatial and temporal analysis of annual rainfall variations in Turkey. *International Journal of Climatology*, 16: 1057-1076.
- UK Met. Office. (2014). *What is climate change?* 3 February. Accessed: September 5, 2014. <http://www.metoffice.gov.uk/climate-guide/climate-change>.
- Van der Linden, P. And Mitchell, J.F.B. (eds.) (2009). ENSEMBLES: Climate Change and its Impacts: Summary of research and results from the ENSEMBLES project. Met Office Hadley Centre. Exeter, UK. 160 pp.
- Viana, H., Aranha, J., Lopes, D., and Cohen, W.B. (2012). Estimation of crown biomass of Pinus pinaster stands and shrubland above-ground biomass using forest inventory data, remotely sensed imagery and spatial prediction models. *Ecological Modelling*, 226: 22 – 35.
- Vieux, B. (2001). Distributed Hydrologic Modeling using GIS. *Kluwer Academic Publishers*, Dordrecht, the Netherlands.
- Vineis, P., Chan, Q., and Khan, A. (2011). Climate change impacts on water salinity and health. *Journal of Epidemiology and Global Health*, 1, 5-10.
- Visbeck, M.H., Hurrell, J.W., Polvanis, L., and Cullen, H.M. (2001). The North Atlantic Oscillation: Past, present, and future. *Proceedings of the National Academy of Sciences of the United States of America*. Irvine: PNAS. 12876–12877.
- Vörösmarty, C.J., McIntyre, P.B., Gessner, M.O., Dudgeon, D., Prusevich, A., Green, P., Glidden, S., Bunn, S.E., Sullivan, C.A., Liermann, C.R., and Davies, P.M. (2010). Global threats to human water security and river biodiversity. *Nature*, 467(7315): 555-561.
- Vrochidou, A.E.K., Tsanis, I.K., Grillakis, M.G., and Koutroulis, A.G. (2013). The impact of climate change on hydrometeorological droughts at a basin scale. *Journal of Hydrology*, 476: 290–301.

- Wada, Y., Wisser, D., Eisner, S., Flörke, M., Gerten, D., Haddeland, I., Hanasaki, N., Masaki, Y., Portmann, F.T., Stacke, T., Tessler, Z., and Schewe, J. (2013). Multi-model projections and uncertainties of irrigation water demand under climate change. *Geophysical Research Letters*, 40(17): 4626-4632.
- Wagner, P.D., Fiener, P., Wilken, F., Kumar, S., and Schneider, K. (2012). Comparison and evaluation of spatial interpolation schemes for daily rainfall in data scarce regions. *Journal of Hydrology*, 464-465: 388-400.
- Wang, A., Lettenmaier, D.P., and Sheffield, J. (2011). Soil Moisture Drought in China, 1950-2006. *Journal of Climate*, 24(13): 3257-3271.
- Werner, A.D., Ward, J.D., Morgan, L.K., Simmons, C.T., Robinson, N.I., and Teubner, M.D. (2012). Vulnerability indicators of sea water intrusion. *Ground Water*, 50(1): 48-58.
- Willems P. (2009). A time series tool to support the multi-criteria performance evaluation of rainfall-runoff models. *Environmental Modelling & Software*, 24(3), 311-321.
- Willems, P. and Vrac, M. (2013). Statistical precipitation downscaling for small-scale hydrological impact investigations of climate change. *Journal of Hydrology*, 402: 1015-1030.
- Williams, D., Elghali, L., Wheeler, R., and France, C. (2012). Climate change influence on building lifecycle greenhouse gas emissions: Case study of a UK mixed-use development. *Energy and Buildings*, 48: 112-126.
- Wilson, D., Hisdal, H., and Lawrence, D. (2010). Has streamflow changed in the Nordic countries? - Recent trends and comparisons to hydrological projections. *Journal of Hydrology*, 394(3-4): 334-346.
- Xie, Z.C., Wang, X., Feng, Q.H., Kang, E.S., Li, Q.Y., and Cheng, L. (2006). Glacial runoff in China: an evaluation and prediction for the future 50 years. *Journal of Glaciology and Geocryology*, 28(4): 457-466.
- Yıldız, M. and Saraç, M. (2008). Türkiye akarsularındaki akımların trendleri ve bu trendlerin hidroelektrik enerji üretimine etkileri. *VII. Ulusal Temiz Enerji Sempozyumu*. İstanbul. 503-516.
- Yılmaz, K.K. and Yazıcıgil, H., (2011). Potential Impacts of Climate Change on Turkish Water Resources: A Review. In *Climate Change and its Effects on Water Resources*, by A. Baba, G. Tayfur, O. Gündüz, K.W.F. Howard, M.J. Friedel and A. Chambel, 105-114. Netherland: *Springer*.

- Yucel, I., Güventürk, A., and Sen, O.L. (2014). Climate change impacts on snowmelt runoff for mountainous transboundary basins in eastern Turkey. *International Journal of Climatology*, xxx: xxx-xxx.
- Zhang, X. and Cai, X. (2013). Climate change impacts on global agricultural water deficit. *Geophysical Research Letters*, 40(6): 1111-1117.
- Zhang, X., Zwiers, F.W., Hegerl, G.C., Lambert, F.H., Gillett, N.P., Solomon, S., Stott, P.A., and Nozawa, T. (2007). Detection of human influence on twentieth-century precipitation trends. *Nature*, 448(7152): 461-465.
- Zhenyao, S., Lei, C., Ruimin, L., and Qian, H. (2012). Impact of spatial rainfall variability on hydrology and nonpoint source pollution modeling. *Journal of Hydrology*, 472-473: 205-215.
- Ziadat, F.M. (2007). Land suitability classification using different sources of information: Soil maps and predicted soil attributes in Jordan. *Geoderma*, 140: 73-80.

APPENDIX A

PARAMETER FILE OF SUB-CATCHMENT 02-67

```
START 1grid
2 0 1 PNO Number of precipitation stations
2 0 Zone1 PID1 Identification for precip station 1
2 0 147.00 PHOH1 Altitude precip station 1
2 0 1 PWGT1 Weight precip station 1
2 0 1 TNO Number of temperature stations
2 0 Zone1 TID1 Identification for temp station 1
2 0 147.00 THOH1 Altitude temp station 1
2 0 1 TWGT1 Weight temp station 1
2 0 1 QNO
2 0 OEMERLI_2 QID
2 0 1 QWGT
2 0 145 AREAL
2 4 0.000 MAGDEL
2 5 64.00 HYP SO (1,1)
2 6 147.00 HYP SO (2,1)
2 7 168.00 HYP SO (3,1)
2 8 184.00 HYP SO (4,1)
2 9 200.00 HYP SO (5,1)
2 10 215.00 HYP SO (6,1)
2 11 231.00 HYP SO (7,1)
2 12 251.00 HYP SO (8,1)
2 13 279.00 HYP SO (9,1)
2 14 314.00 HYP SO (10,1)
2 15 479.00 HYP SO (11,1)
2 16 0.000 HYP SO (1,2)
2 17 0.100 HYP SO (2,2)
2 18 0.200 HYP SO (3,2)
2 19 0.300 HYP SO (4,2)
2 20 0.400 HYP SO (5,2)
2 21 0.500 HYP SO (6,2)
2 22 0.600 HYP SO (7,2)
2 23 0.700 HYP SO (8,2)
2 24 0.800 HYP SO (9,2)
2 25 0.900 HYP SO (10,2)
2 26 1.000 HYP SO (11,2)
```

2	27	0.000	BREPRO(1),		
2	28	0.000	BREPRO(2),		
2	29	0.000	BREPRO(3),		
2	30	0.000	BREPRO(4),		
2	31	0.000	BREPRO(5),		
2	32	0.000	BREPRO(6),		
2	33	0.000	BREPRO(7),		
2	34	0.000	BREPRO(8),		
2	35	0.000	BREPRO(9),		
2	36	0.000	BREPRO(10),		
2	37	0.000	BREPRO(11),		
2	38				
2	39	270.0000	NDAG	Day no for conversion of glacier snow to ice	
2	40	-.2650954128	TX	Threshold temperature for snow/ice	[C]
2	41	2.0000000000	TS	Threshold temperature fo no melt	[C]
2	42	1.9674446523	CX	Melt index	[mm/deg/day]
2	43	0.0200	CFR	Refreeze efficiency	[1]
2	44	0.0800	LV	Max rel. water content in snow	[1]
2	45	.99328928799	PKORR	Precipitaion correction for rain	[1]
2	46	1.3278375759	SKORR	Additional precipitation corection for snow at gauge	[1]
2	47		GRADALT		
2	48		PGRAD1		
2	49	0.0200	CALB	Ageing factor for albedo	[1/day]
2	50	0.3300	CRAD	Radiation melt component	[1]
2	51	0.3300	CONV	Convection melt component	[1]
2	52	0.3300	COND	Condensation melt component	[1]
2	60	1.1000	CEVPL	Lake evapotranspiration adjustment fact	[1]
2	61	0.5000	ERED	Evapotranspiration red. during interception	[1]
2	62	30.0000	ICEDAY	Lake temperature time constant	[d]
2	63	-.5002344066	TTGRAD	Temperature gradient for days without precip	[deg/100 m]
2	64	-.7000000000	TVGRAD	Temperature gradient for days with precip	[deg/100 m]
2	65	3.6000000E-4	PGRAD	Precipitation altitude gradient	[1/100 m]
2	66	1.5000	CBRE	Melt increase on glacier ice	[1]
2	67	0.1000	EP	EP(1), Pot evapotranspiration, Jan	[mm/day] or [1]
2	68	0.2000	EP	EP(2), Pot evapotranspiration, Feb	[mm/day] or [1]
2	69	0.3000	EP	EP(3)	
2	70	0.8000	EP	EP(4)	
2	71	2.1000	EP	EP(5)	
2	72	2.3000	EP	EP(6)	
2	73	2.4000	EP	EP(7)	
2	74	2.0000	EP	EP(8)	
2	75	1.4000	EP	EP(9)	
2	76	0.5000	EP	EP(10)	

2	77	0.2000	EP	EP(11)	
2	78	0.1000	EP	EP(12)), Pot evapotranspiration, Dec	[mm/day] or [1]
2	79	199.85415574	FC	Maximum soil water content	[mm]
2	80	1.0000	FCDEL	Pot.evapotr when content = FC*FCDEL	[1]
2	81	1.2922754110	BETA	Non-linearity in soil water zone	[1]
2	82	100.0000	INFMAX	Maximum infiltration capacity	[mm/day]
2	85	.19999989634	KUZ2	Quick time constant upper zone	[1/day]
2	86	10.000000000	UZ1	Threshold quick runoff	[mm]
2	87	.38886504297	KUZ1	Slow time constant upper zone	[1/day]
2	88	2.000000000	PERC	Percolation to lower zone	[mm/day]
2	89	.03757788816	KLZ	Time constant lower zone	[1/day]
2	90	0.0000	ROUT	(1), Routing constant (lake area, km2)	
2	91	0.0000	ROUT	(2), Routing constant (rating curve const)	
2	92	0.0000	ROUT	(3), Routing constant (rating curve zero)	
2	93	0.0000	ROUT	(4), Routing constant (rating curve exp)	
2	94	0.0000	ROUT	(5), Routing constant (drained area ratio)	
2	95	0.0000	DECAY	(1), Feedback constant	
2	96	0.0000	DECAY	(2), Feedback constant	
2	97	0.0000	DECAY	(3), Feedback constant	
2	98	0.1700	CE	Evapotranspiration constant	[mm/deg/day]
2	99	0.5000	DRAW	"draw up" constant	[mm/day]
2	100	59.0000	LAT	Latitude	[deg]
2	101	-0.6000	TGRAD(1)	Temperature gradient Jan	[deg/100m]
2	102	-0.6000	TGRAD(2)	Temperature gradient Feb	[deg/100m]
2	103	-0.6000	TGRAD(3)	Temperature gradient Mar	[deg/100m]
2	104	-0.6000	TGRAD(4)	Temperature gradient Apr	[deg/100m]
2	105	-0.6000	TGRAD(5)	Temperature gradient May	[deg/100m]
2	106	-0.6000	TGRAD(6)	Temperature gradient Jun	[deg/100m]
2	107	-0.6000	TGRAD(7)	Temperature gradient Jul	[deg/100m]
2	108	-0.6000	TGRAD(8)	Temperature gradient Aug	[deg/100m]
2	109	-0.6000	TGRAD(9)	Temperature gradient Sep	[deg/100m]
2	110	-0.6000	TGRAD(10)	Temperature gradient Oct	[deg/100m]
2	111	-0.6000	TGRAD(11)	Temperature gradient Nov	[deg/100m]
2	112	-0.6000	TGRAD(12)	Temperature gradient Dec	[deg/100m]
2	113	20.0000	SPDIST	Uniformly distributed snow acc	[mm]
2	114	30.0000	SMINI	Initial soil moisture content	[mm]
2	115	0.0000	UZINI	Initial upper zone content	[mm]
2	116	20.0000	LZINI	Initial lower zone content	[mm]
2	121	2	VEGT(1,1)	Vegetation type	
2	122	4	VEGT(2,1)	Vegetation type	
2	123	0.250	VEGA(1)	Vegetation 2 area	
2	124	0.000	LAKE(1)	Lake area	
2	125	2	VEGT(1,2)	Vegetation type	
2	126	4	VEGT(2,2)	Vegetation type	
2	127	0.250	VEGA(2)	Vegetation 2 area	
2	128	0.000	LAKE(2)	Lake area	

2 129	2	VEGT(1,3) Vegetation type
2 130	4	VEGT(2,3) Vegetation type
2 131	0.250	VEGA(3) Vegetation 2 area
2 132	0.000	LAKE(3) Lake area
2 133	2	VEGT(1,4) Vegetation type
2 134	4	VEGT(2,4) Vegetation type
2 135	0.250	VEGA(4) Vegetation 2 area
2 136	0.000	LAKE(4) Lake area
2 137	2	VEGT(1,5) Vegetation type
2 138	4	VEGT(2,5) Vegetation type
2 139	0.250	VEGA(5) Vegetation 2 area
2 140	0.000	LAKE(5) Lake area
2 141	2	VEGT(1,6) Vegetation type
2 142	4	VEGT(2,6) Vegetation type
2 143	0.250	VEGA(6) Vegetation 2 area
2 144	0.000	LAKE(6) Lake area
2 145	2	VEGT(1,7) Vegetation type
2 146	4	VEGT(2,7) Vegetation type
2 147	0.250	VEGA(7) Vegetation 2 area
2 148	0.000	LAKE(7) Lake area
2 149	2	VEGT(1,8) Vegetation type
2 150	4	VEGT(2,8) Vegetation type
2 151	0.250	VEGA(8) Vegetation 2 area
2 152	0.000	LAKE(8) Lake area
2 153	2	VEGT(1,9) Vegetation type
2 154	4	VEGT(2,9) Vegetation type
2 155	0.250	VEGA(9) Vegetation 2 area
2 156	0.000	LAKE(9) Lake area
2 157	2	VEGT(1,10) Vegetation type
2 158	4	VEGT(2,10) Vegetation type
2 159	0.250	VEGA(10) Vegetation 2 area
2 160	0.000	LAKE(10) Lake area

FINIS

APPENDIX B

A SAMPLE INPUT FILE FOR THE HBV MODEL

Year	Month	Day	Precipitatio	Temperature	Discharge
1978	10	1	0.00	13.20	0.08
1978	10	2	0.00	17.60	0.10
1978	10	3	0.00	20.40	0.10
1978	10	4	0.00	17.40	0.10
1978	10	5	0.00	16.30	0.10
1978	10	6	0.00	15.10	0.10
1978	10	7	0.00	15.80	0.10
1978	10	8	0.00	15.80	0.10
1978	10	9	0.00	17.20	0.10
1978	10	10	0.00	16.50	0.10
1978	10	11	0.00	15.30	0.10
1978	10	12	0.00	15.40	0.10
1978	10	13	0.00	16.10	0.10
1978	10	14	0.00	15.40	0.10
1978	10	15	0.00	12.00	0.10
1978	10	16	0.00	12.40	0.08
1978	10	17	0.00	13.00	0.08
1978	10	18	0.00	12.50	0.08

1978	10	19	0.00	13.80	0.08	
1978	10	20	0.00	13.70	0.10	
1978	10	21	0.00	14.00	0.10	
1978	10	22	7.00	11.20	0.12	
1978	10	23	8.00	8.50	0.12	
1978	10	24	0.00	8.30	0.14	
1978	10	25	0.00	12.50	0.14	...

APPENDIX C

A SAMPLE RESULT FILE OF THE HBV MODEL

```

Simulation for grid      period: 1/ 9 1979 - 30/ 8 1995
States
      prec  temp  evap  snowres  snowcov  soilmoist  upperzn
lowerzn  qsim  qobs
1979  9  1  0.099  17.672  1.344  0.000  0.000  29.053  0.000  18.961
0.740  0.286
1979  9  2  1.590  19.472  1.984  0.000  0.000  28.853  0.000  18.062
0.705  0.191
1979  9  3  0.000  20.023  1.400  0.000  0.000  27.726  0.000  17.122
0.669  0.167
1979  9  4  0.000  18.823  1.258  0.000  0.000  26.729  0.000  16.227
0.634  0.268
1979  9  5  0.000  19.523  1.252  0.000  0.000  25.727  0.000  15.376
0.600  0.131
1979  9  6  0.000  20.423  1.255  0.000  0.000  24.711  0.000  14.569
0.569  0.119
1979  9  7  0.000  20.923  1.229  0.000  0.000  23.711  0.000  13.801
0.539  0.107
1979  9  8  0.099  20.072  1.176  0.000  0.000  22.853  0.000  13.072
0.510  0.107
1979  9  9  0.000  19.323  1.040  0.000  0.000  22.021  0.000  12.380
0.483  0.095
1979  9 10  0.000  19.123  0.988  0.000  0.000  21.232  0.000
11.723  0.458  0.083
1979  9 11  0.000  18.923  0.939  0.000  0.000  20.483  0.000
11.099  0.433  0.083
1979  9 12  0.000  19.223  0.917  0.000  0.000  19.747  0.000
10.508  0.410  0.072
1979  9 13  0.000  19.623  0.899  0.000  0.000  19.020  0.000  9.947
0.388  0.072
1979  9 14  0.000  20.823  0.916  0.000  0.000  18.269  0.000  9.415
0.368  0.072
1979  9 15  0.000  20.223  0.851  0.000  0.000  17.575  0.000  8.911
0.348  0.072
1979  9 16  0.000  14.023  0.565  0.000  0.000  17.158  0.000  8.433
0.329  0.072

```


CURRICULUM VITAE

PERSONAL INFORMATION

Surname, Name: Kara, Fatih

Nationality: Turkish (TC)

Date and Place of Birth: 1 February 1974, Düzce

Marital Status: Married

Email: e160027@metu.edu.tr

EDUCATION

Degree	Institution	Year of Graduation
MA	Fatih Unv. Dept. of Geography	2007
BA	Dokuz Eylul Unv. Dept. of Geography Educ.	1996
High School	Düzce Lisesi	1990

WORK EXPERIENCE

Year	Place	Enrollment
2011-present	Fatih University	Lecturer
2006-2011	Fatih University	Research Assist.

FOREIGN LANGUAGES

Advanced in English.

PUBLICATIONS

- Egresi, I., Kara, F., "Motives of Tourists Attending Small-Scale Events: The Case of Three Local Festivals and Events in Istanbul, Turkey", *GeoJournal of Tourism and Geosites*, Vol. 14, No. 2, Jul. 2014, pp. 94-111.
- Kara, F., Egresi, I., "Accessibility of health care institutions: a case study by using GIS", *International Journal of Scientific Knowledge*, Vol. 3, No. 4, Aug. 2013, pp. 16-27
- Kara, F., Tuna, F., "A geographical research of facilities brought by high resolution satellite images in determining plant species", *International Journal of Scientific Knowledge*, Vol. 3, No. 3, Jul. 2013, pp. 1-10.
- Egresi, I., Bayram, B., Kara, F., "Economic Impact of Religious Tourism in Mardin, Turkey", *Journal of Economics and Business Research*, Vol. 18, No. 2, Nov. 2012, pp. 7-22.
- Egresi, I., Bayram, B., Kara, F., "Tourism at religious sites: a case from Mardin, Turkey", *Geographica Timisiensis*, Vol. 21, No. 1, Aug. 2012, pp. 5-15.
- Karaburun, A., Demirci, A., and Kara, F., "Analysis of Spatially Distributed Annual, Seasonal, and Monthly Temperatures in Marmara Region from 1975 to 2006", *Ozean Journal of Applied Sciences*, Vol. 5, No. 2, Jun. 2012, pp. 131-149.
- Kara, F., "Investigation of Effects of Spatial Resolution on Image Classification", *Ozean Journal of Applied Sciences*, Vol. 5, No. 2, Jun. 2012, pp. 169-184.
- Egresi, I., Bayram, B., Kara, F., Kesik, O.A., "Unlocking the potential of religious tourism in Turkey", *GeoJournal of Tourism and Geosites*, Vol. 9, No. 1, May. 2012, pp. 63-80.
- Kara, F., Usul, N., "Highway route design through the use of GIS and multi-criteria analysis: a case study of Istanbul ", *Ozean Journal of Applied Sciences*, Vol. 5, No. 1, Mar. 2012, pp. 71-84.
- Karaburun, A., Demirci, A., Kara, F., "Analysis of Spatially Distributed Annual, Seasonal and Monthly Temperatures in Istanbul from 1975 to 2006", *World Applied Sciences Journal*, Vol. 12, No. 10, May. 2011, pp. 1662-1675.
- Kara, F., "Determination of land-use/land-cover change and urban growth by using remote sensing: a case study of Duzce province in Turkey", *Fresenius Environmental Bulletin*, Vol. 19, No. 7, Jul. 2010, pp. 1312-1319.

Kara, F., Demirci, A., "Spatial analysis and facility characteristics of outdoor recreational areas in Istanbul", *Environmental Monitoring And Assessment*, Vol. 164, No. 1-4, May. 2010, pp. 593-603.

Kara, F., Demirci, A., "An assessment of outdoor recreational behaviors and preferences of the residents in Istanbul", *Scientific Research and Essays*, Vol. 5, No. 1, Jan. 2010, pp. 93-104.

McAdams, M. A., Kocaman, S., Kara, F., "The use of remote sensing in the protection and management of archaeological sites: A case study of the Anastasian wall", *Scientific Research and Essays*, Vol. 5, No. 1, Jan. 2010, pp. 55-62.

HOBBIES

Traveling, football, computer technologies.